UNIVERSITY OF CALIFORNIA

Santa Barbara

Role of Monomer Sequence in Polymer Coatings and Self-Assembly

A dissertation submitted in partial satisfaction
of the requirements for the degree
Doctor of Philosophy in Materials

by

Anastasia Lily Patterson

Committee in charge:

Professor Rachel Segalman, Chair

Professor Glenn Fredrickson

Professor Craig Hawker

Professor Omar Saleh

March 2019

The dissertation of Anastasia Lily Patterson is approved.

Professor Glenn Fredrickson

Professor Craig Hawker

Professor Omar Saleh

Professor Rachel Segalman, Committee Chair

March 2019

Role of Monomer Sequence in Polymer Coatings and Self-Assembly

Anastasia Lily Patterson

ACKNOWLEDGEMENTS

First, I am indebted to my advisor, Rachel Segalman: for gauging my interests and fit from just a Skype call 6 years ago, for showing me how to bring energy and tenacity to every discussion, for understanding me both as a researcher and as a person, and for supporting me in exploring the unknown, even if it takes a little longer than we'd both like. Thank you also for being a role model in building a deliberate and positive group culture—something that I benefited from as a group member and will take with me everywhere I go.

For my committee: Glenn Fredrickson, who made possible the insights from theory in our collaborative studies and who warmly offered advice on both scientific and professional pursuits; Craig Hawker, who brought fresh perspectives to the design of my synthetic systems and to my eventual job search; and Omar Saleh, who rooted me in a physical intuition of materials through courses, TAing, and discussions around the committee table.

For the Segalman group, for providing a community that was both inspiring and comforting, offering constant and unconditional support that posed a stable backdrop to the inevitable highs and lows of the PhD journey. To Emily, for welcoming me into the group and going above and beyond to support me and others in their research and personal goals. And to George, whose camaraderie, chemical insight, and unending patience with a first-year graduate student formed the foundation of my PhD work. Thank you for the morning catch-ups, sash-side discussions, runaway puns, and even battles with La Fleur.

For instrument scientists, for working tirelessly to enable and inform the measurements that formed the bulk of my and many others' work. To Rachel Behrens, for long chats while working on chromatography and an easy acceptance that steadied me at my most harried. To James Pavlovich, for training me in a mass spectrometry technique commonly accepted to be "black magic" that would be a workhorse of my PhD, and Dmitriy Uchenik for picking up the torch. For Tom Mates, who spent hours tuning instruments with me and always offered a friendly face. To beamline scientists, Eric Schaible, Chenhui Zhu, Masafumi Fukuto, and

Ruipeng Li, for answering midnight phone calls and generously extending their expertise in X-ray scattering, which enabled much of this dissertation. To Ron Zuckermann and the entire NanoBio staff, for training me in how to make the materials that formed the foundation of my thesis, and for demonstrating with grace the gold standard of a respectful, motivated, and collaborative research environment.

For friends near and far. Thank you to my Santa Barbara crew for bringing fun and lightness to my life, and for welcoming me back to group events after I'd disappear for weeks into the lab and at beamtime. To the mountain goats Caitlin and Julija: thank you for 5 years of friendship—since even before we decided to come to UCSB—and for reminding me to take care of myself by continually including me in activities outside of the lab. To my Harvey Mudd friends, thank you for being an important part of how I became who I am now, and for the adventures and commitment to seeing each other, even when life takes us in different directions. To Andrew, for being my rock through thick and thin, and bringing me joy and comfort when I need them most. To my "LA" friends, who remind me of my roots, whose deep-seated friendship I look forward to revisiting every winter, and who embrace me even though I left engineering to study chemistry.

For Dave, without whom I would not have known my soon-to-be advisor was even moving to UCSB, and Teresa, who, among other things, welcomed me into their home during an impactful and tough summer program. Together with Marianne, Lewis, and Irene, I am grateful for your advice and acceptance that has supported me through every step of my journey. And for Ken, whose graciousness stoked a seven-year-old's enthusiasm for understanding the world around her.

For my family. To my parents, who have always supported my wide interests and aspirations with total love and understanding—from driving a pink taxi, to running a pastry shop, to being a scientist—and who painted a backdrop of balance, creativity, and respect that I will always keep with me. To my sister, who sends me funny images when I am down and is always up for an adventure with her little sister in tow. To my aunts, cousins, nieces,

nephew, and all branches of the family tree for consistently encouraging me at every holiday and get together—I am grateful to have never questioned that I had the support of my family at every step of the way. And for my grandmother, Susan, whose wit and sass brought perspective to my studious bubble, who gave me that "sparkle" gene, and who reminded me that sometimes what seems like a rainstorm will only be a showah.

VITA OF ANASTASIA LILY PATTERSON

March 2019

EDUCATION

Doctor of Philosophy in Materials — March 2019
University of California, Santa Barbara, CA

Bachelor of Science in Chemistry — May 2014
Harvey Mudd College, Claremont, CA

HONORS AND AWARDS

Fellowships and Scholarships

- NSF Graduate Fellowship Research Program — Spring 2015
- National Defense Science and Engineering Fellowship Program — Spring 2015
- Harvey S. Mudd Merit Scholarship — 2010–2014
- Achievement Rewards for College Scientists (ARCS) Scholar — 2011–2014
- Rose Hills Scholar — 2011–2014

Awards

- *Journal of Polymer Science* Poster Prize, 3rd place, APS March Meeting — Spring 2016
- Poster Award, Edward J. Kramer Memorial Conference — Spring 2016
- Best Student Poster Award, Symposium B, MRS Spring Meeting — Spring 2014
- American Chemical Society Polyed Award — 2013
- Harvey Mudd College Alumni Professional Presentation Award — 2012

TEACHING EXPERIENCE

MATRL 200A: Thermodynamic Foundation of Materials TA (HMC) — Fall 2015
Held weekly office hours, graded weekly homeworks and wrote solutions, graded exams

Analytical Chemistry Choice Lab TA (HMC) — Spring 2012
Taught experimental design and chemical analysis of local soil, advised field work

Academic Excellence Facilitator (HMC) — 2011–2014
Tutored students in Core chemistry concepts

SERVICE

Co-founder and editorial board member, UCSB Materials Minute — 2018–2019

Executive board member, UCSB Chemical Sciences Student Seminar	2015–2019
Lab safety officer	2015–2018
Secretary, UCSB Chemical Engineering Grad Student Association	2015
Graduate Students for Diversity in Science, UCSB	2014–2019

PUBLICATIONS

"Role of Monomer Sequence in Polymer Coatings and Self-Assembly," A. L. Patterson. Unpublished thesis submitted in partial fulfillment of the requirements for the Ph.D. degree in Materials, University of California, Santa Barbara, 2019.

"Effects of Helical Chain Shape on Lamellae-Forming Block Copolymer Self-Assembly," B. Yu, S. P. O. Danielsen, A. L. Patterson, E. C. Davidson, R. A. Segalman. *Macromolecules*, 2019, Articles ASAP.

"The Role of Hydrogen Bonding in Peptoid-Based Marine Antifouling Coatings," M. E. Barry, E. C. Davidson, C. Zhang, A. L. Patterson, B. Yu, A. K. Leonardi, N. Duzen, K. Malaviya, J. L. Clarke, J. A. Finlay, A. S. Clare, Z. Chen, C. K. Ober, R. A. Segalman. *Macromolecules*, 2019, 52, 3, 1287–1295.

"Sequence Effects on Block Copolymer Self-Assembly through Tuning Chain Conformation and Segregation Strength Utilizing Sequence-Defined Polypeptoids," A. L. Patterson, S. P. O. Danielsen, B. Yu, E. C. Davidson, G. H. Fredrickson, R. A. Segalman. *Macromolecules*, 52, 3, 1277–1286.

"Impact of Helical Chain Shape in Sequence-Defined Polymers on Polypeptoid Block Copolymer Self-Assembly," E. C. Davidson, A. Rosales, A. L. Patterson, B. Yu, R. N. Zuckermann, R. A. Segalman. *Macromolecules*, 2018, 51, 5, 2089–2098.

"Role of Backbone Chemistry and Monomer Sequence in Amphiphilic Oligopeptide- and Oligopeptoid-Functionalized PDMS- and PEO-Based Block Copolymers for Marine Antifouling and Fouling Release Coatings," A. L. Patterson, B. Wenning, G. Rizis, D. R. Calabrese, J. A. Finlay, S. C. Franco, R. N. Zuckermann, A. S. Clare, E. J. Kramer, C. K. Ober, R. A. Segalman. *Macromolecules*, 2017, 50, 2656–67.

"Solvent-free Synthesis and Fluorescence of a Thiol-reactive Sensor for Undergraduate Organic Laboratories," A. L. Patterson, M. D. May, B. J. Visser, A. A. Kislukhin, D. A. Vosburg. *Journal of Chemical Education* 2013, 90, 1685–1687.

PRESENTATIONS

Invited Presentations

"Tuning Segregation Strength with Sequence-Defined Polypeptoid Copolymers." A. L. Patterson, S. P. O. Danielsen, B. Yu, E. C. Davidson, G. H. Fredrickson, R. A. Segalman. UCSB–Korea Mini-Symposium with KAIST and Korea University, Santa Barbara, CA. March 2018.

"Sequence-Specific Polymers for Antifouling Surfaces: Materials Comparison Toward New Design Rules." A. L. Patterson, B. Wenning, G. Rizis, D. R. Calabrese, J. A. Finlay, S. C. Franco, R. N. Zuckermann, A. S. Clare, E. J. Kramer, C. K. Ober, R. A. Segalman. Edward J. Kramer Memorial Conference, Santa Barbara, CA. February 2016. (Poster, Poster Prize)

Contributed Presentations

"Sequence Effects on Block Copolymer Self-Assembly through Tuning Chain Conformation and Segregation Strength Utilizing Sequence-Defined Polypeptoids." A. L. Patterson, S. P. O. Danielsen, B. Yu, E. C. Davidson, G. H. Fredrickson, R. A. Segalman. APS March Meeting. March 2019.

"Tuning Segregation Strength with Sequence-Defined Polypeptoid Copolymers." A. L. Patterson, S. P. O. Danielsen, B. Yu, E. C. Davidson, G. H. Fredrickson, R. A. Segalman. Gordon Research Seminar/Conference on Polymer Physics, South Hadley, MA. July 2018. (Poster)

"Tuning Segregation Strength with Sequence-Defined Polypeptoid Diblock Copolymers." A. L. Patterson, S. P. O. Danielsen, B. Yu, E. C. Davidson, G. H. Fredrickson, R. A. Segalman. American Physical Society March Meeting, Los Angeles, CA. March 2018.

"Role of Monomer Sequence and Backbone Chemistry in Polypeptoid Copolymers for Marine Antifouling Coatings." A. L. Patterson, B. Wenning, G. Rizis, D. R. Calabrese, J. A. Finlay, S. C. Franco, R. N. Zuckermann, A. S. Clare, E. J. Kramer, C. K. Ober, R. A. Segalman. American Physical Society March Meeting, New Orleans, LA. March 2017.

"Role of Backbone Chemistry and Monomer Sequence in Amphiphilic Oligopeptide-and Oligopeptoid-Functionalized Block Copolymers for Marine Antifouling Coatings." A. L. Patterson, B. Wenning, G. Rizis, D. R. Calabrese, J. A. Finlay, S. C. Franco, R. N. Zuckermann, A. S. Clare, E. J. Kramer, C. K. Ober, R. A. Segalman. Materials Research Outreach Program, Santa Barbara, CA. January 2017. (Poster)

"Role of Monomer Sequence and Backbone Structure in Polypeptoid and Polypeptide Polymers for Antifouling Applications." A. L. Patterson, B. Wenning, G. Rizis, D. R. Calabrese, J. A. Finlay, S. C. Franco, R. N. Zuckermann, A. S. Clare, E. J. Kramer, C. K. Ober, R. A. Segalman. Materials Research Outreach Program, Santa Barbara, CA. January 2017. (Poster, 3rd place Poster Prize)

"Coupling of a Homologous Series of Porphyrin Dyes to Zinc Oxide Nanorod and Nanotube Photoanodes in Dye-Sensitized Solar Cells." S. V. Shah, A. L. Patterson, H. Van Ryswyk. MRS Spring Meeting, San Francisco, CA. April 2014.

"Synthesis and Fluorescence of a Thiol-Reactive Probe for Organic Laboratories." A. L. Patterson, B. J. Visser, A. A. Kislukhin, and D. A. Vosburg. American Chemical Society National Conference, San Diego, CA. March 2012. (Poster, Best Student Poster Award)

ABSTRACT

Role of Monomer Sequence in Polymer Coatings and Self-Assembly

by

Anastasia Lily Patterson

Polymeric materials that incorporate multiple functionalities are crucial in a variety of applications, from adhesives and membranes to thermoplastic elastomers and electrolytes. Control over the length scale of each component is key to designing the structure and resulting properties, driving efforts for greater control in copolymer systems. Controlling comonomer sequence is an attractive tool to reach this goal, as the length scales of assembly can be set by tuning the size and connectivity of different chemistries. However, materials systems that bridge the sequence-specificity of biopolymers and robustness of synthetic polymers are needed to experimentally understand the role of comonomer sequence in multicomponent polymer materials. This work utilizes versatile and scalable polypeptoid chemistry to install sequence-defined chains into traditional polymer systems, focusing on two potential applications. First, the roles of polymer sequence and functionality are investigated in a modular surface-active coating, achieving optimal marine antifouling and fouling release properties with finer length scales of amphiphilicity. Second, the role of comonomer sequence is investigated in self-assembling diblock copolymers, forming lamellae with tunable thermal and morphological properties based on sequence. The findings in this work emphasize the utility of comonomer sequence as a design tool to target both surface and bulk properties of multicomponent polymer materials.

TABLE OF CONTENTS

Chapter 1

Introduction

Polymeric materials that incorporate multiple chemistries are crucial in a variety of applications, from adhesives and membranes to thermoplastic elastomers and electrolytes. A key factor in each of these applications is the ability for multi-component polymer materials to rearrange their distinct components with no external direction. At surfaces, surface free energy dictates which components are present, while in the bulk, tradeoffs between mixing and chain stretching penalties drive self-assembly into periodic morphologies, imparting both mechanical and functional properties. Control over the length scales of each component is crucial in determining the behavior and resulting performance, driving a push for even greater control in copolymer systems.

Polymer sequence is an attractive tool to reach this goal, as the length scales of assembly can be set by tuning the size and connectivity of different chemistries. While natural biopolymers are inherently and robustly sequence-defined, they are limited in functionality, molecular weight, and stability, making them less suited for materials development. Furthermore, biopolymers such as polypeptides and nucleic acids employ strong and specific interactions to drive their natural structures (i.e., hydrogen bonding and charge–charge interactions) that make them intractable for solvent-free, bulk applications. On the other hand, traditional polymer synthesis is by nature statistical, producing stable and

diverse polymers but with limited control over sequence at the monomer level, mainly relying on monomer reactivity ratios, which are difficult to control. Materials systems that bridge the specificity of biopolymers and the robustness of synthetic polymers are needed to understand the role of comonomer sequence in self-assembly and harness sequence control as a design tool for new materials.

The adaptation of solid-phase synthesis to chemistries beyond peptides has enabled significant progress in reaching this middle ground of sequence-defined polymers. Polypeptoids (*N*-substituted polyglycines) are ideal materials for studying the role of sequence in self-assembly, and while they have their roots in solution foldamer and nanostructure assembly, polypeptoids are emerging materials for answering key questions in traditional polymeric settings. Utilizing polypeptoids as a model system, this work investigates the effect of comonomer sequence on the self-assembly of multi-component polymeric systems—both at surfaces (targeting marine antifouling and fouling release properties) and in the bulk (tuning morphological and thermal properties of block copolymers). First, a background in other synthetic approaches is presented to give context to polypeptoid materials. Next, the states of each field—marine antifouling and sequence-defined self-assembly—are briefly summarized. Finally, a note is offered on the impact of imperfection in these sequence-defined materials.

1.1 Synthesis of sequence-defined polymers

In order for polymer physicists to tackle questions about the role of comonomer sequence, flexible and reliable syntheses of sequence-defined polymers must be established first. In recent years, a number of strategies have been developed toward controlling polymer composition on the monomer length scale. The approaches generally fall into one of five categories: reactivity ratio control, batch-fed copolymerization, macronomer extension, iterative exponential growth, and solid-phase synthesis (Figure 1.1).

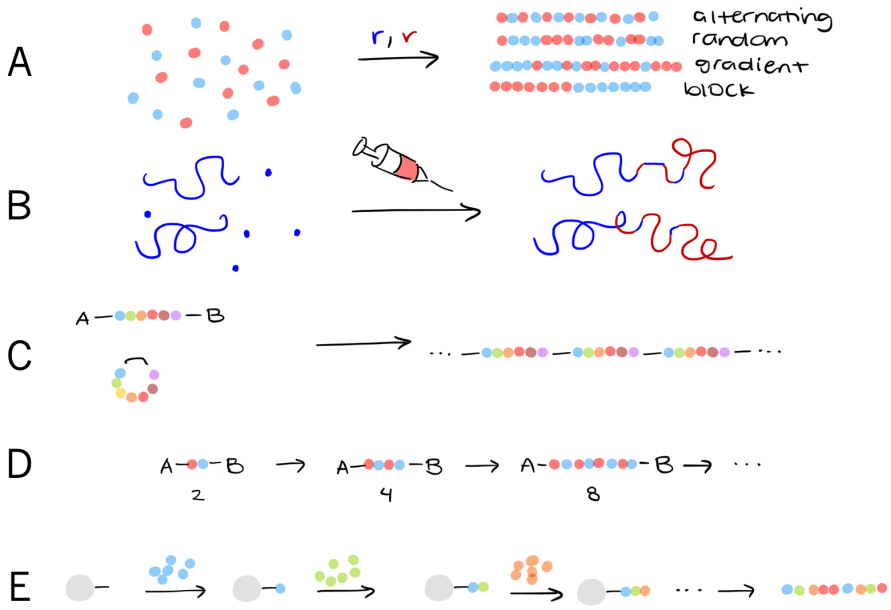

Figure 1.1 Polymerization approaches for controlling comonomer placement

Approaches to controlling comonomer placement typically fall into one of five categories: A) reactivity ratio control, B) batch-fed copolymerization, C) macromonomer extension, D) iterative exponential growth, and E) solid-phase synthesis.

(Jean-François Lutz has written prolifically on the synthesis and unusual applications of sequence-defined polymers, and the reader is directed to his many publications on the topic.[2-6]) The following is a summary of these synthetic techniques, with references to point the reader toward further reading. Ultimately, this work relies on the fifth category—solid-phase synthesis—due to its absolute sequence control, flexible chemistry, and relatively high production scale.

1.1.1 Reactivity ratio control

In traditional copolymerizations, two or more monomers are present in solution during the reaction, and the growing chain incorporates each in a statistical manner depending on the identity of the chain end. Taking a snapshot of a copolymerization of A and B monomers, any given chain end is a just-incorporated A or B monomer, and so AA, AB, BA, and BB pairs are all possible next steps with different probabilities depending on the ratio of propagation

rate constants. For example, if monomers are more likely to react with chain ends of their same identity, long sequences of ···AAA··· and ···BBB··· will grow before switching to the other monomer and an overall "blocky" distribution of comonomers will develop. Careful kinetics studies[7] partnered with judicious monomer synthesis[8] can create sets of monomers that produce desired composition profiles (alternating, blocky, gradient, or—elusively—truly random). However, this approach is ill-suited to studies of comonomer sequence, as the resulting materials are inherently statistical (produce variation from chain to chain) and cannot realize arbitrary sequences of comonomers. Lessons learned from more careful synthetic systems, though, could be adapted to this approach, especially where blockiness (or the average block size) is an important parameter.

1.1.2 Semibatch copolymerization

Another approach toward controlling the distribution of comonomers is to temporally control the addition of monomers during a polymerization to produce average profiles that vary in composition over the length of the chain (Figure 1.2). This approach is termed "semibatch polymerization", after reactors that allow for the addition of reactants over time. Torkelson and coauthors synthesized and studied a variety of gradient copolymers, which vary smoothly from one monomer identity to another over the entire length of the chain.[9-11]

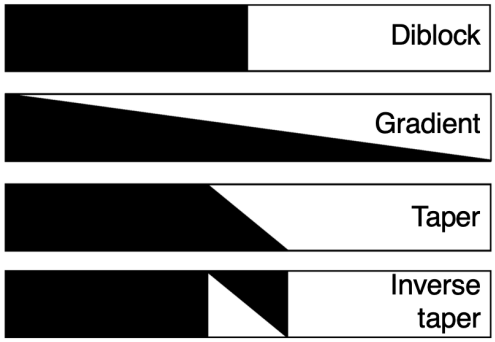

Figure 1.2 Semibatch copolymerization approach to controlling composition profiles
Reproduced (adapted) with permission from reference 12.

While the composition of the reaction mixture is well-controlled using this method, the target composition profiles are difficult to confirm, only by analyzing aliquots during the reaction time.[13] Similar to gradient copolymers, tapered copolymers are prepared via semibatch methods, where the transition from monomer A to B occurs only over a portion of the chain, rather than along the entire chain length. Epps and coauthors are well-known for work in tapered copolymers, synthesized by well-defined, small injections of comonomer that are allowed to reach high conversion at each step to more finely control the taper shape.[12,14,15] Semibatch methods can produce smoothly-varying composition profiles, but the populations of chains is disperse in both length and composition, and arbitrary or fine sequences cannot be synthesized.

1.1.3 Macromonomer and iterative exponential growth approaches

Sequence control on the monomer length scale can be achieved by synthesizing precise macromonomers, in which a small number of repeat units have been incorporated in a specific order, and polymerizing them to create polymers composed of repeating sequences. A variety of polymerization mechanisms can be employed under this general approach, such as ring-opening metathesis polymerization,[16,17] click chemistry,[18] and acyclic diene metathesis (ADMET) polymerization.[19,20] While this approach controls sequence on a monomer length scale, it does not control sequence on a whole-chain basis, and is thus limited in its application. Similarly, a process termed "iterative exponential growth" relies on potentially sequence-defined building blocks that are iteratively coupled in what resembles a highly controlled step-growth polymerization.[21-24] This iterative synthesis produces, primarily, highly controlled polymer lengths, and the many reaction steps required have more recently been streamlined into flow reactors to make the technique more accessible.[25] However, outside of alternating or repeating sequences, none of these synthetic techniques can control sequence along the entire length of the polymer chain.

1.1.4 Solid-phase synthesis

Solid-phase approaches to polymerization take advantage of the control afforded by iterative reaction steps, but have two practical benefits: 1) no purification steps are needed between reactions (the growing polymer chain is bound to a substrate, and excess reagent can simply be rinsed off), and 2) the use of excess chemistry can drive reactions to >99.9% completion (and depending on the chemistry, the concentrated solutions of reagents can be recovered and reused). The combination of these two factors make solid-phase synthesis an attractive approach for producing reasonable amounts of sequence-defined polymers. First introduced by Merrifield in 1963 to synthesize a tetrapeptide,[26] solid-phase synthesis has since expanded to include non-peptide chemistries.[27-30] In principle, any two-step or orthogonal chain extension reactions can be adapted to solid-phase synthesis, and are limited only by reaction efficiency and chemistry compatibility.

One such solid-phase approach is the synthesis of polypeptoids (*N*-substituted polyglycines). Developed in 1992 by Ron Zuckermann,[31] polypeptoids are built up via a submonomer process: 1) amide coupling to an alkyl halide acid, 2) displacement of the halide by a primary amine carrying the side chain of interest (Figure 1.3).

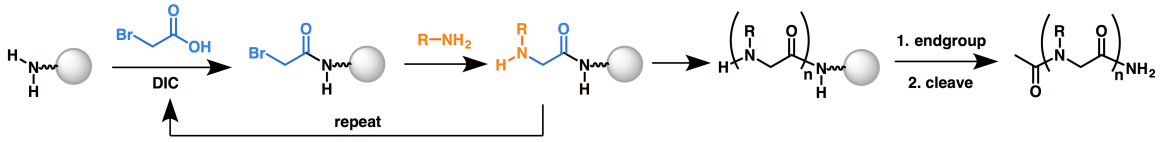

Figure 1.3 Solid-phase synthesis of polypeptoids via the submonomer approach

Polypeptoids are truly sequence-defined materials, can reach degrees of polymerization of ~50 with high fidelity, and incorporate a substantial variety of side chain functionalities, readily available as simple primary amines. Furthermore, polypeptoids have no inherent specific interactions, such as hydrogen bonding or charged groups, which makes them practical candidates for bulk and melt studies. This work utilizes polypeptoid materials in two contexts: 1) surface design for antifouling (where the length scale of comonomer

placement is relevant for interactions with biological adhesives), and 2) block copolymer design for bulk self-assembly.

1.2 Length scale effects in antifouling coating design

Since the banning of biocidal antifouling paints in the early 2000s, there has been an enormous research effort to design non-toxic alternatives.[32] A challenge thwarting the advent of universal antifouling coatings is the diversity and complexity of proteinaceous biological adhesives,[33] secreted by single-celled or larval organisms upon settling onto a surface. The length scale for the interactions that cause adhesion is somewhere between the size of the protein's adhering moieties and the size of the organism—nanometers to microns. Surfaces designed to prevent the settlement and attachment of fouling organisms must then incorporate features on this relevant length scale. Two approaches have been pursued in creating disruptive surface features: topographic patterning (physical disruption) and functionality patterning (chemical disruption). This work only explores the use of incorporating amphiphilic functionalities on ~1-nanometer length scales, but a brief overview of topographic effects is offered for context.

1.2.1 Topographic patterning

Inspired by the fouling resistance of fish (especially sharks), the hypothesis behind topographic antifouling is that a surface with texture on the length scale of the fouling organism will prevent settlement by offering cramped, and therefore undesirable, local environments. The body of work on topographical antifouling is reviewed here.[34] To briefly illustrate this concept, Long, et al. simulates algal spore settlement on commercial SharkLet AF™ topographic surfaces and demonstrates the accuracy of the simulations with spore settlement studies (Figure 1.4).[35]

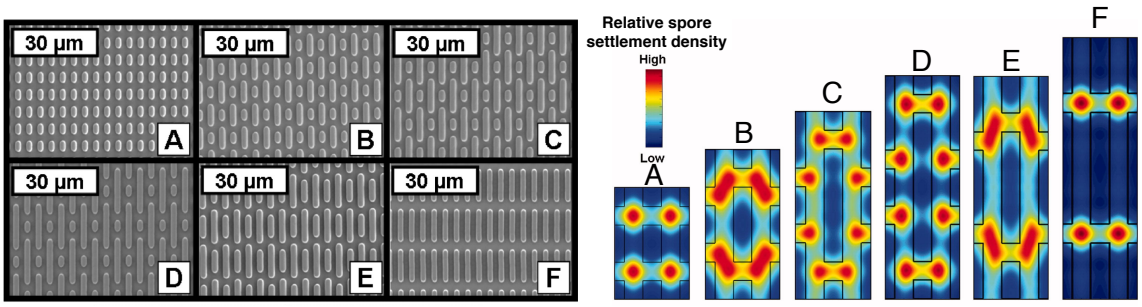

Figure 1.4 Topographic antifouling with SharkLet AF™ surfaces by Long, et al.
Reproduced (adapted) with permission from reference 35.

The spores are expected to settle in the regions with the least crowding, and bioassay experiments confirm this hypothesis. While targeted antifouling can be achieved with these topographical approaches, the wide variety of organism sizes and the challenge of carefully patterning large areas make this physical strategy more cumbersome than chemical approaches.

1.2.2 Functional patterning

A more approachable antifouling coating strategy lies in chemical modifications to the surface, rather than specialized topographic patterning. This strategy relies on physicochemical interactions between foulants and the surface layer of a coating, so the design and quantification of functionalities at the surface is crucial. However, a complicating factor in using polymer coatings for antifouling is that the interfacial free energy, which dictates the composition of the surface, varies depending on environment. In film preparation and annealing, the air/vacuum–coating interface is dominated by coating components with the lowest surface free energy. In testing and application, the presence of an aqueous environment causes rearrangement in rubbery coating materials such that coating components with the lowest interfacial energy are present at the surface. This rearrangement is demonstrated in a handful of cryogenic spectroscopy techniques, where the sample is hydrated with bulk water, cryogenically frozen, and dried via sublimation of the

water droplet, revealing the underlying coating in its "hydrated" state (Figure 1.5).[36,37] Cryo-spectroscopy is a useful technique for getting insight into the hydrated state of these rearranging coatings, but is not always feasible and additionally can introduce artifacts from mechanical damage to the sample on freezing. Experiments are ongoing in the Segalman group to adapt synchrotron ambient pressure X-ray photoelectron spectroscopy (AP-XPS) to polymer surfaces to dynamically measure surface presentation in humid environments.

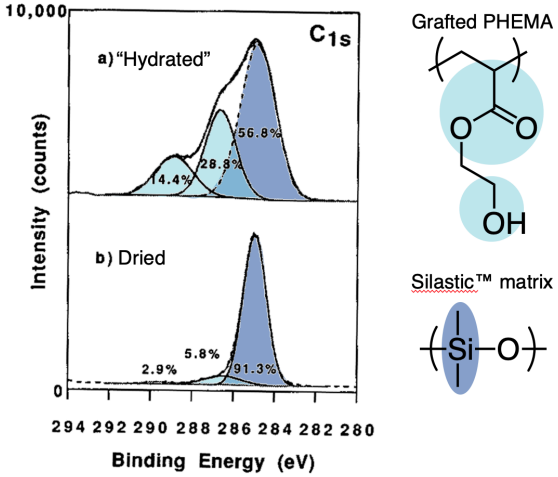

Figure 1.5 Rearrangement of PHEMA-grafted Silastic™ using cryo-ESCA
Aadapted with permission from reference 37.

There is a large body of literature aimed toward understanding the interaction of surface functionalities with marine foulants. With thousands of identified marine fouling organisms and a variety of adhesion mechanisms, it is no wonder that this body of work is so expansive. A number of model organisms have been identified (such as *Ulva linza* algae and *Balanus amphitrite* barnacles) as representatives of the various attachment mechanisms, and well-controlled bioassay protocols have been developed to make composition–structure–performance comparisons between a wide range of polymeric coatings.[38-40]

It is has been seen that amphiphilic surfaces (those that contain both hydrophilic and hydrophobic components) are some of the strongest candidates for "universal" antifouling coatings and resist or release a wide range of fouling organisms. Many amphiphilic polymer

coating designs exist, often based on fluorinated groups as the hydrophobic component.[41-46] While distinct regions of functionalities can be lithographically patterned,[47] the covalent connectivity of different groups is more often used to tune the mixed presentation of these materials and to prevent macrophase separation. Work from van Zoelen, et al. and Calabrese, et al. introduced length scale control on the molecular level by incorporating amphiphilic, sequence-defined oligomers as side chains.[48,49] Utilizing polypeptoids, van Zoelen, et al. showed that the ratio of hydrophilic ether and hydrophobic fluorinated groups had a strong impact on fouling release of *U. linza* sporelings, and the placement of fluorinated groups relative to the graft point affected the initial settlement of algal spores (Figure 1.6).

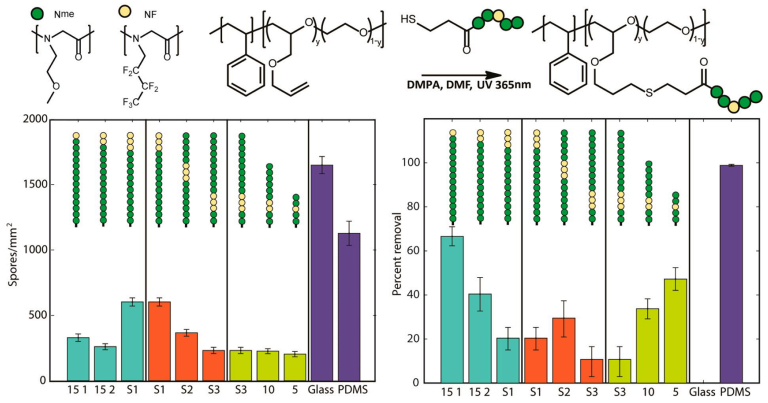

Figure 1.6 Peptoid-based amphiphilic marine antifouling and fouling-release coatings
Reproduced (adapted) with permission from reference 48.

In addition to controlling the length scale of amphiphilicity, the approaches taken in van Zoelen, et al. and Calabrese, et al. have the advantage of a modular coating platform with which direct materials comparisons can be made. With so many polymer scaffolds studied, it is difficult make direct comparisons between literature studies. There is room still for systematic studies of mixed functionalities and their length scales. The work included in this thesis describes such a comparison, stemming from the two studies highlighted here.

1.3 Sequence effects in block copolymer self-assembly

While comonomer sequence has been utilized to set a length scale of amphiphilicity in coating design, control over sequence is best known for driving complex and specific self-assembled structures. The majority of the literature on sequence-driven self-assembly is set in aqueous environments: micelles, sheets, and foldamers are just a few examples. In the polypeptoid community alone, elegant aqueous self-assembled structures have been produced, including nanosheets,[50] nanotubes,[51,52] single-chain and hierarchical helices,[53-59] and other foldamer building blocks.[60-62]

In this thesis, inspiration is taken from aqueous sequence-dependent self-assembly and extended to melt self-assembly of block copolymers. In both aqueous and melt environments, the enthalpic interactions between dissimilar components are balanced with entropic conformational penalties. There is great opportunity to harness the sequence-specific synthesis outlined above in melt self-assembly.

1.3.1 Classical diblock copolymer self-assembly

Diblock copolymer self-assembly has been extensively studied since the first studies in the 1960s,[63] and formalized thermodynamic understanding has been well-established since the 1980s.[64,65] The classic diblock copolymer is a Gaussian (random-walk) chain composed of two distinct chemistries joined at a block junction, with symmetric statistical segment lengths (or "step" sizes). At small degrees of polymerization (N) or low enthalpic penalties of mixing (parameterized by the Flory–Huggins parameter χ), diblock copolymers form disordered melts, as the entropy gained by disordering outweighs the enthalpic penalty of mixing dissimilar blocks. However, at sufficiently large degrees of polymerization or χ parameters (sufficiently large segregation strength χN), the enthalpic drive to demix overcomes the entropic penalties of chain stretching and these materials self-assemble into

periodic, microphase-separated structures, whose interfacial curvatures and thus morphologies are determined by the relative volumes of each distinct block (Figure 1.7).

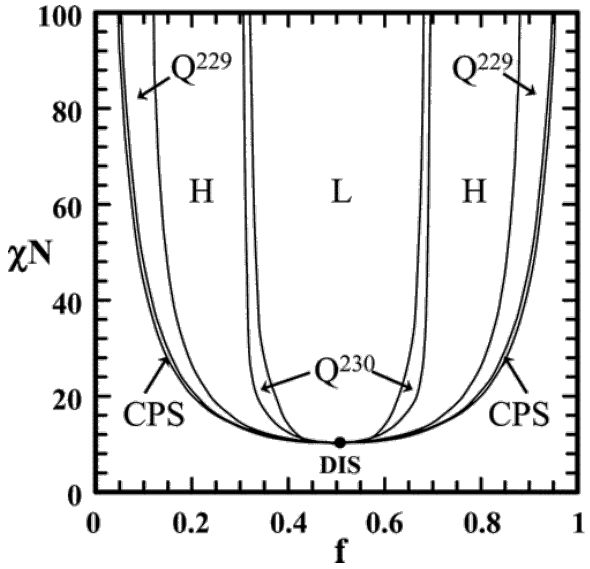

Figure 1.7 The diblock copolymer phase diagram calculated using SCFT

The labels signify the following: CPS (hexagonally-packed spheres), Q^{229} (body-centered spheres), H (hexagonally-packed cylinders), Q^{230} (double-gyroid), L (lamellae), DIS (disordered). Reproduced with permission from reference 66.

The almost 10,000 publications to date containing the phrase "block copolymer self-assembly" are evidence for the vast interest in and utility of block copolymers across fields, from medicine to energy to mechanics. Work in this thesis focuses on one mostly unexplored parameter in the wide design space for block copolymer materials: comonomer sequence.

1.3.2 Sequence effects in diblock copolymer self-assembly

The majority of work done on sequence-controlled block copolymers has been in manipulating composition profiles via the semibatch methods described above. Torkelson and coauthors have extensively studied the properties of gradient copolymers, and over a series of prolific studies, found that thermal properties,[9,13,67,68] blend compatibilization,[11,69,70] and self-assembly[71-73] depend on factors such as gradient profile shape, segregation strength, and the presence of specific interactions such as hydrogen bonds. In general, the presence of

a gradient broadens the interface between dissimilar components, resulting in "uniquely-broad" glass transition temperatures, greatly compatibilized blends, and suppressed segregation-driven self-assembly of the neat copolymers. A number of other experimental studies concerning gradient copolymer self-assembly have been performed,[74,75] and the reader is directed to a review for even more applications.[76] Theoretical and simulation work has also been pursued to understand the phase behavior of gradient copolymers.[77-82]

Concurrently, Epps and coauthors have explored many aspects of tapered copolymer self-assembly, including thermal transitions,[12] stabilized network phases,[1,14] and interfacial mixing[83] (reviewed here[84]). In general, the presence of a tapered composition profile in the center of the block strongly depresses order–disorder transition temperatures of self-assembled phases, as well as stabilizes phases with complex curvature (Figure 1.8). More recently, tapered copolymers have been predicted to have faster dynamics than traditional block copolymers,[85] and subsequently showed increased ionic conductivity following this prediction.[15]

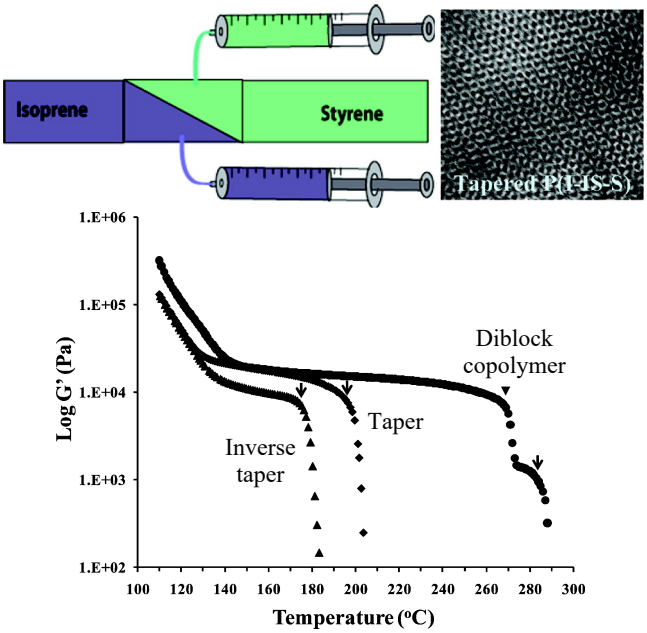

Figure 1.8 Tapered copolymers have lower order–disorder transition temperatures

Reproduced (adapted) with permission from reference 1.

In all of these experimental systems, the comonomer composition profile is controlled, but the monomer-by-monomer sequence is not. With precise control over comonomer placement, simulations are well-suited to predict the behavior of sequence-defined copolymers. Hall and coworkers have shown that the strength, volume fraction, and direction of precisely-defined tapered composition profiles alter the chain conformations of copolymer chains.[85,86] Ganesan and coworkers have investigated the role of "blockiness" (or the average length of consecutive monomers of a single type) in gradient copolymer systems, and have found that blockier gradients have expanded regions of morphologies with curved interfaces, such as cylindrical phases, compared to gradients with finer distributions of comonomers.[82] With a range of interesting behaviors predicted for these precise materials, there is an opportunity for experiments with sequence-defined block copolymers. Chapters 3 and 4 of this dissertation describe the thermal and morphological effects of precisely-controlled comonomer sequence.

1.4 Note on imperfections: Polymer dispersity and impurities

While the polymer experimentalist can do their best to avoid imperfections in their materials, it is common to have both dispersity in chain length and small amounts of impurities (especially polymeric ones) in the final system. It is crucial to understand the quantification and impact of these imperfections so that results can be interpreted accurately. This section briefly comments on the definitions and potential effects of dispersity and excess homopolymer in both surface design and bulk self-assembly.

Dispersity, or the variation in degree of polymerization from chain to chain, is present in all polymer systems (although is negligible in polypeptoids). Quantified by the ratio of the weight-averaged molecular weight (M_w) and the number-averaged molecular weight (M_n), dispersity (Đ) is a measure of the narrowness of the distribution of chain lengths:

$$Đ = \frac{M_w}{M_n} \geq 1 \tag{1.1}$$

where M_w and M_n are calculated as sums over all chains i:

$$M_w = \frac{\sum_i w_i M_i}{\sum_i w_i} = \frac{\sum_i n_i M_i^2}{\sum_i n_i M_i} \tag{1.2}$$

$$M_n = \frac{\sum_i n_i M_i}{\sum_i n_i} \tag{1.3}$$

with weight fraction w_i, number fraction n_i, and chain molecular weight M_i. To demonstrate these concepts pictorially, dispersities are calculated in Figure 1.9 for two hypothetical polymer distributions. In general, Đ~1.1–1.2 is considered "low dispersity"; however, it is clear from the example below that even low calculated dispersities can have a wide range of chain lengths.

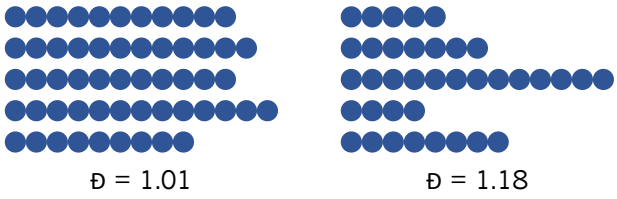

Figure 1.9 Schematic representation of dispersity

In surface design, dispersity of the main polymer matrix has a relatively low impact on final properties (although it plays a stronger role in thin films[87]). However, if the surface composition is being controlled by short-chain, sequence-defined surface-active groups (as in this work), dispersity in *composition* and *sequence* is more important than dispersity in length (Figure 1.10). These dispersities are discussed in the previous section on sequence-defined polymer synthesis.

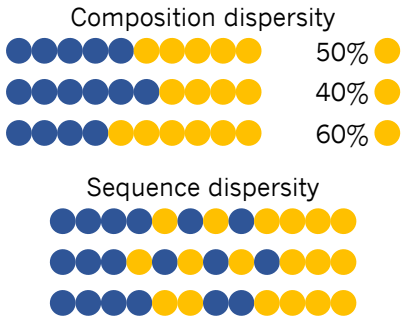

Figure 1.10 Composition and sequence dispersity

In block copolymer self-assembly, dispersity in chain *length* partially relieves the chain stretching required to fill space within each domain, especially in morphologies with curved interfaces.[88-90] For example, in the double gyroid morphology, the width of the domain varies between the arms of the network to nodes of the network, and chains in those regions must compress and extend to fill space, respectively.[91,92] Lynd and Hillmyer synthesized over 30 PEP–PLA diblock copolymers with a range of volume fractions and dispersities, and found that the degree of dispersity can even cause morphological changes, where dispersity in the minority phase drives the formation of morphologies with larger mean interfacial curvature and dispersity in the majority phase does the opposite.[93] A systematic study of dispersity in very low-molecular-weight diblock coöligomers demonstrated that disperse diblocks have increased domain spacings and more stable disordered phases (lower order–disorder transition temperatures) compared to their discrete analogs.[94] Because dispersity impacts self-assembly in these ways, it is important that studies of comonomer sequence use polymers with very low dispersities so that the results are not dominated by dispersity effects.

At low concentrations, homopolymer impurities play a similar role as dispersity in block copolymer assembly. The main source of potential introduction of homopolymer in these cases is the incomplete purification of the block copolymer after two or more homopolymers have been conjugated together, i.e., homopolymers that are the same molecular weight as the

incorporated blocks. The role of these impurities in the self-assembled structure is then in the "wet brush" regime, where the homopolymer mixes intimately with the matching block arranged at the block–block interface.[95] (This is in contrast to the "dry brush" regime when $MW_{homopolymer} > \sim 10 \times MW_{block}$, where the center of the domain becomes predominantly homopolymer and avoids penetrating the brush-like arrangement of blocks at the interface. This regime will not be discussed in detail, but becomes the focus of work in blend compatibilization of high-molecular-weight homopolymers.) For the experimentalist, it is useful to understand the effects of unpurified homopolymer ("wet-brush") so that results are not confounded by this factor. The main effect of excess homopolymer is the swelling of the domain composed of the same type of polymer, where the homopolymer resides mainly in the center of the domain (away from the interface). The presence of homopolymer in one domain relaxes the complementary block in the other domain, so the overall domain spacing can, perhaps surprisingly, increase *or* decrease upon the addition of homopolymer. The amount of homopolymer also influences the area occupied by each chain, increasing the area at low concentrations/molecular weights, and decreasing it at higher concentrations/molecular weights.[96,97] This thesis demonstrates that effects due to sequence, while significant, are relatively small in magnitude and could be masked by small amounts of unreacted homopolymer. It is suggested that sequence-defined block copolymers synthesized via conjugation of a sequence-defined block to a homopolymer block be thoroughly purified, via precipitation or, preferably, by chromatography (preparatory GPC or careful adsorption chromatography[98]).

1.5 Outline

This thesis describes the application of comonomer sequence control to design both surface and bulk properties of multi-component polymeric systems. First, the use of sequence in imparting fine length scales of amphiphilicity in marine antifouling coatings is

described in Chapter 2. Next, the role of comonomer sequence is investigated in a study of bulk chain conformation and segregation strength of lamellae-forming block copolymers (Chapter 3) and the effect these have on interfacial mixing (Chapter 4). Appendices of Chapters 2–4 contain useful information for those looking to repeat these materials syntheses or data analyses. Finally, perspectives on this work and future directions are offered in Chapter 5.

1.6 Permissions

Parts of this dissertation were reproduced in part with permissions from:

1. Patterson, A. L.; Wenning, B.; Rizis, G.; Calabrese, D. R.; Finlay, J. A.; Franco, S. C.; Zuckermann, R. N.; Clare, A. S.; Kramer, E. J.; Ober, C. K.; Segalman, R. A. Role of Backbone Chemistry and Monomer Sequence in Amphiphilic Oligopeptide- and Oligopeptoid-Functionalized PDMS- and PEO-Based Block Copolymers for Marine Antifouling and Fouling Release Coatings. *Macromolecules*, 2017, 50, 7, 2656–2667. Copyright 2017 American Chemical Society.
2. A. L. Patterson, S. P. O. Danielsen, B. Yu, E. C. Davidson, G. H. Fredrickson, R. A. Segalman. Sequence Effects on Block Copolymer Self-Assembly through Tuning Chain Conformation and Segregation Strength Utilizing Sequence-Defined Polypeptoids. *Macromolecules*, 2019, 52, 3, 1277–1286. Copyright 2019 American Chemical Society.
3. Patterson, A. L.; Yu, B.; Danielsen, S. P. O.; Davidson, E. C.; Fredrickson, G. H.; Segalman, R. A. Comonomer sequence effects on interfacial mixing of self-assembled diblock copolymers. In preparation.

1.7 References

(1) Roy, R.; Park, J. K.; Young, W. S.; Mastroianni, S. E.; Tureau, M. S.; Epps, T. H., III Double-Gyroid Network Morphology in Tapered Diblock Copolymers. *Macromolecules* **2011,** *44* (10), 3910-3915.

(2) Lutz, J. F. Sequence-controlled polymerizations: the next Holy Grail in polymer science? *Polym. Chem.* **2010,** *1* (1), 55-62.

(3) Lutz, J. F.; Liu, S. Y.; Sumerlin, B. Polymer Science: The Next Generation. *Macromol. Rapid Commun.* **2012,** *33* (9), 721-721.

(4) Lutz, J. F. Coding Macromolecules: Inputting Information in Polymers Using Monomer-Based Alphabets. *Macromolecules* **2015,** *48* (14), 4759-4767.

(5) Lutz, J. F.; Lehn, J. M.; Meijer, E. W.; Matyjaszewski, K. From precision polymers to complex materials and systems. *Nat Rev Mater* **2016,** *1* (5).

(6) Lutz, J. F. Defining the Field of Sequence-Controlled Polymers. *Macromol. Rapid Commun.* **2017,** *38* (24).

(7) Beckingham, B. S.; Sanoja, G. E.; Lynd, N. A. Simple and Accurate Determination of Reactivity Ratios Using a Nonterminal Model of Chain Copolymerization. *Macromolecules* **2015,** *48* (19), 6922-6930.

(8) Leibig, D.; Müller, A. H. E.; Frey, H. Anionic Polymerization of Vinylcatechol Derivatives: Reversal of the Monomer Gradient Directed by the Position of the Catechol Moiety in the Copolymerization with Styrene. *Macromolecules* **2016**.

(9) Gray, M. K.; Zhou, H. Y.; Nguyen, S. T.; Torkelson, J. M. Synthesis and glass transition behavior of high molecular weight styrene/4-acetoxystyene and styrene/4-hydroxystyrene gradient copolymers made via nitroxide-mediated controlled radical polymerization. *Macromolecules* **2004,** *37* (15), 5586-5595.

(10) Dettmer, C. M.; Gray, M. K.; Torkelson, J. M.; Nguyen, S. T. Synthesis and functionalization of ROMP-based gradient copolymers of 5-substituted norbornenes. *Macromolecules* **2004,** *37* (15), 5504-5512.

(11) Kim, J.; Zhou, H. Y.; Nguyen, S. T.; Torkelson, J. M. Synthesis and application of styrene/4-hydroxystyrene gradient copolymers made by controlled radical polymerization: Compatibilization of immiscible polymer blends via hydrogen-bonding effects. *Polymer* **2006,** *47* (16), 5799-5809.

(12) Singh, N.; Tureau, M. S.; Epps, T. H., III Manipulating ordering transitions in interfacially modified block copolymers. *Soft Matter* **2009,** *5* (23), 4757-4762.

(13) Mok, M. M.; Kim, J.; Wong, C. L. H.; Marrou, S. R.; Woo, D. J.; Dettmer, C. M.; Nguyen, S. T.; Ellison, C. J.; Shull, K. R.; Torkelson, J. M. Glass Transition Breadths and Composition Profiles of Weakly, Moderately, and Strongly Segregating Gradient Copolymers: Experimental Results and Calculations from Self-Consistent Mean-Field Theory. *Macromolecules* **2009,** *42* (20), 7863-7876.

(14) Kuan, W. F.; Roy, R.; Rong, L. X.; Hsiao, B. S.; Epps, T. H. Design and Synthesis of Network-Forming Triblock Copolymers Using Tapered Block Interfaces. *ACS Macro Lett.* **2012,** *1* (4), 519-523.

(15) Kuan, W. F.; Remy, R.; Mackay, M. E.; Epps, T. H. Controlled ionic conductivity via tapered block polymer electrolytes. *Rsc Adv* **2015,** *5* (17), 12597-12604.

(16) Gutekunst, W. R.; Hawker, C. J. A General Approach to Sequence-Controlled Polymers Using Macrocyclic Ring Opening Metathesis Polymerization. *J. Am. Chem. Soc.* **2015,** *137* (25), 8038-8041.

(17) Zhang, J. H.; Matta, M. E.; Hillmyer, M. A. Synthesis of Sequence-Specific Vinyl Copolymers by Regioselective ROMP of Multiply Substituted Cyclooctenes. *ACS Macro Lett.* **2012,** *1* (12), 1383-1387.

(18) Chen, Y. L.; Guan, Z. B. Bioinspired Modular Synthesis of Elastin-Mimic Polymers To Probe the Mechanism of Elastin Elasticity. *J. Am. Chem. Soc.* **2010,** *132* (13), 4577-4579.

(19) Atallah, P.; Wagener, K. B.; Schulz, M. D. ADMET: The Future Revealed. *Macromolecules* **2013,** *46* (12), 4735-4741.

(20) Li, Z. L.; Lv, A.; Du, F. S.; Li, Z. C. Intrachain Cyclization via Postmodification of the Internal Alkenes of Periodic ADMET Copolymers: The Sequence Matters. *Macromolecules* **2014,** *47* (17), 5942-5951.

(21) Trinh, T. T.; Laure, C.; Lutz, J. F. Synthesis of Monodisperse Sequence-Defined Polymers Using Protecting-Group-Free Iterative Strategies. *Macromol. Chem. Phys.* **2015,** *216* (14), 1498-1506.

(22) Barnes, J. C.; Ehrlich, D. J. C.; Gao, A. X.; Leibfarth, F. A.; Jiang, Y. V.; Zhou, E.; Jamison, T. F.; Johnson, J. A. Iterative exponential growth of stereo- and sequence-controlled polymers. *Nat. Chem.* **2015,** *7* (10), 810-815.

(23) Jiang, Y.; Golder, M. R.; Nguyen, H. V. T.; Wang, Y. F.; Zhong, M. J.; Barnes, J. C.; Ehrlich, D. J. C.; Johnson, J. A. Iterative Exponential Growth Synthesis and Assembly of Uniform Diblock Copolymers. *J. Am. Chem. Soc.* **2016,** *138* (30), 9369-9372.

(24) Binauld, S.; Damiron, D.; Connal, L. A.; Hawker, C. J.; Drockenmuller, E. Precise Synthesis of Molecularly Defined Oligomers and Polymers by Orthogonal Iterative Divergent/Convergent Approaches. *Macromol. Rapid Commun.* **2011,** *32* (2), 147-168.

(25) Leibfarth, F. A.; Johnson, J. A.; Jamison, T. F. Scalable synthesis of sequence-defined, unimolecular macromolecules by Flow-IEG. *P Natl Acad Sci USA* **2015,** *112* (34), 10617-10622.

(26) Merrifield, R. B. Solid Phase Peptide Synthesis .1. Synthesis of a Tetrapeptide. *J. Am. Chem. Soc.* **1963,** *85* (14), 2149-&.

(27) Hill, S. A.; Gerke, C.; Hartmann, L. Recent Developments in Solid-Phase Strategies towards Synthetic, Sequence-Defined Macromolecules. *Chem-Asian J* **2018,** *13* (23), 3611-3622.

(28) Espeel, P.; Carrette, L. L. G.; Bury, K.; Capenberghs, S.; Martins, J. C.; Du Prez, F. E.; Madder, A. Multifunctionalized Sequence-Defined Oligomers from a Single Building Block. *Angew. Chem., Int. Ed.* **2013,** *52* (50), 13261-13264.

(29) Yang, C. J.; Flynn, J. P.; Niu, J. Facile Synthesis of Sequence-Regulated Synthetic Polymers Using Orthogonal SuFEx and CuAAC Click Reactions. *Angew. Chem., Int. Ed.* **2018,** *57* (49), 16194-16199.

(30) Al Ouahabi, A.; Charles, L.; Lutz, J. F. Synthesis of Non-Natural Sequence-Encoded Polymers Using Phosphoramidite Chemistry. *J. Am. Chem. Soc.* **2015,** *137* (16), 5629-5635.

(31) Zuckermann, R. N.; Kerr, J. M.; Kent, S. B. H.; Moos, W. H. Efficient Method for the Preparation of Peptoids [Oligo(N-substituted glycines)] by Submonomer Solid-Phase Synthesis. *J. Am. Chem. Soc.* **1992,** *114* (26), 10646-10647.

(32) In *On the Control of Harmful Anti-Fouling Systems on Ships, 2001*, International Convention on the Control of Harmful Anti-fouling Systems on Ships, 18 October, 2001; International Maritime Organization: 2001.

(33) Hennebert, E.; Becker, P.; Flammang, P., Lessons from Sea Organisms to Produce New Biomedical Adhesives. In *Biomimetic Approaches for Biomaterials Development*, Wiley-VCH Verlag GmbH & Co. KGaA: 2012; pp 273-291.

(34) Myan, F. W. Y.; Walker, J.; Paramor, O. The interaction of marine fouling organisms with topography of varied scale and geometry: a review. *Biointerphases* **2013,** *8*.

(35) Long, C. J.; Finlay, J. A.; Callow, M. E.; Callow, J. A.; Brennan, A. B. Engineered antifouling microtopographies: mapping preferential and inhibitory microenvironments for zoospore attachment. *Biofouling* **2010,** *26* (8), 941-952.

(36) Delcroix, M. F.; Zuyderhoff, E. M.; Genet, M. J.; Dupont-Gillain, C. C. Optimization of cryo-XPS analyses for the study of thin films of a block copolymer (PS-PEO). *Surf. Interface Anal.* **2012,** *44* (2), 175-184.

(37) Lewis, K. B.; Ratner, B. D. Observation of Surface Rearrangement of Polymers Using ESCA. *J. Colloid Interface Sci.* **1993,** *159* (1), 77-85.

(38) Briand, J. F. Marine antifouling laboratory bioassays: an overview of their diversity. *Biofouling* **2009,** *25* (4), 297-311.

(39) Salta, M.; Chambers, L.; Wharton, J.; Wood, R.; Briand, J.-F.; Blache, Y.; Stokes, K., Marine fouling organisms and their use in antifouling bioassays. In *EUROCORR 2009*, 2009; Vol. 6.

(40) Callow, M. E.; Callow, J. A.; Pickett-Heaps, J. D.; Wetherbee, R. Primary adhesion of *Enteromorpha* (Chlorophyta, Ulvales) propagules: Quantitative settlement studies and video microscopy. *J. Phycol.* **1997,** *33* (6), 938-947.

(41) Youngblood, J. P.; Andruzzi, L.; Ober, C. K.; Hexemer, A.; Kramer, E. J.; Callow, J. A.; Finlay, J. A.; Callow, M. E. Coatings based on side-chain ether-linked poly(ethylene glycol) and fluorocarbon polymers for the control of marine biofouling. *Biofouling* **2003,** *19*, 91-98.

(42) Gan, D. J.; Mueller, A.; Wooley, K. L. Amphiphilic and hydrophobic surface patterns generated from hyperbranched fluoropolymer/linear polymer networks: Minimally adhesive coatings via the crosslinking of hyperbranched fluoropolymers. *Journal of Polymer Science Part a-Polymer Chemistry* **2003,** *41* (22), 3531-3540.

(43) Gudipati, C. S.; Finlay, J. A.; Callow, J. A.; Callow, M. E.; Wooley, K. L. The antifouling and fouling-release perfomance of hyperbranched fluoropolymer (HBFP)-poly(ethylene glycol) (PEG) composite coatings evaluated by adsorption of biomacromolecules and the green fouling alga *Ulva*. *Langmuir* **2005,** *21* (7), 3044-3053.

(44) Park, D.; Weinman, C. J.; Finlay, J. A.; Fletcher, B. R.; Paik, M. Y.; Sundaram, H. S.; Dimitriou, M. D.; Sohn, K. E.; Callow, M. E.; Callow, J. A.; Handlin, D. L.; Willis, C. L.; Fischer, D. A.; Kramer, E. J.; Ober, C. K. Amphiphilic Surface Active Triblock Copolymers with Mixed Hydrophobic and Hydrophilic Side Chains for Tuned Marine Fouling-Release Properties. *Langmuir* **2010,** *26* (12), 9772-9781.

(45) Zhou, Z.; Calabrese, D. R.; Taylor, W.; Finlay, J. A.; Callow, M. E.; Callow, J. A.; Fischer, D.; Kramer, E. J.; Ober, C. K. Amphiphilic triblock copolymers with PEGylated

hydrocarbon structures as environmentally friendly marine antifouling and fouling-release coatings. *Biofouling* **2014,** *30* (5), 589-604.

(46) Stafslien, S. J.; Christianson, D.; Daniels, J.; VanderWal, L.; Chernykh, A.; Chisholm, B. J. Combinatorial materials research applied to the development of new surface coatings XVI: fouling-release properties of amphiphilic polysiloxane coatings. *Biofouling* **2015,** *31* (2), 135-149.

(47) Finlay, J. A.; Krishnan, S.; Callow, M. E.; Callow, J. A.; Dong, R.; Asgill, N.; Wong, K.; Kramer, E. J.; Ober, C. K. Settlement of *Ulva* zoospores on patterned fluorinated and PEGylated monolayer surfaces. *Langmuir* **2008,** *24* (2), 503-510.

(48) van Zoelen, W.; Buss, H. G.; Ellebracht, N. C.; Lynd, N. A.; Fischer, D. A.; Finlay, J.; Hill, S.; Callow, M. E.; Callow, J. A.; Kramer, E. J.; Zuckermann, R. N.; Segalman, R. A. Sequence of Hydrophobic and Hydrophilic Residues in Amphiphilic Polymer Coatings Affects Surface Structure and Marine Antifouling/Fouling Release Properties. *ACS Macro Lett.* **2014,** *3* (4), 364-368.

(49) Calabrese, D. R.; Wenning, B.; Finlay, J. A.; Callow, M. E.; Callow, J. A.; Fischer, D.; Ober, C. K. Amphiphilic oligopeptides grafted to PDMS-based diblock copolymers for use in antifouling and fouling release coatings. *Polym. Adv. Technol.* **2015,** *26* (7), 829-836.

(50) Sanii, B.; Kudirka, R.; Cho, A.; Venkateswaran, N.; Olivier, G. K.; Olson, A. M.; Tran, H.; Harada, R. M.; Tan, L.; Zuckermann, R. N. Shaken, Not Stirred: Collapsing a Peptoid Monolayer To Produce Free-Floating, Stable Nanosheets. *J. Am. Chem. Soc.* **2011,** *133* (51), 20808-20815.

(51) Vollrath, S. B. L.; Hu, C. H.; Brase, S.; Kirshenbaum, K. Peptoid nanotubes: an oligomer macrocycle that reversibly sequesters water via single-crystal-to-single-crystal transformations. *Chem. Commun.* **2013,** *49* (23), 2317-2319.

(52) Sun, J.; Jiang, X.; Lund, R.; Downing, K. H.; Balsara, N. P.; Zuckermann, R. N. Self-assembly of crystalline nanotubes from monodisperse amphiphilic diblock copolypeptoid tiles. *P Natl Acad Sci USA* **2016,** *113* (15), 3954-3959.

(53) Armand, P.; Kirshenbaum, K.; Falicov, A.; Dunbrack, R. L.; Dill, K. A.; Zuckermann, R. N.; Cohen, F. E. Chiral N-substituted glycines can form stable helical conformations. *Folding Des.* **1997,** *2* (6), 369-375.

(54) Armand, P.; Kirshenbaum, K.; Goldsmith, R. A.; Farr-Jones, S.; Barron, A. E.; Truong, K. T. V.; Dill, K. A.; Mierke, D. F.; Cohen, F. E.; Zuckermann, R. N.; Bradley, E. K. NMR

determination of the major solution conformation of a peptoid pentamer with chiral side chains. *P Natl Acad Sci USA* **1998,** *95* (8), 4309-4314.

(55) Wu, C. W.; Sanborn, T. J.; Huang, K.; Zuckermann, R. N.; Barron, A. E. Peptoid oligomers with alpha-chiral, aromatic side chains: Sequence requirements for the formation of stable peptoid helices. *J. Am. Chem. Soc.* **2001,** *123* (28), 6778-6784.

(56) Wu, C. W.; Sanborn, T. J.; Zuckermann, R. N.; Barron, A. E. Peptoid oligomers with alpha-chiral, aromatic side chains: Effects of chain length on secondary structure. *J. Am. Chem. Soc.* **2001,** *123* (13), 2958-2963.

(57) Wu, C. W.; Kirshenbaum, K.; Sanborn, T. J.; Patch, J. A.; Huang, K.; Dill, K. A.; Zuckermann, R. N.; Barron, A. E. Structural and spectroscopic studies of peptoid oligomers with alpha-chiral aliphatic side chains. *J. Am. Chem. Soc.* **2003,** *125* (44), 13525-13530.

(58) Gorske, B. C.; Mumford, E. M.; Gerrity, C. G.; Ko, I. A Peptoid Square Helix via Synergistic Control of Backbone Dihedral Angles. *J. Am. Chem. Soc.* **2017,** *139* (24), 8070-8073.

(59) Murnen, H. K.; Rosales, A. M.; Jaworsk, J. N.; Segalman, R. A.; Zuckermann, R. N. Hierarchical Self-Assembly of a Biomimetic Diblock Copolypeptoid into Homochiral Superhelices. *J. Am. Chem. Soc.* **2010,** *132* (45), 16112-16119.

(60) Kirshenbaum, K.; Barron, A. E.; Goldsmith, R. A.; Armand, P.; Bradley, E. K.; Truong, K. T. V.; Dill, K. A.; Cohen, F. E.; Zuckermann, R. N. Sequence-specific polypeptoids: A diverse family of heteropolymers with stable secondary structure. *P Natl Acad Sci USA* **1998,** *95* (8), 4303-4308.

(61) Huang, K.; Wu, C. W.; Sanborn, T. J.; Patch, J. A.; Kirshenbaum, K.; Zuckermann, R. N.; Barron, A. E.; Radhakrishnan, I. A threaded loop conformation adopted by a family of peptoid nonamers. *J. Am. Chem. Soc.* **2006,** *128* (5), 1733-1738.

(62) Renfrew, P. D.; Crayen, T. W.; Butterfoss, G. L.; Kirshenbaum, K.; Bonneau, R. A Rotamer Library to Enable Modeling and Design of Peptoid Foldamers. *J. Am. Chem. Soc.* **2014,** *136* (24), 8772-8782.

(63) Block Copolymers. In *Journal of Polymer Science, Part C, POLYMER SYMPOSIA*, Jioacanin, J.; Holden, G.; Tschoegl, N. W., Eds. Interscience Publishers, a Division of John Wiley & Sons, Inc. : 1969; Vol. 26.

(64) Leibler, L. Theory of Microphase Separation in Block Copolymers. *Macromolecules* **1980,** *13* (6), 1602-1617.

(65) Fredrickson, G. H.; Helfand, E. Fluctuation Effects in the Theory of Microphase Separation in Block Copolymers. *J. Chem. Phys.* **1987,** *87* (1), 697-705.

(66) Cochran, E. W.; Garcia-Cervera, C. J.; Fredrickson, G. H. Stability of the gyroid phase in diblock copolymers at strong segregation. *Macromolecules* **2006,** *39* (7), 2449-2451.

(67) Kim, J.; Mok, M. M.; Sandoval, R. W.; Woo, D. J.; Torkelson, J. M. Uniquely broad glass transition temperatures of gradient copolymers relative to random and block copolymers containing repulsive comonomers. *Macromolecules* **2006,** *39* (18), 6152-6160.

(68) Wong, C. L. H.; Kim, J.; Torkelson, J. M. Breadth of glass transition temperature in styrene/acrylic acid block, random, and gradient copolymers: Unusual sequence distribution effects. *J. Polym. Sci. Pol. Phys.* **2007,** *45* (20), 2842-2849.

(69) Kim, J.; Gray, M. K.; Zhou, H. Y.; Nguyen, S. T.; Torkelson, J. M. Polymer blend compatibilization by gradient copolymer addition during melt processing: Stabilization of dispersed phase to static coarsening. *Macromolecules* **2005,** *38* (4), 1037-1040.

(70) Kim, J.; Sandoval, R. W.; Dettmer, C. M.; Nguyen, S. T.; Torkelson, J. M. Compatibilized polymer blends with nanoscale or sub-micron dispersed phases achieved by hydrogen-bonding effects: Block copolymer vs blocky gradient copolymer addition. *Polymer* **2008,** *49* (11), 2686-2697.

(71) Mok, M. M.; Pujari, S.; Burghardt, W. R.; Dettmer, C. M.; Nguyen, S. T.; Ellison, C. J.; Torkelson, J. M. Microphase separation and shear alignment of gradient copolymers: Melt rheology and small-angle X-ray scattering analysis. *Macromolecules* **2008,** *41* (15), 5818-5829.

(72) Mok, M. M.; Ellison, C. J.; Torkelson, J. M. Effect of Gradient Sequencing on Copolymer Order-Disorder Transitions: Phase Behavior of Styrene/n-Butyl Acrylate Block and Gradient Copolymers. *Macromolecules* **2011,** *44* (15), 6220-6226.

(73) Mok, M. M.; Torkelson, J. M. Imaging of phase segregation in gradient copolymers: Island and hole surface topography. *J. Polym. Sci. Pol. Phys.* **2012,** *50* (3), 189-197.

(74) Jouenne, S.; Gonzalez-Leon, J. A.; Ruzette, A.-V.; Lodefier, P.; Tence-Girault, S.; Leibler, L. Styrene/butadiene gradient block copolymers: Molecular and mesoscopic structures. *Macromolecules* **2007,** *40* (7), 2432-2442.

(75) Milonaki, Y.; Kaditi, E.; Pispas, S.; Demetzos, C. Amphiphilic gradient copolymers of 2-methyl- and 2-phenyl-2-oxazoline: self-organization in aqueous media and drug

encapsulation. *Journal of Polymer Science Part a-Polymer Chemistry* **2012,** *50* (6), 1226-1237.

(76) Beginn, U. Gradient copolymers. *Colloid. Polym. Sci.* **2008,** *286* (13), 1465-1474.

(77) Pakula, T.; Matyjaszewski, K. Copolymers with controlled distribution of comonomers along the chain .1. Structure, thermodynamics and dynamic properties of gradient copolymers. Computer simulation. *Macromol. Theory Simul.* **1996,** *5* (5), 987-1006.

(78) Aksimentiev, A.; Holyst, R. Phase behavior of gradient copolymers. *J. Chem. Phys.* **1999,** *111* (5), 2329-2339.

(79) Lefebvre, M. D.; de la Cruz, M. O.; Shull, K. R. Phase segregation in gradient copolymer melts. *Macromolecules* **2004,** *37* (3), 1118-1123.

(80) Jiang, R.; Jin, Q. H.; Li, B. H.; Ding, D. T.; Wickham, R. A.; Shi, A. C. Phase behavior of gradient copolymers. *Macromolecules* **2008,** *41* (14), 5457-5465.

(81) Tito, N. B.; Milner, S. T.; Lipson, J. E. G. Self-Assembly of Lamellar Microphases in Linear Gradient Copolymer Melts. *Macromolecules* **2010,** *43* (24), 10612-10620.

(82) Ganesan, V.; Kumar, N. A.; Pryamitsyn, V. Blockiness and Sequence Polydispersity Effects on the Phase Behavior and Interfacial Properties of Gradient Copolymers. *Macromolecules* **2012,** *45* (15), 6281-6297.

(83) Luo, M.; Browns, J. R.; Remy, R. A.; Scott, D. M.; Mackay, M. E.; Halv, L. M.; Epps, T. H. Determination of Interfacial Mixing in Tapered Block Polymer Thin Films: Experimental and Theoretical Investigations. *Macromolecules* **2016,** *49* (14), 5213-5222.

(84) Mastroianni, S. E.; Epps, T. H., III Interfacial Manipulations: Controlling Nanoscale Assembly in Bulk, Thin Film, and Solution Block Copolymer Systems. *Langmuir* **2013,** *29* (12), 3864-3878.

(85) Seo, Y.; Brown, J. R.; Hall, L. M. Effect of Tapering on Morphology and Interfacial Behavior of Diblock Copolymers from Molecular Dynamics Simulations. *Macromolecules* **2015,** *48* (14), 4974-4982.

(86) Brown, J. R.; Seo, Y. M.; Sides, S. W.; Hall, L. M. Unique Phase Behavior of Inverse Tapered Block Copolymers: Self Consistent Field Theory and Molecular Dynamics Simulations. *Macromolecules* **2017,** *50* (14), 5619-5626.

(87) Tanaka, K.; Takahara, A.; Kajiyama, T. Effect of polydispersity on surface molecular motion of polystyrene films. *Macromolecules* **1997,** *30* (21), 6626-6632.

(88) Lynd, N. A.; Meuler, A. J.; Hillmyer, M. A. Polydispersity and block copolymer self-assembly. *Prog. Polym. Sci.* **2008,** *33* (9), 875-893.

(89) Cooke, D. M.; Shi, A. C. Effects of polydispersity on phase behavior of diblock copolymers. *Macromolecules* **2006,** *39* (19), 6661-6671.

(90) Schröder-Turk, G. E.; Fogden, A.; Hyde, S. T. Local v/a variations as a measure of structural packing frustration in bicontinuous mesophases, and geometric arguments for an alternating Im(3-bar)m (I-WP) phase in block-copolymers with polydispersity. *Eur Phys J B* **2007,** *59* (1), 115-126.

(91) Meuler, A. J.; Ellison, C. J.; Hillmyer, M. A.; Bates, F. S. Polydispersity-induced stabilization of the core-shell gyroid. *Macromolecules* **2008,** *41* (17), 6272-6275.

(92) Widin, J. M.; Schmitt, A. K.; Schmitt, A. L.; Im, K.; Mahanthappa, M. K. Unexpected Consequences of Block Polydispersity on the Self-Assembly of ABA Triblock Copolymers. *J. Am. Chem. Soc.* **2012,** *134* (8), 3834-3844.

(93) Lynd, N. A.; Hillmyer, M. A. Influence of polydispersity on the self-assembly of diblock copolymers. *Macromolecules* **2005,** *38* (21), 8803-8810.

(94) Oschmann, B.; Lawrence, J.; Schulze, M. W.; Ren, J. M.; Anastasaki, A.; Luo, Y.; Nothling, M. D.; Pester, C. W.; Delaney, K. T.; Connal, L. A.; McGrath, A. J.; Clark, P. G.; Bates, C. M.; Hawker, C. J. Effects of Tailored Dispersity on the Self-Assembly of Dimethylsiloxane–Methyl Methacrylate Block Co-Oligomers. *ACS Macro Lett.* **2017,** *6* (7), 668-673.

(95) Dai, K. H.; Kramer, E. J. Molecular-Weight Dependence of Diblock Copolymer Segregation at a Polymer/Polymer Interface. *J. Polym. Sci. Pol. Phys.* **1994,** *32* (11), 1943-1950.

(96) Winey, K. I.; Thomas, E. L.; Fetters, L. J. Swelling a Lamellar Diblock Copolymer with Homopolymer - Influences of Homopolymer Concentration and Molecular-Weight. *Macromolecules* **1991,** *24* (23), 6182-6188.

(97) Shull, K. R.; Winey, K. I. Homopolymer Distributions in Lamellar Copolymer Homopolymer Blends. *Macromolecules* **1992,** *25* (10), 2637-2644.

(98) Lawrence, J.; Lee, S. H.; Abdilla, A.; Nothling, M. D.; Ren, J. M.; Knight, A. S.; Fleischmann, C.; Li, Y. L.; Abrams, A. S.; Schmidt, B. V. K. J.; Hawker, M. C.; Connal, L. A.; McGrath, A. J.; Clark, P. G.; Gutekunst, W. R.; Hawker, C. J. A Versatile and Scalable Strategy to Discrete Oligomers. *J. Am. Chem. Soc.* **2016,** *138* (19), 6306-6310.

Part I: Non-Toxic Antifouling Coatings

Chapter 2

Polymer Backbone and Sequence in Marine Antifouling Coatings

Poly(dimethyl siloxane) (PDMS)- and poly(ethylene oxide) (PEO)-based block copolymer coatings functionalized with amphiphilic, surface-active, and sequence-controlled oligomer side chains were studied to directly compare the effects of hydrophilicity, hydrogen bonding, and monomer sequence on antifouling performance. Utilizing a modular coating architecture, structurally similar copolymers were used to make direct and meaningful comparisons. Amphiphilic character was imparted with non-natural oligopeptide and oligopeptoid pendant chains made from oligo-PEO and surface-segregating fluoroalkyl monomer units. Surface analysis revealed rearrangement for all surfaces when moved from vacuum to wet environments. X-ray photoelectron spectroscopy (XPS) spectra indicated that the polymer backbone and oligomer interactions play key roles in the surface presentation. Biofouling assays using the macroalga *Ulva linza* showed that the presence of peptoid side chains facilitated the removal of sporelings on the PDMS block copolymer, with removal matching that of a PDMS elastomer standard. The lack of a hydrogen bond donor in the peptoid backbone likely contributed to the lower adhesion

strength of sporelings to these surfaces. Both the initial attachment and adhesion strength of the diatom *Navicula incerta* were lower on the coatings based on PEO than on those based on PDMS. Surprisingly, on the PEO coating bearing the blocky peptoid sequence, initial attachment of *N. incerta* showed no measurable cell density.

This chapter was reproduced in part with permission from: Patterson, A. L.; Wenning, B.; Rizis, G.; Calabrese, D. R.; Finlay, J. A.; Franco, S. C.; Zuckermann, R. N.; Clare, A. S.; Kramer, E. J.; Ober, C. K.; Segalman, R. A. Role of Backbone Chemistry and Monomer Sequence in Amphiphilic Oligopeptide- and Oligopeptoid-Functionalized PDMS- and PEO-Based Block Copolymers for Marine Antifouling and Fouling Release Coatings. *Macromolecules*, 2017, 50, 7, 2656–2667. Copyright 2017 American Chemical Society.

2.1 Introduction

Marine fouling is caused by the settlement and adhesion of a wide range of marine organisms on surfaces in the marine environment, and begins within minutes of immersion with early colonizers such as bacteria, diatoms, and algal spores.[1] When surfaces such as ships' hulls or other manufactured marine structures become fouled, the costs of operation and maintenance are significantly increased.[2,3] Frequent cleaning adds cost and lowers operational time, and the higher drag penalties induced by a build-up of fouling organisms cause efficiency loss for marine vessels, resulting in increased fuel consumption and greenhouse gas production (representing an extra $180–260M per year for the U.S. Navy alone).[2,4] Paints that contain biocidal compounds have proven successful in reducing biofouling and the associated maintenance and efficiency penalties,[5] however some of these compounds are very persistent in marine environments and have negative effects on non-target organisms.[6,7] Environmental concerns have led to increased regulation of these biocidal compounds,[8] creating a demand for non-toxic alternatives.

Effective coatings should have both antifouling and fouling release properties (both reduce initial settlement of marine organisms, and disrupt or weaken adhesion of those organisms that do attach). Many strategies have been studied extensively, including control of surface topology,[9-11] as well as chemically modifying surfaces using bioactive molecules,[12-17] zwitterionic groups,[18-22] fluoroalkyl groups,[23,24] and fluoroether networks.[25,26] Particularly successful coatings have been produced using poly(ethylene oxide) (PEO) polymers and oligomers[27-31] as well as polydimethylsiloxane (PDMS).[32-36] Hydrophilic PEO-based block copolymers have shown excellent protein adsorption resistance[37-39] when compared to hydrophobic materials such as PDMS, while PDMS-based materials exhibit high fouling release due to low elastic modulus[40-45] and low surface energy, as described by the Baier curve.[46-48]

The incorporation of both hydrophilic and hydrophobic components into amphiphilic block copolymers has been shown to produce highly effective antifouling and fouling release coatings.[30,35,37,49-55] These surfaces incorporate the protein resistance of hydrophilic materials such as PEO with the low surface energy and high fouling release of hydrophobic materials containing siloxane, fluoroalkyl, or alkyl groups. Because of the chemical complexity of these multi-component materials, the surfaces are environmentally responsive, exhibiting chemical reconstruction underwater.[55] An effective strategy for incorporating multiple chemical components into a single coating is attaching side chains of various chemistries onto a polymeric backbone. A wide range of amphiphilic side chains have been designed and attached to a variety of polymer backbones to impart amphiphilicity and improved performance.[31,36,49,52,54,56,57] An advantage to incorporating amphiphilicity via side chains is that structurally similar polymers can be produced, but with modular components that facilitate direct comparisons.

Another advantage to polymer architectures with modular amphiphilic side chains is that the length scale of amphiphilicity can be systematically explored. For chemically heterogeneous coatings, the length scale between different chemical functionalities at the surface is important for antifouling properties, with a critical length scale for low *U. linza* zoospore settlement being on the micron scale.[58] Furthermore, subtle changes in the monomer sequence and spatial distribution of functionalities can have large effects on the chemical surface presentation.[31,54,59,60] These effects present an opportunity to study how variations in sequence and composition at the molecular length scale can be used to optimize antifouling and fouling release performance, using components that are already in common use.

Surface-active block copolymers (SABCs) have been made with pendant oligomers that are sequence-defined and surface-segregating, produced using peptide and peptoid chemistry, and allow modular incorporation of amphiphilic sequences that can tune the chemical composition of the surface and spatial proximity of functional groups down to the monomer level. Peptoids are peptide isomers, produced via a submonomer approach to solid phase synthesis, in which the residue functionalities are incorporated simply as primary amines and result in an *N*-substituted glycine repeat unit.[61] Previous work has studied oligopeptides on PDMS block copolymers[36] and oligopeptoids on PEO block copolymers,[31,62,63] all utilizing amphiphilic, surface-active, sequence-defined structures to modify the performance of a polymeric backbone material. In one study with oligopeptoid sequences, fluoroalkyl groups were placed at different positions within the sequence, resulting in dramatically different surface and bulk properties.[62] At least one fluoroalkyl group was necessary to surface segregate the peptoid within the PEO coating, and positioning fluoroalkyl groups farthest from the block copolymer attachment point produced coatings with the highest surface presentation of peptoid groups. In applying

similar materials in antifouling coatings, strong trends were seen in *U. linza* settlement with peptoid sequence, and in removal with peptoid composition and length.[31] Work with oligopeptides has shown that using very long PEO-like and alkyl side groups is necessary to enhance antifouling and fouling release performance.[36] The long side groups, however, eliminate the effects of sequence on the surface properties of the final coatings. Until now, these materials have been studied independently with structures that make direct comparisons difficult.

In this study, structurally similar PEO- and PDMS-based triblock copolymers were synthesized and functionalized with oligopeptide and oligopeptoid side chains (Figure 2.1) to determine how polymer chemistry, oligomer backbone chemistry, and molecular-scale amphiphilicity independently contribute to the antifouling and fouling release performance of a coating. By making sequence-defined side chains containing nearly identical subunits, the effects of the backbone chemistry within the side chains could be compared directly. The primary difference between the two is that the peptide backbone is able to both donate and accept hydrogen bonds, whereas the peptoid with a nitrogen-linked functional group has no hydrogen bond donating groups. Since the adhesives of many fouling organisms contain a protein component, interactions between the side chains in the coating with marine bioadhesives could be affected by the presence of hydrogen bonding capabilities. The oligomers contain equal numbers of either PEO-like or fluoroalkyl groups in two different sequences. The fluoroalkyl groups were used not only as the hydrophobic components of the amphiphilic coating, but also as surface-segregating units that define the surface chemistry. Each sequence contained six monomers, with three PEO-like and three fluoroalkyl side chains, and a terminal unit containing a thiol to allow the oligomer to be functionalized onto the block copolymer via thiol–ene "click" chemistry. The sequences studied include one that alternates the hydrophilic and hydrophobic units to produce the smallest length scale of

amphiphilicity ("alternating") and a second with these groups in segments of three units of each type ("blocky").

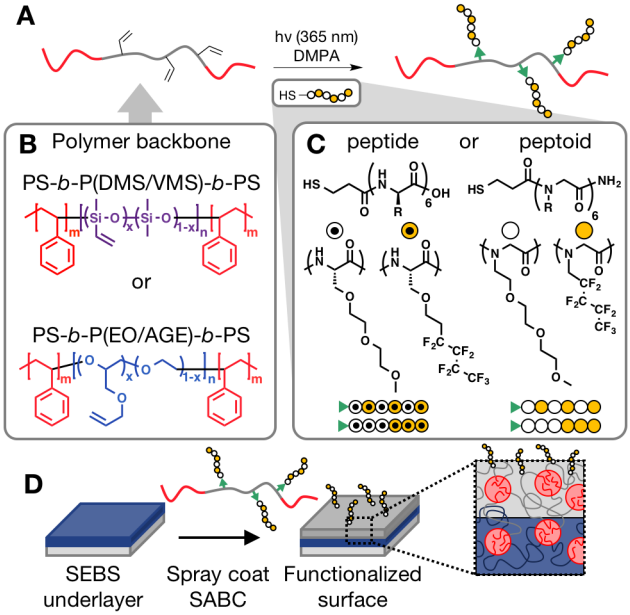

Figure 2.1 Materials for comparison

A) Functional oligomers are clicked onto triblock copolymer scaffolds for surface presentation. B) Polymer backbones: PS-*b*-P(EO/AGE)-*b*-PS and PS-*b*-P(DMS-VMS)-*b*-PS, each with m = 5–7 kDa PS end blocks and n = ~70 kDa midblocks containing x = 2.5 mol% vinyl groups. C) Oligomer structures: peptide and peptoid, each with alternating and blocky sequences. D) Functionalized surface-active block copolymers (SABCs) are spray-coated onto an SEBS underlayer and annealed to form the final surface.

2.2 Experimental methods

2.2.1 Materials

All materials were purchased from Sigma-Aldrich and used as received, unless otherwise noted. Polystyrene-*block*-poly(ethylene-*ran*-butylene)-*block*-polystyrene (SEBS, MD6945) and SEBS grafted with maleic anhydride (MA-SEBS, FG1901X) were generously provided by Kraton Polymers. Wang resin (100–200 mesh) was purchased from Novabiochem. Dimethylformamide (DMF), diisopropylcarbodiimide, trifluoroacetic acid, and low-loaded (0.20 mmol/g) Rink amide MBHA resin were purchased from Protein Technologies, Inc. 1H,1H-perluoropentylamine was purchased from Manchester Organics.

2.2.2 Synthesis of siloxane block copolymer

Siloxane triblock copolymer (polystyrene-*b*-poly(dimethyl siloxane-*co*-vinylmethylsiloxane)-*b*-polystyrene, PS-*b*-P(DMS/VMS)-*b*-PS) was synthesized as previously described.[36] In short, dried styrene was polymerized anionically in benzene with the use of *sec*-butyl lithium as an initiator (Scheme 2.1). An aliquot was removed for analysis by GPC. The active chain ends were extended with the addition of purified hexamethylcyclotrisiloxane (D3) monomer to initiate siloxane polymerization. Then, the appropriate amount of 1,3,5-trivinyl-1,3,5-trimethylcyclotrisiloxane (V3) was added in THF via syringe pump over 48 hours and allowed to react for an additional 48 hours. Samples were analyzed via GPC and ^{1}H-NMR to monitor the reaction. At the desired conversion, the active chain ends were coupled with dichlorodimethylsilane in THF, and stirred for 16 hours before additional coupling agent was added via syringe pump over 24 hours to ensure complete coupling. The final triblock was precipitated in methanol, filtered, and dried. The polymer was characterized by GPC to determine final molecular weight, and by ^{1}H-NMR to determine vinyl content.

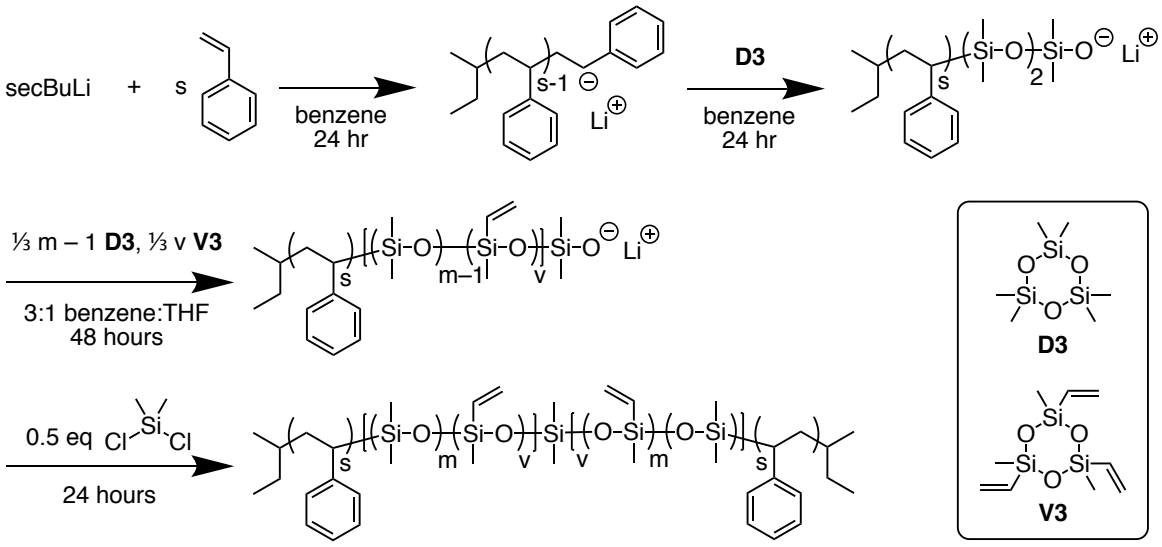

Scheme 2.1 Anionic polymerization of PS-*b*-P(DMS-*stat*-VMS)-*b*-PS

2.2.3 Synthesis of ethylene oxide block copolymer

The P(EO-*co*-AGE) midblock was synthesized as described previously[30] and in appendix **Error! Reference source not found.**. In short, ethylene glycol was used as an initiator for t he anionic co-polymerization of ethylene oxide and allyl glycidyl ether in THF. The midblock was terminated with isopropyl alcohol to produce terminal alcohol groups. The molecular weight of the midblock was determined via GPC and vinyl content was determined by ^{1}H-NMR. These groups were converted to macroinitiators with N-tert-butyl-O-[1-[4-(chloromethyl)phenyl]ethyl]-N-(2-methyl-1-phynylpropyl)hydroxylamine (chloromethyl-TIPNO) in the presence of sodium hydride, and then used to grow polystyrene endblocks via nitroxide-mediated radical polymerization. The triblock was washed with hexanes to remove auto-polymerized polystyrene homopolymer, and analyzed by GPC and ^{1}H-NMR to determine polystyrene endblock molecular weight.

2.2.4 Synthesis of non-natural amino acids for oligopeptide side chains

First, organosulfonates were prepared by reacting 3,3,4,4,5,5,6,6,6-nonafluoro 1-hexanol or diethylene glycol monomethyl ether with methanesulfonyl chloride under nitrogen in THF for 18 hours (Scheme 2.2). Excess methanesulfonyl chloride was removed by passing the reaction solution through a plug of silica gel, and the solvent was removed by rotary evaporation.

Non-natural amino acids were synthesized by the nucleophilic displacement of the desired mesylate-bearing side chains by serine-Fmoc in acetonitrile and diisopropylethylamine (DIEA) (Scheme 2.2). The reaction was refluxed under nitrogen for 24 hours and quenched with DI water. The functionalized amino acids were extracted into ethyl acetate, dried over sodium sulfate, and isolated by removal of solvent by rotary evaporation.

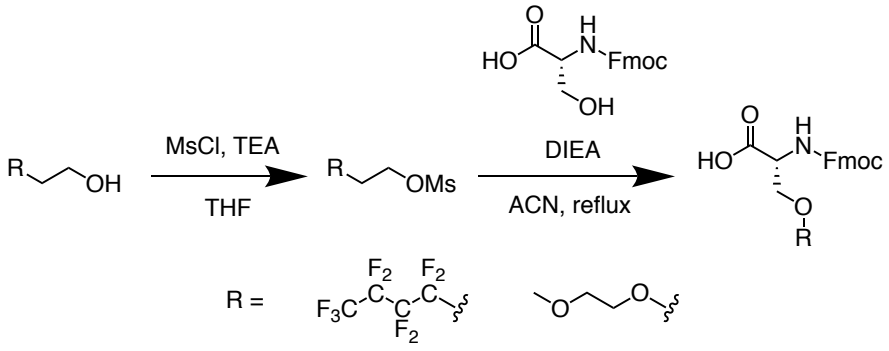

Scheme 2.2 Synthesis of non-natural amino acids

2.2.5 Synthesis of oligopeptides

The synthesis of oligopeptides via solid-phase synthesis was carried out using published procedures on Wang resin.[64] Two sequences of hexamer oligopeptides were made, one with three fluorinated amino acids followed by three triethylene glycol amino acids and the other alternating fluorinated and triethylene glycol amino acids. These will be referred to as "blocky" and "alternating" oligopeptides, respectively. The N-terminus was capped with 3-mercaptopropionic acid to yield a thiol-terminated oligomer to be attached to a polymer backbone via thiol–ene "click" chemistry. To prevent disulfides from forming, 1.5 equivalents of triethyl silane was added as a reducing agent.

2.2.6 Synthesis of 2-[2-(2-methoxyethoxy)ethoxy]ethanamine for oligopeptoids

2-[2-(2-methoxyethoxy)ethoxy] ethanamine submonomer was synthesized via published procedures.[65] In short, triethylene glycol monomethyl ether was converted to a mesylate and isolated following procedures outlined above. The mesylate was combined with sodium azide in DMF and stirred at 60 °C for 24 hours. The mixture was diluted with excess DI water (taking care to avoid acidic pHs to prevent the formation of toxic and explosive hydrazoic acid), and the azide product was extracted into diethyl ether, washed

with water, dried over magnesium sulfate, and concentrated under vacuum. The azide was then reduced with triphenylphosphine in THF under nitrogen overnight. The solids were removed by filtration, and the solution washed with toluene and dichloromethane before concentrating in vacuo.

2.2.7 Synthesis of oligopeptoids

The synthesis of oligopeptoids via solid-phase submonomer synthesis was carried out using published procedures using Rink amide MBHA resin.[61] Peptoids were redissolved in 50:50 acetonitrile/water and washed with hexanes before lyophilizing to yield isolated oligomers. Two sequences of hexamer oligopeptoids were made, one with the incorporation of three 1H,1H-perfluoropentylamine submonomers followed by three 2-[2-(2-methoxyethoxy)ethoxy]ethanamine submonomers and the other with alternating fluorinated and triethylene glycol submonomers. These will be referred to as "blocky" and "alternating" oligopeptoids, respectively. The N-terminus was capped with 3-mercaptopropionic acid to yield a thiol-terminated oligomer to be attached to a polymer backbone via thiol–ene "click" chemistry.

2.2.8 Thiol–ene "click" of oligomers to polymer backbones

Thiol-terminated oligopeptide and oligopeptoid sequences were attached to the siloxane- and PEO-based block copolymers using thiol–ene "click" chemistry. For all cases, 800 mg of triblock copolymer was dissolved in 3 mL of dichloromethane with 1 g of peptide or peptoid and 26 mg of 2,2-dimethoxy-2-phenyl acetophenone (DMPA). The reaction solution was first purged with nitrogen, and then irradiated with 365 nm UV light from a handheld UV lamp for 1 hour. The functionalized PDMS-based copolymers were precipitated into methanol, filtered, and dried. The functionalized PEO-based copolymers were thoroughly dialyzed in a solution of 15% water in ethanol, and dried *in vacuo*. Click

completion was determined by ^{1}H-NMR analysis. A total of eight samples were produced, based on four peptide and peptoid side chains, including two sequences, attached to two separate block copolymer backbones.

2.2.9 Surface preparation

Coated glass slides for biofouling assays were prepared as previously reported using SEBS materials.[66] Briefly, standard microscope glass slides (3 × 1 in.) were treated with freshly prepared piranha solution (5:3 v/v, mixture of concentrated H_2SO_4 and 30 wt% H_2O_2 solution) overnight, and then sequentially rinsed with distilled water and anhydrous ethanol. The dried clean glass slides were then immersed in 3.5% 3-(aminopropyl)trimethoxysilane solution (v/v in anhydrous ethanol) at room temperature overnight, followed by washing with water and anhydrous ethanol. The aminosilane treated glass slides were cured at 120 °C under reduced pressure for 2 hours before slowly cooling to room temperature. The first layer coating was then immediately applied by spin coating with SEBS/MA-SEBS solution (7% w/v SEBS and 2% w/v MA-SEBS) in toluene (2500 rpm, 30 sec), followed by curing at 120 °C in a vacuum oven at reduced pressure for 12 hours, allowing the maleic anhydride groups on the polymer backbone react with amine groups on the glass surfaces, therefore improving the bonding of the coating to the glass. The second layer was spin coated with SEBS solution (12 % w/v SEBS solution) three times (2500 rpm, 30 sec), followed by annealing at 120 °C in a vacuum oven at reduced pressure for 12 hours to give a base layer thickness about 1 mm. The functionalized PDMS- and PEO-based SABCs were dissolved in 19:1 dichloromethane/toluene and spray coated onto the surface using a Badger model 250 airbrush, annealed in a vacuum oven at reduced pressure at 60 °C for 6 hours, then 120 °C for 24 hours to ensure complete removal of solvents.

2.2.10 ^{1}H NMR

^{1}H NMR spectra were recorded using a Varian Gemini 400 MHz spectrometer (Cornell) and a Varian VNMRS 600 MHz spectrometer (UCSB) in $CDCl_3$ solution.

2.2.11 Gel permeation chromatography (GPC)

GPC was performed on a Waters Ambient Temperature GPC with a Waters 1515 Isocratic HPLC pump (Cornell) and a Waters e2695 GPC (UCSB), both using THF as an eluent. The instruments are equipped with both a Waters 2414 differential refractive index detector as well as a Waters 2489 UV-Vis detector (Cornell) and a Waters 2998 PDA detector (UCSB). Both instruments were calibrated using polystyrene standards.

2.2.12 Water contact angle measurements

Water contact angle measurements were taken using an NRL contact angle goniometer (ramé-hart model 100-00) using the captive bubble method previously described.[67,68] Briefly, the surfaces were immersed upside-down in deionized water at room temperature, and an air bubble was trapped against the immersed surface by releasing it from the tip of a 22 gauge stainless steel needle. For each coating, the water contact angle (measured in the external liquid phase) was measured three times from three separate bubbles at different locations on the surface and averaged. These measurements were taken immediately after immersion in water over a total of 7 days, with measurements taken every 24 hours to study the reconstruction of the surfaces upon immersion in water. Because the captive bubble method is performed *in situ*, the measurements reflect the operating condition of full immersion.

2.2.13 X-ray photoelectron spectroscopy (XPS)

Measurements were performed on a Kratos Axis Ultra Spectrometer (Kratos Analytical, Manchester, UK) with a monochromatic aluminum K_α X-ray source (1486.6 eV) operating at

225 W under a vacuum of 10^{-8} Torr. Charge compensation was carried out by injection of low-energy electrons into the magnetic lens of the electron spectrometer. High resolution spectra were recorded at 20 eV pass energy at intervals of 0.05 eV. Survey spectra were recorded at 80 eV pass energy at intervals of 0.5 eV. Samples were measured as-annealed, as well as after at least 11 days of undisturbed soaking in Millipore deionized water, after which they were wicked dry of macroscopic water droplets and immediately analyzed. Spectra were calibrated to the major peak (285.00 eV for the aliphatic peak of PS, 286.45 eV for PEO, 284.38 eV for PDMS),[69] the background was subtracted, and peaks were fit using CasaXPS 2.3.16 software.

2.2.14 Settlement, growth, and removal bioassays of Ulva linza

For *Ulva linza* assays, nine slides were equilibrated in 0.22 gm-filtered artificial seawater (ASW, Tropic Marin) for 72 hours before beginning the assays. Zoospores were released into ASW from mature plants using a standard method[70] then suspended in a solution of filtered ASW at a concentration of 6.66×10^5 mL^{-1}. Coated glass slides were placed in the wells of quadriPERM dishes and 10 mL of the spore suspension added to each well. Spores were allowed to settle in complete darkness for 45 minutes. After this time period, all slides were washed gently using filtered ASW. Three of the slides for each material were immediately fixed using 2.5% glutaraldehyde in seawater to determine the spore settlement densities. These slides were analyzed under a Zeiss Axioscop 2 fluorescence microscope using AxioVision 4 image analysis software.[71] Counting was performed using an automated program for 30 fields of view of 0.15 mm^2 per slide.

The remaining six slides were immersed in a nutrient supplemented ASW[72] and cultured in an illuminated incubator at 18 °C for seven days. The biomass on the surfaces was measured indirectly by fluorescence of the chlorophyll contained in the plants using a Tecan fluorescence plate reader (GENios Plus), the output recorded in relative fluorescence units

(RFU) as the mean of 70 point fluorescence readings taken from the central portion of each slide.

The strength of sporeling attachment was determined using a water jet with an impact pressure of 70 kPa.[73] The biomass on the surfaces was again determined using the Tecan plate reader to determine the removal of sporelings.

2.2.15 Attachment and removal bioassays of Navicula incerta

For *Navicula incerta* assays, six slides were equilibrated in 0.22 gm filtered ASW for 24 hours prior to testing. Cultured *N. incerta* cells were diluted to an approximate chlorophyll content of 0.25 gg mL^{-1}. 10 mL of the suspension was added to each of six replicate slides of each coating type and allowed to settle for 2 hours. After that time, slides were exposed to 5 minutes of shaking on an orbital shaker at 60 rpm and rinsed with seawater. Three slides were removed and fixed in 2.5% glutaraldehyde for measurement of initial attachment. The samples were air dried and the density of cells attached to the surface was counted on each slide by eye using a fluorescence microscope to illuminate the samples. Counts were made for 15 fields of view (each 0.15 mm^2) on each slide.

The strength of diatom attachment was determined for 3 slides of each coating type using a water channel with a shear stress of 33 Pa.[74] After exposure to shear stress, samples were fixed and the number of cells remaining was counted, as described above.

2.2.16 Statistical analysis for bioassays

For settlement *U. linza* and initial attachment of *N. incerta,* a one-way analysis of variance was performed to determine if there was a statistically significant difference between groups ($p<0.05$), followed by a post hoc pairwise Tukey comparison test. For percent removal, these statistical tests were performed on arcsine transformed data of fractional removal of organisms.

2.3 Polymer backbone: Comparing PEO- and PDMS-based coatings

Functional surface active block copolymers were synthesized from triblocks of PS and vinyl-containing PEO- or PDMS-based midblocks, to which sequence-specific and surface-segregating oligomers (based on peptide or peptoid chemistry) were attached via thiol–ene "click" chemistry. The resulting amphiphilic copolymers were spray-coated onto an SEBS underlayer to form the final antifouling surface. Surfaces were evaluated for chemical presentation via captive bubble water contact angle measurements and X-ray photoelectron spectroscopy, and for antifouling and fouling release performance via bioassays of *Ulva linza* and *Navicula incerta.* The key results from comparing polymer backbone material, oligomer side chain chemistry, and oligomer sequence are discussed below.

PEO- and PDMS-based block copolymers have been extensively studied as antifouling and fouling release coating materials, but the diversity of coating chemistries has made it difficult to determine universal design rules. In directly comparing these materials side-by-side, differences in surface rearrangement (determined by captive bubble water contact angle and XPS measurements) led to differences in fouling performance with the model organisms *Ulva linza* and *Navicula incerta*.

In comparing polymer scaffolds, the relative surface energies of the polymer backbone and side chains define the composition of the surface. In the annealed (dry) state, XPS indicates that PDMS dominates the surface of all PDMS-based coatings (Figure 2.3Figure 2.2a), which also had similar water contact angles equal to that of the unfunctionalized SABC (approximately 71°, Figure 2.2b). For all PEO-based SABCs, XPS indicates that fluorocarbon-containing oligomers accumulate at the surface in the dry state, and unlike the PDMS-based coatings, the initial difference between water contact angles of the unfunctionalized PEO coating (56°) and all PEO-based functionalized coatings (32–37°) was quite large. This difference in initial water contact angle is further evidence that the side chains populate the

interface more readily in PEO-based systems than on a siloxane-based backbone, likely due to the low surface energy of the fluorocarbon moieties that drives surface segregation even in the dry state. Conversely, the unfunctionalized PEO SABC surface is enriched in carbon over the theoretical bulk value (89% and 71%, respectively), consistent with an enrichment of carbon-rich polystyrene at the surface in the dry state and a larger initial water contact angle.

Upon exposure to water, surface rearrangement was observed via XPS for all coatings except two (both peptoid sequences on PEO, which consistently display a surface enriched in peptoid side chains). High resolution C1s XPS confirms the increase of C–O bonds (286.45 eV) on both PDMS and PEO SABC surfaces (indicated by arrows in Figure 2.2a). For PDMS-based coatings, this suggests the migration of oligomer side chains to the surface, as C–O ether bonds appear only in the side chains of the PDMS SABC structure and not the polymer backbone. As the coatings hydrated, differences between the water contact angles of functionalized and control materials became more prominent. Within one week, all functionalized siloxane SABCs became more hydrophilic than the unfunctionalized siloxane coating and approached similar values in the 26–30° range. Some factors responsible for these changes are surface rearrangement of functionalized coatings that results in more PEO-like groups at the surface, as well as likely a stable hydration layer forming and water filling the rougher surface created by spray-coating (even the unmodified PDMS SABC becomes more hydrophilic, approaching 35° after 7 days).[75] The rearrangement of functional groups accounts for the lower contact angles, and thus greater apparent hydrophilicity, of the functionalized coatings as compared to the unfunctionalized PDMS SABC.

For PEO-based coatings, a similar trend of increased hydrophilicity with time was seen. As the coatings hydrated, the contact angles of functionalized and bare PEO samples approach similar values, indicating that underwater the PEO and PEO-like side chains gradually dominate the surface.

Overall, all samples become more hydrophilic when immersed in water, with all functionalized coatings approaching similar equilibrium values (in the range of 26–31°) distinct from those of either polymer backbone (PEO 22 ± 2°, PDMS 35 ± 2°) (Figure 2.2b). That functionalized coatings based on such dissimilar materials as PEO and PDMS show similar water contact angles indicates that their common peptide and peptoid side chains, not the polymer backbones, define the equilibrium contact angle under water. PDMS-based coatings experience more dramatic rearrangement under hydration, and PEO-based coatings have more consistent side chain presentation regardless of environment. After soaking, the surface presentation of hydrophilic side chains does increase when measured by XPS, but it is difficult to know how closely the structure corresponds to that of the fully hydrated surface due to unknown reconstruction kinetics in vacuum during the measurement, so only qualitative comparisons can be made.

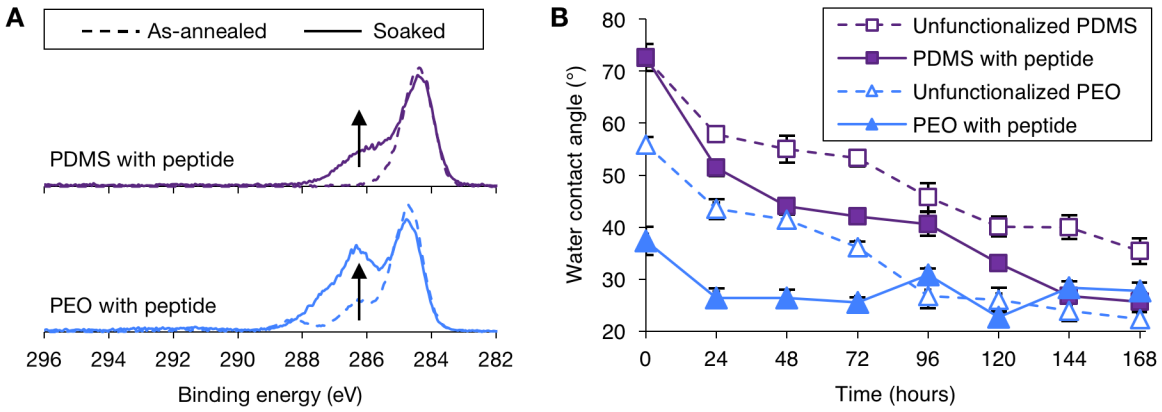

Figure 2.2 Evidence for rearrangement upon soaking

For ease of presentation, only alternating peptide side chains are shown. **A**) High resolution C1s XPS spectra of functionalized PEO and PDMS SABCs. Upon soaking, both PDMS- and PEO-based coatings exhibit more C–O bond character (peak at 286.45 eV). **B**) Water contact angles via captive bubble contact angle measurements (values reported are measured in the external water phase). All coatings become more hydrophilic over days, with functionalized coatings approaching very similar values regardless of polymer backbone. Error bars show standard deviation of three measurements.

Antifouling and fouling release performance was evaluated using settlement and removal bioassays of the macroalga *Ulva linza* and the diatom *Navicula incerta*. Initial attachment

studies using spores of *U. linza* showed that most samples had similar settlement densities to those of the unfunctionalized PEO and PDMS SABC controls. Two samples (alternating peptoid on PEO and alternating peptide on PDMS) outperformed their unfunctionalized SABC controls, indicating possible synergy between polymer backbone and pendant functional groups (Figure 2.3c).

Exposure of the coatings to a 70 kPa waterjet indicated significant differences in sporeling adhesion strength to the surface depending on polymer backbone (one-way analysis of variance on arcsine transformed data, $F_{9,50} = 36$, $p<0.05$). In general, the fouling release properties of the PDMS-based coatings were superior to those of the PEO-based coatings (Figure 2.3d). When functionalized onto the PEO SABC, none of the side chains improved sporeling removal relative to that of the PEO control. On the PDMS SABC, all side chains exhibited fouling release superior to those based on the PEO SABC. In particular, the peptoid side chains on PDMS exhibited much higher removal than both the PDMS control and analogues based on the PEO backbone, with 91–95% of sporelings being removed.

Initial attachment of the diatom *Navicula incerta* was reduced on all the functionalized PEO-based coatings versus the functionalized PDMS-based coatings (one-way analysis of variance, $F_{9,440} = 52.2$, $p<0.05$). Each functionalized PEO-based coating had significantly reduced initial attachment of diatoms relative to the unfunctionalized control (Figure 2.3e), with the coating functionalized with a blocky peptoid side chain having zero observed cells attached. Except for one (blocky peptoid), the addition of side chains to the PDMS backbone did not improve *N. incerta* attachment.

Exposure to a shear stress of 33 Pa indicated significant differences in cell adhesion strength depending on polymer backbone (one-way analysis of variance on arcsine transformed data, $F_{9,440} = 133$, $p<0.05$). In general, the fouling release properties of the PEO-based coatings were superior to those of the PDMS-based coatings, with percent cell

removals of 77–89% for PEO-based coatings and 0–12% for PDMS-based coatings (Figure 2.3f). The superior performance of PEO-based coatings over PDMS-based coatings is consistent with the findings of previous studies that have shown cells of *N. incerta* tend to be more weakly attached to hydrophilic than to hydrophobic surfaces.[76-78] The bubble contact angles indicated that the PEO-based coatings had become more hydrophilic than those based on the PDMS SABC after the 24 hours of soaking before introduction to diatoms, which is consistent with the trend observed in release performance.

The polymer backbone plays a critical role in the performance of coatings, especially in fouling release. The fouling release of *U. linza* was superior on PDMS-based coatings, while PEO-based coatings were superior for removal of *N. incerta.* In terms of organism settlement and initial attachment, the trends were less clear, and superior performance depended on specific pairings of both polymer and side chain backbone chemistries. The standout performance against *U. linza* of the alternating peptoid on the PEO SABC and alternating peptide on the PDMS SABC, and against *N. incerta* of the blocky peptoid on the PEO SABC indicates synergy between polymer backbone and pendant functional groups in antifouling.

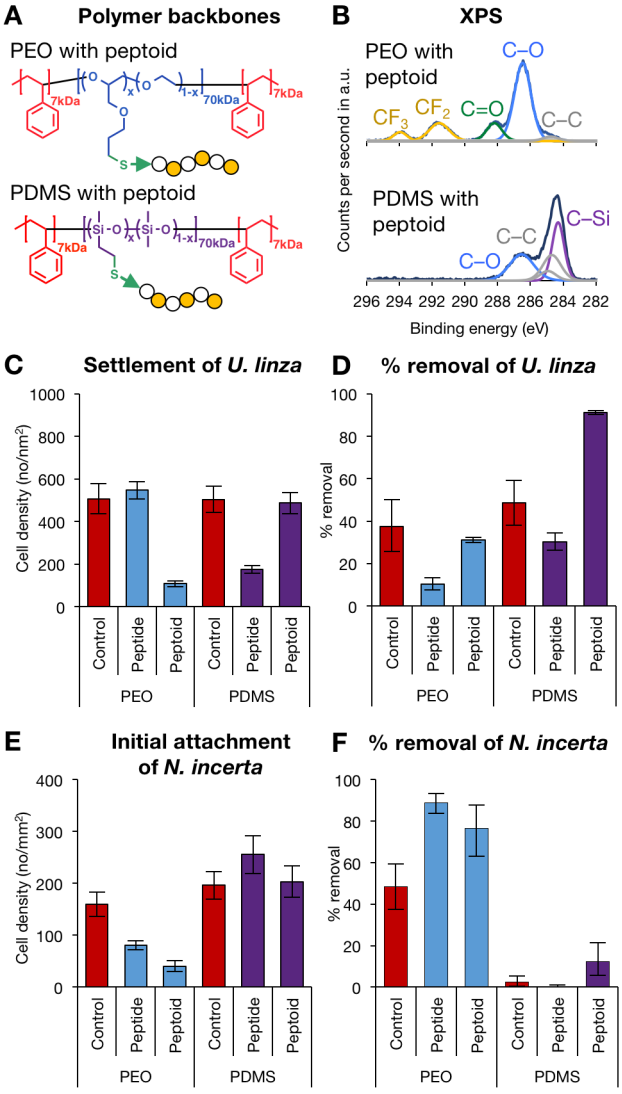

Figure 2.3 Polymer backbone comparison

For ease of presentation, results from just the alternating sequence are shown. A) Materials for comparison. B) High resolution C1s XPS of soaked surfaces soaked. C) Settlement results of *Ulva linza* spores. Achieving low settlement depends on a combination of polymer backbone and side chain. D) Percent removal of *U. linza* sporelings after 1 week of growth. PDMS-based SABCs achieve higher removal than PEO-based coatings. E) Settlement of *N. incerta* cells. PEO-based coatings have lower settlement than PDMS-based coatings. F) Percent removal of *N. incerta* cells. PEO-based coatings have higher removal than PDMS-based coatings. For C, E, and F, error bars show 95% confidence limits, and for D error bars show standard error of the mean.

2.4 Side chain chemistry: Comparing peptide and peptoid oligomers

In comparing oligopeptide and oligopeptoid pendant side chains, the main objective was to elucidate the effect of hydrogen bonding in the side chain backbone on surface presentation and antifouling and fouling release performance. Significant differences emerged in rearrangement kinetics upon soaking, as well as in antifouling and fouling release performance, pointing to distinct interactions of side chain backbones with water and fouling biomolecules. In all surface measurements and fouling performances, it was found

that the polymer backbone strongly influenced the results in comparing side chain chemistries.

Equilibrated bubble contact angle values were similar for all functionalized coatings, and there were no significant differences between peptide- and peptoid-functionalized PEO SABCs over 7 days of measurements. However, the rearrangement kinetics of the functionalized PDMS SABCs varied depending on the side chain. On PDMS, the peptide-functionalized coatings exhibited much faster surface reconstruction than their analogous peptoid-functionalized coatings, reaching lower water contact angle values earlier in the experiment (deviating significantly within 24 hours, and accumulating an approximately 20° difference by 48 hours). It seems that the peptide-functionalized PDMS-based coatings have a stronger driving force for rearrangement and hydration, distinct from the peptoid-functionalized and unfunctionalized PDMS SABCs. It is possible that the oligopeptide's ability to hydrogen bond causes a faster migration to the surface, as the peptide backbone can interact more strongly with water as both a hydrogen bond donor and acceptor. The peptoid backbone is only a hydrogen bond acceptor, which could lead to slower hydration. However, high resolution C1s XPS for peptide- and peptoid-functionalized PDMS SABCs were identical, in both the as-annealed and soaked states. In examining the survey spectra, only the peptoid-functionalized PDMS SABCs display a very small F1s signal after soaking (comprising ≤1% of the total surface composition), corresponding to the fluorocarbon moieties of the side chains. This could be further evidence for the peptide-functionalized PDMS SABCs rearranging on a faster timescale than their peptoid analogues, resulting in a faster rearrangement to the "dry" state where the PDMS backbone dominates and there is no side chain presentation. However, as previously mentioned, the rearrangement kinetics in vacuum are not known, so we can only make qualitative comparisons.

Both peptide- and peptoid-functionalized PEO surfaces showed similar trends in contact angle with soaking time, becoming mildly more hydrophilic over 7 days. After soaking, surface rearrangement was observed via XPS for the peptide-functionalized coatings only, with oligopeptoids presenting at the surface in both the dry and soaked states (Figure 2.4b). However, after soaking, none of the peptide-functionalized coatings showed signal in the high resolution N1s or F1s spectra, indicating that the peptide backbone was below the top ~10 nm of the surface during the measurement, and that the only the backbone PEO and PEO-like sidechains were segregating to the surface. A possible explanation is that the hydrogen-bonding oligopeptides are interacting with each other in the hydrated PEO bulk and are either unable to segregate as strongly to the surface as the oligopeptoids or migrate away from the surface in the XPS due to exposure to air/vacuum on time scales similar to those of the measurement.

In the settlement of spores of *U. linza*, the response to side chain chemistry was dependent on polymer backbone. There was no clear trend with side chain chemistry on PEO SABCs, but peptide-functionalized PDMS coatings had lower spore settlement than their peptoid analogues. In removal of *U. linza* sporelings, there was again a dependence on polymer backbone, with no clear trend on the PEO SABCs with side chain chemistry, but a clear difference on the PDMS SABC, with the peptoid samples showing higher removal of sporelings than the peptide samples (Figure 2.4c). While previous work with oligopeptide-functionalized coatings has been able to increase removal from PDMS,[35] the amino acids in that study had longer amphiphilic side groups than those studied here, which likely masked any effect of hydrogen bonding in the peptide backbone.

In the settlement of cells of *N. incerta*, as mentioned above, the PEO-based materials outperformed the PDMS-based coatings, with the peptoid-functionalized coatings having particularly low cell attachment (there were no measurable cells on the PEO–peptoid

coating with a blocky sequence) (Figure 2.4e). This superior performance is likely due to the combination of an inherently hydrophilic PEO backbone and an amphiphilic antifouling side chain that lacks hydrogen bonding. In removal of diatoms, there is no trend with side chain (Figure 2.4f).

Overall, trends with polymer backbone dominated over those with side chain chemistry, but a few effects with side chain stand out. The addition of peptoid side chains significantly enhanced the removal of organisms from already high-performing polymer backbones: peptoid-functionalization of PDMS SABCs improved removal of *U. linza* sporelings, and peptoid-functionalization PEO SABCs reduced *N. incerta* cell attachment. The addition of peptoid side chains also lowered the *N. incerta* settlement on PDMS as compared to the peptide-functionalized analogues. We hypothesize that the superior performance of peptoid side chains stems from the key chemical difference between these otherwise identical oligomers: peptoids lack the ability to donate a hydrogen bond, while peptides have both hydrogen bond donors and acceptors. These intermolecular forces may be the reason that the peptoid-functionalized coatings outperformed the peptide-functionalized coatings.

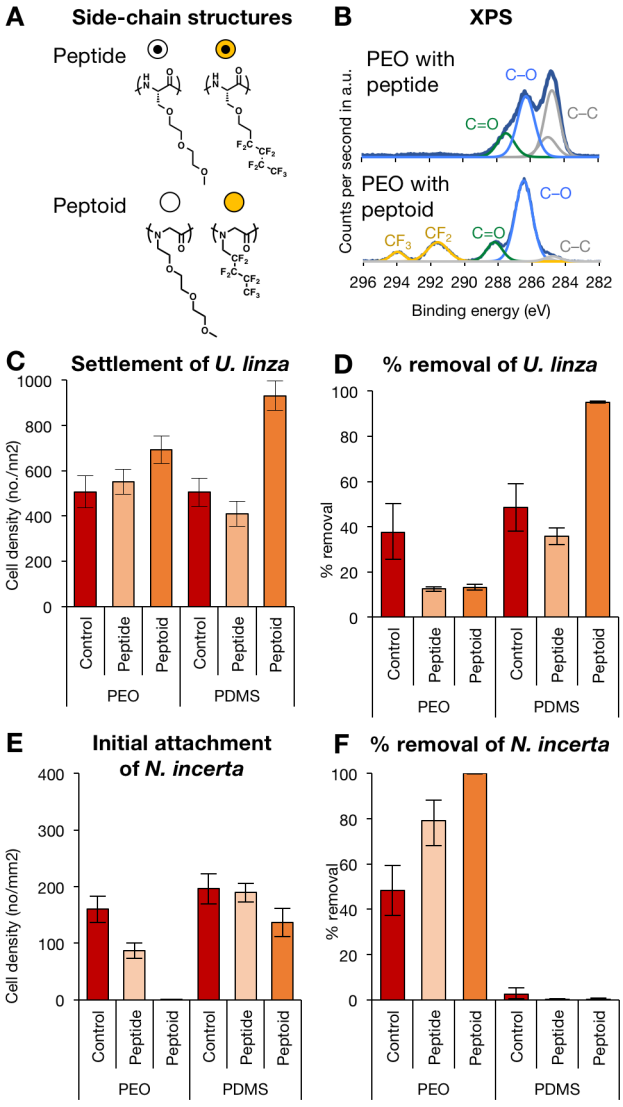

Figure 2.4 Comparison of side chains

For ease of presentation, results for just alternating sequences are shown. A) Amphiphilic side chain chemistries. B) High-resolution C1s XPS of soaked PEO-based surfaces. Peptoids present more strongly than peptides. C) Settlement results of *Ulva linza* spores. Side chain chemistry has an effect only on the PDMS SABC, where peptide-functionalized coatings have lower settlement. D) Percent removal of *U. linza* sporelings after 1 week of growth. Side chain chemistry has an effect only on the PDMS SABC, where peptoid-functionalized coatings have remarkably high removal. E) Settlement of *N. incerta* cells. There is little trend with side chain chemistry. F) Percent removal of *N. incerta* cells. Removal is dictated by polymer backbone, with no effect of side chain. For C, E, and F, error bars show 95% confidence limits, and for D error bars show standard error of the mean.

2.5 Sequence and length scale of amphiphilicity

The main objective in comparing oligomer sequences was to understand how the length scale of amphiphilicity impacts surface presentation and coating performance. Incorporating alternating and blocky sequences of fluoroalkyl and oligo-PEO groups (Figure 2.5a) resulted in subtle differences in surface chemistry measured with XPS, and only affected performance in one bioassay (attachment of *N. incerta*). Overall, sequence effects were less clear than those from side chain or backbone chemistries.

In the dry, annealed state, there was no difference by XPS within pairs of alternating- and blocky-functionalized coatings. After soaking, with the exception of the peptoid-functionalized PEO SABCs, which always present surfaces enriched in peptoid regardless of wet/dry state or sequence, almost all alternating-functionalized coatings showed larger increases in C–O at the surface than the blocky-functionalized coatings (Figure 2.5b). In a previous study, it was found that surfaces that incorporated oligopeptoids with consecutive (or blocky) fluoroalkyl groups had increased intermolecular interactions.[62] In the current study, it possible that the blocky oligomers exhibit similar strong fluorocarbon–fluorocarbon interactions when exposed to air or vacuum, causing the blocky oligomers to become buried below the surface in the vacuum conditions of the XPS and resulting in spectra very similar to those of the unfunctionalized controls. However, we found that blocky-functionalized coatings performed differently from the controls in fouling tests and achieved the same low water contact angles as their alternating-sequence analogues, indicating that the blocky oligomers are in fact at the surface when in the hydrated state.

For *U. linza* settlement and removal, the sequence of hydrophilic and hydrophobic groups in the side chain made little difference in the efficacy of the coating (Figure 2.5c), with slightly better performance of alternating sequences over blocky ones. Although a previous study found that increasing the number of consecutive fluoroalkyl groups was worse for both antifouling and fouling release,[31] the sequences used in this study may not have enough monomer units in each side chain for significant differences to appear. Further studies with longer sequences would likely give further insight into the role of sequence in coating performance.

For initial attachment of *N. incerta*, there was no effect of sequence on PEO SABCs, but PDMS-based coatings functionalized with alternating sequences had statistically higher settlement than their blocky analogues (Figure 2.5e). There was no difference with sequence

in diatom removal (Figure 2.5f). Overall, differences arising from sequence in surface presentation and antifouling performance were much subtler than differences stemming from side chain or polymer backbone chemistries.

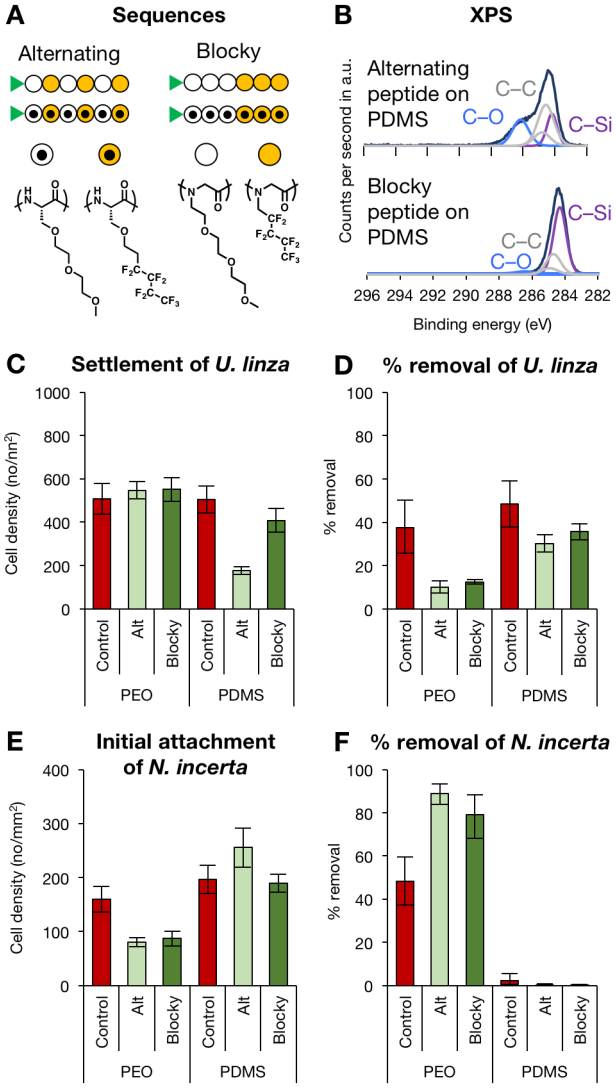

Figure 2.5 Sequence comparison

For ease of presentation, results for just oligopeptide side chains are shown. A) Alternating and blocky hexamers. B) High resolution C1s XPS of soaked surfaces. C) Settlement results of *Ulva linza* spores. There is no significant trend with sequence. D) Percent removal of *U. linza* sporelings after 1 week of growth. There is no significant trend with sequence. E) Settlement of *N. incerta* cells. On PDMS SABCs, blocky coatings have lower settlement. F) Percent removal of *N. incerta* cells. Removal is dictated by polymer backbone, with no effect of sequence. For C–F, only peptide side chains are shown for ease of presentation. Error bars show 95% confidence limits. For C, E, and F, error bars show 95% confidence limits, and for D error bars show standard error of the mean.

2.6 Conclusions

PEO- and PDMS-based block copolymers have been extensively studied as antifouling and fouling release coating materials, but the diversity of coating chemistries has made universal design rules difficult to determine. The impact of polymer scaffold choice and

incorporation of hydrogen bonding capabilities have been studied independently with different structures, which made direct comparisons difficult. In this study, PEO- and PDMS-based SABCs were functionalized with amphiphilic surface-active oligopeptides or oligopeptoids. Each of these side chain structures incorporated sequence control into a traditional block copolymer architecture, and allowed the study of different length scales of amphiphilicity. With this hierarchical and modular design, meaningful conclusions about the role of subtle functional group differences, surface chemistry design, and environmental response can be gathered. By correlating surface characterization with the results from *U. linza* and *N. incerta* biofouling assays, design rules and trends in performance can be used to improve the design of antifouling and fouling release coatings.

After soaking in water, all coatings become more hydrophilic over the time scale of days. All functionalized coatings approach very similar water contact angle values after 7 days, distinct from either unfunctionalized control, indicating a migration of their similar side chains to the surface. PDMS-based coatings have a larger change in water contact angle, correlating to the superior release of *U. linza* sporelings. Furthermore, high resolution XPS spectra indicate an increase in C–O ether bond character upon soaking for all coatings, corresponding to a migration of ether-bearing side chains to the surface. Peptide-functionalized coatings do not display a fluorine signal after soaking, possibly indicating fast rearrangement kinetics in vacuum that bury peptide oligomers due to hydrogen bonding interactions between side chains within the coating.

Fouling release performance was largely determined by polymer backbone chemistry, with *U. linza* having lower adhesion strength on PDMS-based coatings and *N. incerta* having lower adhesion strength on PEO-based coatings. For *U. linza*, peptoid-functionalized PDMS SABCs had the best removal, improved most by peptoid side chains, which had percent removal values of up to 95%. Settlement of *U. linza* spores did not show a clear trend with any

of the variables studied, with two coatings showing improved performance (alternating peptoid on PEO SABC and alternating peptide on PDMS SABC). Initial attachment of *N. incerta* was also lower on PEO-based coatings, with standout performance from the blocky peptoid PEO SABC, which had zero observed cells.

Differences arising from sequence were much less pronounced than those arising from either polymer or side chain chemistry. Blocky sequences consistently presented less side chain via XPS, indicating possible self-interaction within the coating of consecutive of fluoroalkyl groups.

In considering the choice of polymer backbone, this work emphasizes that synergies between these materials can lead to dramatic improvements in performance. Overall, for both fouling species, the peptoid-functionalized coatings outperformed the peptide-functionalized coatings, improving both *U. linza* removal and *N. incerta* settlement, suggesting that coatings devoid of hydrogen bond donors may achieve better overall performance.

2.7 Acknowledgements

This work was supported by the Office of Naval Research in the form of a Presidential Early Career Award in Science and Engineering (PECASE) (R.A.S.) and by awards N0001411103 (C.K.O.), and N00014-13-1-0633 and N00014-13-1-0634 (A.S.C). A.L.P gratefully acknowledges the National Science Foundation for a graduate fellowship. The authors acknowledge support through the Molecular Foundry, a Lawrence Berkeley National Laboratory User Facility supported by the Office of Science, Office of Basic Energy Sciences, U.S. Department of Energy, under Contract DE-AC02-05CH11231. The authors also thank Gabriel Sanoja for synthesis of the P(EO/AGE) midblock, and Dr. Thomas Mates for help with acquisition of X-ray photoelectron spectroscopy data.

2.8 References

(1) Callow, J. A.; Callow, M. E., Biofilms. In *Antifouling Compounds*, Springer: Berlin Heidelberg, Germany, 2006; Vol. 42, pp 141–169.

(2) Schultz, M. P.; Bendick, J. A.; Holm, E. R.; Hertel, W. M. Economic impact of biofouling on a naval surface ship. *Biofouling* **2011,** *27* (1), 87-98.

(3) Townsin, R. L. The ship hull fouling penalty. *Biofouling* **2003,** *19*, 9-15.

(4) Corbett, J. J.; Koehler, H. W. Updated emissions from ocean shipping. *J. Geophys. Res.: Atmos.* **2003,** *108* (D20), 4650.

(5) Thomas, K. V.; Brooks, S. The environmental fate and effects of antifouling paint biocides. *Biofouling* **2010,** *26* (1), 73-88.

(6) Champ, M. A. Economic and environmental impacts on ports and harbors from the convention to ban harmful marine anti-fouling systems. *Marine Pollution Bulletin* **2003,** *46* (8), 935-940.

(7) Earley, P. J.; Swope, B. L.; Barbeau, K.; Bundy, R.; McDonald, J. A.; Rivera-Duarte, I. Life cycle contributions of copper from vessel painting and maintenance activities. *Biofouling* **2014,** *30* (1), 51-68.

(8) In *On the Control of Harmful Anti-Fouling Systems on Ships, 2001*, International Convention on the Control of Harmful Anti-fouling Systems on Ships, 18 October, 2001; International Maritime Organization: 2001.

(9) Scardino, A. J.; Guenther, J.; de Nys, R. Attachment point theory revisited: the fouling response to a microtextured matrix. *Biofouling* **2008,** *24* (1), 45-53.

(10) Scardino, A. J.; de Nys, R. Mini review: Biomimetic models and bioinspired surfaces for fouling control. *Biofouling* **2011,** *27* (1), 73-86.

(11) Long, C. J.; Schumacher, J. F.; Robinson, P. A. C., II; Finlay, J. A.; Callow, M. E.; Callow, J. A.; Brennan, A. B. A model that predicts the attachment behavior of *Ulva linza* zoospores on surface topography. *Biofouling* **2010,** *26* (4), 411-419.

(12) McMaster, D. M.; Bennett, S. M.; Tang, Y.; Finlay, J. A.; Kowalke, G. L.; Nedved, B.; Bright, F. V.; Callow, M. E.; Callow, J. A.; Wendt, D. E.; Hadfield, M. G.; Detty, M. R. Antifouling character of 'active' hybrid xerogel coatings with sequestered catalysts for the activation of hydrogen peroxide. *Biofouling* **2009,** *25* (1), 21-33.

(13) Qian, P.-Y.; Xu, Y.; Fusetani, N. Natural products as antifouling compounds: recent progress and future perspectives. *Biofouling* **2010,** *26* (2), 223-234.

(14) Olsen, S. M.; Pedersen, L. T.; Laursen, M. H.; Kiil, S.; Dam-Johansen, K. Enzyme-based antifouling coatings: a review. *Biofouling* **2007,** *23* (5), 369-383.

(15) Leroy, C.; Delbarre-Ladrat, C.; Ghillebaert, F.; Compere, C.; Combes, D. Influence of subtilisin on the adhesion of a marine bacterium which produces mainly proteins as extracellular polymers. *J. Appl. Microbiol.* **2008,** *105* (3), 791-799.

(16) Aldred, N.; Phang, I. Y.; Conlan, S. L.; Clare, A. S.; Vancso, G. J. The effects of a serine protease, Alcalase®, on the adhesives of barnacle cyprids (*Balanus amphitrite*). *Biofouling* **2008,** *24* (2), 97-107.

(17) Tasso, M.; Pettitt, M. E.; Cordeiro, A. L.; Callow, M. E.; Callow, J. A.; Werner, C. Antifouling potential of Subtilisin A immobilized onto maleic anhydride copolymer thin films. *Biofouling* **2009,** *25* (6), 505-516.

(18) Carr, L. R.; Xue, H.; Jiang, S. Functionalizable and nonfouling zwitterionic carboxybetaine hydrogels with a carboxybetaine dimethacrylate crosslinker. *Biomaterials* **2011,** *32* (4), 961-968.

(19) Jiang, S.; Cao, Z. Ultralow-Fouling, Functionalizable, and Hydrolyzable Zwitterionic Materials and Their Derivatives for Biological Applications. *Adv. Mater.* **2010,** *22* (9), 920-932.

(20) Cheng, G.; Xue, H.; Li, G.; Jiang, S. Integrated Antimicrobial and Nonfouling Hydrogels to Inhibit the Growth of Planktonic Bacterial Cells and Keep the Surface Clean. *Langmuir* **2010,** *26* (13), 10425-10428.

(21) Zhang, Z.; Finlay, J. A.; Wang, L. F.; Gao, Y.; Callow, J. A.; Callow, M. E.; Jiang, S. Y. Polysulfobetaine-Grafted Surfaces as Environmentally Benign Ultralow Fouling Marine Coatings. *Langmuir* **2009,** *25* (23), 13516-13521.

(22) Aldred, N.; Li, G.; Gao, Y.; Clare, A. S.; Jiang, S. Modulation of barnacle (*Balanus amphitrite* Darwin) cyprid settlement behavior by sulfobetaine and carboxybetaine methacrylate polymer coatings. *Biofouling* **2010,** *26* (6), 673-683.

(23) Krishnan, S.; Weinman, C. J.; Ober, C. K. Advances in polymers for anti-biofouling surfaces. *J. Mater. Chem.* **2008,** *18* (29), 3405-3413.

(24) Li, X. F.; Andruzzi, L.; Chiellini, E.; Galli, G.; Ober, C. K.; Hexemer, A.; Kramer, E. J.; Fischer, D. A. Semifluorinated aromatic side-group polystyrene-based block copolymers: Bulk structure and surface orientation studies. *Macromolecules* **2002,** *35* (21), 8078-8087.

(25) Hu, Z.; Finlay, J. A.; Chen, L.; Betts, D. E.; Hillmyer, M. A.; Callow, M. E.; Callow, J. A.; DeSimone, J. M. Photochemically Cross-Linked Perfluoropolyether-Based

Elastomers: Synthesis, Physical Characterization, and Biofouling Evaluation. *Macromolecules* **2009,** *42* (18), 6999-7007.

(26) Gudipati, C. S.; Finlay, J. A.; Callow, J. A.; Callow, M. E.; Wooley, K. L. The antifouling and fouling-release perfomance of hyperbranched fluoropolymer (HBFP)-poly(ethylene glycol) (PEG) composite coatings evaluated by adsorption of biomacromolecules and the green fouling alga *Ulva*. *Langmuir* **2005,** *21* (7), 3044-3053.

(27) Andruzzi, L.; Senaratne, W.; Hexemer, A.; Sheets, E. D.; Ilic, B.; Kramer, E. J.; Baird, B.; Ober, C. K. Oligo(ethylene glycol) containing polymer brushes as bioselective surfaces. *Langmuir* **2005,** *21* (6), 2495-2504.

(28) Ma, H. W.; Hyun, J. H.; Stiller, P.; Chilkoti, A. "Non-fouling" oligo(ethylene glycol)-functionalized polymer brushes synthesized by surface-initiated atom transfer radical polymerization. *Adv. Mater.* **2004,** *16* (4), 338-341.

(29) Hawkins, M. L.; Fay, F.; Rehel, K.; Linossier, I.; Grunlan, M. A. Bacteria and diatom resistance of silicones modified with PEO-silane amphiphiles. *Biofouling* **2014,** *30* (2), 247-258.

(30) Dimitriou, M. D.; Zhou, Z. L.; Yoo, H. S.; Killops, K. L.; Finlay, J. A.; Cone, G.; Sundaram, H. S.; Lynd, N. A.; Barteau, K. P.; Campos, L. M.; Fischer, D. A.; Callow, M. E.; Callow, J. A.; Ober, C. K.; Hawker, C. J.; Kramer, E. J. A general approach to controlling the surface composition of poly(ethylene oxide)-based block copolymers for antifouling coatings. *Langmuir* **2011,** *27* (22), 13762-13772.

(31) van Zoelen, W.; Buss, H. G.; Ellebracht, N. C.; Lynd, N. A.; Fischer, D. A.; Finlay, J.; Hill, S.; Callow, M. E.; Callow, J. A.; Kramer, E. J.; Zuckermann, R. N.; Segalman, R. A. Sequence of Hydrophobic and Hydrophilic Residues in Amphiphilic Polymer Coatings Affects Surface Structure and Marine Antifouling/Fouling Release Properties. *ACS Macro Lett.* **2014,** *3* (4), 364-368.

(32) Martinelli, E.; Guazzelli, E.; Bartoli, C.; Gazzarri, M.; Chiellini, F.; Galli, G.; Callow, M. E.; Callow, J. A.; Finlay, J. A.; Hill, S. Amphiphilic Pentablock Copolymers and their Blends with PDMS for Antibiofouling Coatings. *J. Polym. Sci., Part A: Polym. Chem.* **2015,** *53* (10), 1213-1225.

(33) Marabotti, I.; Morelli, A.; Orsini, L. M.; Martinelli, E.; Galli, G.; Chiellini, E.; Lien, E. M.; Pettitt, M. E.; Callow, M. E.; Callow, J. A.; Conlan, S. L.; Mutton, R. J.; Clare, A. S.; Kocijan, A.; Donik, C.; Jenko, M. Fluorinated/siloxane copolymer blends for fouling

release: chemical characterisation and biological evaluation with algae and barnacles. *Biofouling* **2009,** *25* (6), 481-493.

(34) Sommer, S.; Ekin, A.; Webster, D. C.; Stafslien, S. J.; Daniels, J.; VanderWal, L. J.; Thompson, S. E. M.; Callow, M. E.; Callow, J. A. A preliminary study on the properties and fouling-release performance of siloxane-polyurethane coatings prepared from poly(dimethylsiloxane) (PDMS) macromers. *Biofouling* **2010,** *26* (8), 961-972.

(35) Stafslien, S. J.; Christianson, D.; Daniels, J.; VanderWal, L.; Chernykh, A.; Chisholm, B. J. Combinatorial materials research applied to the development of new surface coatings XVI: fouling-release properties of amphiphilic polysiloxane coatings. *Biofouling* **2015,** *31* (2), 135-149.

(36) Calabrese, D. R.; Wenning, B.; Finlay, J. A.; Callow, M. E.; Callow, J. A.; Fischer, D.; Ober, C. K. Amphiphilic oligopeptides grafted to PDMS-based diblock copolymers for use in antifouling and fouling release coatings. *Polym. Adv. Technol.* **2015,** *26* (7), 829-836.

(37) Youngblood, J. P.; Andruzzi, L.; Ober, C. K.; Hexemer, A.; Kramer, E. J.; Callow, J. A.; Finlay, J. A.; Callow, M. E. Coatings based on side-chain ether-linked poly(ethylene glycol) and fluorocarbon polymers for the control of marine biofouling. *Biofouling* **2003,** *19*, 91-98.

(38) Gu, M.; Vegas, A. J.; Anderson, D. G.; Langer, R. S.; Kilduff, J. E.; Belfort, G. Combinatorial synthesis with high throughput discovery of protein-resistant membrane surfaces. *Biomaterials* **2013,** *34* (26), 6133-6138.

(39) Perry, J. L.; Reuter, K. G.; Kai, M. P.; Herlihy, K. P.; Jones, S. W.; Luft, J. C.; Napier, M.; Bear, J. E.; DeSimone, J. M. PEGylated PRINT Nanoparticles: The Impact of PEG Density on Protein Binding, Macrophage Association, Biodistribution, and Pharmacokinetics. *Nano Lett.* **2012,** *12* (10), 5304-5310.

(40) Kavanagh, C. J.; Quinn, R. D.; Swain, G. W. Observations of barnacle detachment from silicones using high-speed video. *J. Adhes.* **2005,** *81* (7-8), 843-868.

(41) Brady, R. F.; Singer, I. L. Mechanical factors favoring release from fouling release coatings. *Biofouling* **2000,** *15* (1-3), 73-81.

(42) Kim, J.; Chisholm, B. J.; Bahr, J. Adhesion study of silicone coatings: the interaction of thickness, modulus and shear rate on adhesion force. *Biofouling* **2007,** *23* (2), 113-120.

(43) Wynne, K. J.; Swain, G. W.; Fox, R. B.; Bullock, S.; Uilk, J. Two silicone nontoxic fouling release coatings: Hydrosilation cured PDMS and $CaCO_3$ filled, ethoxysiloxane cured RTV11. *Biofouling* **2000,** *16* (2-4), 277-288.

(44) Wendt, D. E.; Kowalke, G. L.; Kim, J.; Singer, I. L. Factors that influence elastomeric coating performance: the effect of coating thickness on basal plate morphology, growth and critical removal stress of the barnacle *Balanus amphitrite*. *Biofouling* **2006,** *22* (1), 1-9.

(45) Kim, J.; Nyren-Erickson, E.; Stafslien, S.; Daniels, J.; Bahr, J.; Chisholm, B. J. Release characteristics of reattached barnacles to non-toxic silicone coatings. *Biofouling* **2008,** *24* (4), 313-319.

(46) Baier, R. E.; Shafrin, E. G.; Zisman, W. A. Adhesion: Mechanisms That Assist or Impede It. *Science* **1968,** *162* (3860), 1360-1368.

(47) Baier, R. E.; Zisman, W. A. Wettability and Multiple Attenuated Internal Reflection Infrared Spectroscopy of Solvent-Cast Thin Films of Polyamides. *Macromolecules* **1970,** *3* (4), 462-468.

(48) Baier, R. E.; Meyer, A. E. Surface Analysis of Fouling-Resistant Marine Coatings. *Biofouling* **1992,** *6* (2), 165-180.

(49) Martinelli, E.; Suffredini, M.; Galli, G.; Glisenti, A.; Pettitt, M. E.; Callow, M. E.; Callow, J. A.; Williams, D.; Lyall, G. Amphiphilic block copolymer/poly(dimethylsiloxane) (PDMS) blends and nanocomposites for improved fouling-release. *Biofouling* **2011,** *27* (5), 529-541.

(50) Martinelli, E.; Sarvothaman, M. K.; Galli, G.; Pettitt, M. E.; Callow, M. E.; Callow, J. A.; Conlan, S. L.; Clare, A. S.; Sugiharto, A. B.; Davies, C.; Williams, D. Poly(dimethyl siloxane) (PDMS) network blends of amphiphilic acrylic copolymers with poly(ethylene glycol)-fluoroalkyl side chains for fouling-release coatings. II. Laboratory assays and field immersion trials. *Biofouling* **2012,** *28* (6), 571-582.

(51) Yasani, B. R.; Martinelli, E.; Galli, G.; Glisenti, A.; Mieszkin, S.; Callow, M. E.; Callow, J. A. A comparison between different fouling-release elastomer coatings containing surface-active polymers. *Biofouling* **2014,** *30* (4), 387-399.

(52) Cho, Y.; Sundaram, H. S.; Weinman, C. J.; Paik, M. Y.; Dimitriou, M. D.; Finlay, J. A.; Callow, M. E.; Callow, J. A.; Kramer, E. J.; Ober, C. K. Triblock Copolymers with Grafted Fluorine-Free, Amphiphilic, Non-Ionic Side Chains for Antifouling and Fouling-Release Applications. *Macromolecules* **2011,** *44* (12), 4783-4792.

(53) Park, D.; Weinman, C. J.; Finlay, J. A.; Fletcher, B. R.; Paik, M. Y.; Sundaram, H. S.; Dimitriou, M. D.; Sohn, K. E.; Callow, M. E.; Callow, J. A.; Handlin, D. L.; Willis, C. L.; Fischer, D. A.; Kramer, E. J.; Ober, C. K. Amphiphilic Surface Active Triblock

Copolymers with Mixed Hydrophobic and Hydrophilic Side Chains for Tuned Marine Fouling-Release Properties. *Langmuir* **2010,** *26* (12), 9772-9781.

(54) Zhou, Z.; Calabrese, D. R.; Taylor, W.; Finlay, J. A.; Callow, M. E.; Callow, J. A.; Fischer, D.; Kramer, E. J.; Ober, C. K. Amphiphilic triblock copolymers with PEGylated hydrocarbon structures as environmentally friendly marine antifouling and fouling-release coatings. *Biofouling* **2014,** *30* (5), 589-604.

(55) Cho, Y.; Sundaram, H. S.; Finlay, J. A.; Dimitriou, M. D.; Callow, M. E.; Callow, J. A.; Kramer, E. J.; Ober, C. K. Reconstruction of Surfaces from Mixed Hydrocarbon and PEG Components in Water: Responsive Surfaces Aid Fouling Release. *Biomacromolecules* **2012,** *13* (6), 1864-1874.

(56) Krishnan, S.; Ayothi, R.; Hexemer, A.; Finlay, J. A.; Sohn, K. E.; Perry, R.; Ober, C. K.; Kramer, E. J.; Callow, M. E.; Callow, J. A.; Fischer, D. A. Anti-biofouling properties of comblike block copolymers with amphiphilic side chains. *Langmuir* **2006,** *22* (11), 5075-5086.

(57) Weinman, C. J.; Gunari, N.; Krishnan, S.; Dong, R.; Paik, M. Y.; Sohn, K. E.; Walker, G. C.; Kramer, E. J.; Fischer, D. A.; Ober, C. K. Protein adsorption resistance of anti-biofouling block copolymers containing amphiphilic side chains. *Soft Matter* **2010,** *6* (14), 3237-3243.

(58) Finlay, J. A.; Krishnan, S.; Callow, M. E.; Callow, J. A.; Dong, R.; Asgill, N.; Wong, K.; Kramer, E. J.; Ober, C. K. Settlement of *Ulva* zoospores on patterned fluorinated and PEGylated monolayer surfaces. *Langmuir* **2008,** *24* (2), 503-510.

(59) Lutz, J.-F.; Ouchi, M.; Liu, D. R.; Sawamoto, M. Sequence-Controlled Polymers. *Science* **2013,** *341* (6146), 1238149.

(60) Rosales, A. M.; Segalman, R. A.; Zuckermann, R. N. Polypeptoids: a model system to study the effect of monomer sequence on polymer properties and self-assembly. *Soft Matter* **2013,** *9* (35), 8400-8414.

(61) Zuckermann, R. N.; Kerr, J. M.; Kent, S. B. H.; Moos, W. H. Efficient Method for the Preparation of Peptoids [Oligo(N-substituted glycines)] by Submonomer Solid-Phase Synthesis. *J. Am. Chem. Soc.* **1992,** *114* (26), 10646-10647.

(62) van Zoelen, W.; Zuckermann, R. N.; Segalman, R. A. Tunable Surface Properties from Sequence-Specific Polypeptoid-Polystyrene Block Copolymer Thin Films. *Macromolecules* **2012,** *45* (17), 7072-7082.

(63) Leng, C.; Buss, H. G.; Segalman, R. A.; Chen, Z. Surface Structure and Hydration of Sequence-Specific Amphiphilic Polypeptoids for Antifouling/Fouling Release Applications. *Langmuir* **2015,** *31* (34), 9306-9311.

(64) Coin, I.; Beyermann, M.; Bienert, M. Solid-phase peptide synthesis: from standard procedures to the synthesis of difficult sequences. *Nat. Protoc.* **2007,** *2* (12), 3247-3256.

(65) Sun, J.; Stone, G. M.; Balsara, N. P.; Zuckermann, R. N. Structure-Conductivity Relationship for Peptoid-Based PEO-Mimetic Polymer Electrolytes. *Macromolecules* **2012,** *45* (12), 5151-5156.

(66) Krishnan, S.; Ward, R. J.; Hexemer, A.; Sohn, K. E.; Lee, K. L.; Angert, E. R.; Fischer, D. A.; Kramer, E. J.; Ober, C. K. Surfaces of fluorinated pyridinium block copolymers with enhanced antibacterial activity. *Langmuir* **2006,** *22* (26), 11255-11266.

(67) Andrade, J. D.; Ma, S. M.; King, R. N.; Gregonis, D. E. Contact Angles at the Solid–Water Interface. *J. Colloid Interface Sci.* **1979,** *72* (3), 488-494.

(68) Andrade, J. D.; King, R. N.; Gregonis, D. E.; Coleman, D. L. Surface Characterization of Poly(Hydroxyethyl methacrylate) and Related Polymers .1. Contact-Angle Methods in Water. *J. Polym. Sci., Part C: Polym. Symp.* **1979,** (66), 313-336.

(69) Beamson, G.; Briggs, D. The XPS of Polymers Database. SurfaceSpectra, Ltd.

(70) Callow, M. E.; Callow, J. A.; Pickett-Heaps, J. D.; Wetherbee, R. Primary adhesion of *Enteromorpha* (Chlorophyta, Ulvales) propagules: Quantitative settlement studies and video microscopy. *J. Phycol.* **1997,** *33* (6), 938-947.

(71) Callow, M. E.; Jennings, A. R.; Brennan, A. B.; Seegert, C. E.; Gibson, A.; Wilson, L.; Feinberg, A.; Baney, R.; Callow, J. A. Microtopographic cues for settlement of zoospores of the green fouling alga *Enteromorpha*. *Biofouling* **2002,** *18* (3), 237-245.

(72) Starr, R. C.; Zeikus, J. A. Utex — The Culture Collection of Algae at the University of Texas at Austin 1993 List of Cultures. *J. Phycol.* **1993,** *29* (2), 1-106.

(73) Finlay, J. A.; Callow, M. E.; Schultz, M. P.; Swain, G. W.; Callow, J. A. Adhesion strength of settled spores of the green alga *Enteromorpha*. *Biofouling* **2002,** *18* (4), 251-256.

(74) Schultz, M. P.; Finlay, J. A.; Callow, M. E.; Callow, J. A. A turbulent channel flow apparatus for the determination of the adhesion strength of microfouling organisms. *Biofouling* **2000,** *15* (4), 243-251.

(75) Mishra, H.; Schrader, A. M.; Lee, D. W.; Gallo, A.; Chen, S. Y.; Kaufman, Y.; Das, S.; Israelachvili, J. N. Time-Dependent Wetting Behavior of PDMS Surfaces with

Bioinspired, Hierarchical Structures. *ACS Appl. Mater. Interfaces* **2016,** *8* (12), 8168-8174.

(76) Holland, R.; Dugdale, T. M.; Wetherbee, R.; Brennan, A. B.; Finlay, J. A.; Callow, J. A.; Callow, M. E. Adhesion and motility of fouling diatoms on a silicone elastomer. *Biofouling* **2004,** *20* (6), 323-329.

(77) Finlay, J. A.; Bennett, S. M.; Brewer, L. H.; Sokolova, A.; Clay, G.; Gunari, N.; Meyer, A. E.; Walker, G. C.; Wendt, D. E.; Callow, M. E.; Callow, J. A.; Detty, M. R. Barnacle settlement and the adhesion of protein and diatom microfouling to xerogel films with varying surface energy and water wettability. *Biofouling* **2010,** *26* (6), 657-666.

(78) Schilp, S.; Rosenhahn, A.; Pettitt, M. E.; Bowen, J.; Callow, M. E.; Callow, J. A.; Grunze, M. Physicochemical Properties of (Ethylene Glycol)-Containing Self-Assembled Monolayers Relevant for Protein and Algal Cell Resistance. *Langmuir* **2009,** *25* (17), 10077-10082.

Part II: Self-Assembly of Sequence-Defined Block Copolymers

Chapter 3

Sequence effects on chain conformation and segregation strength

Polymers with sequence control offer the possibility of tuning segregation strength with comonomer sequence instead of chemical identity. Here, we have synthesized polystyrene-*b*-polypeptoid diblock copolymers that differ only in the sequence of comonomers in the polypeptoid block, where nonpolar phenyl side chains are incorporated to tune compatibility with polystyrene. Using small-angle X-ray scattering, we see that these materials readily self-assemble into lamellae, with domain spacings and order–disorder transition temperatures varying with sequence, despite identical composition. The ordered state is likely governed by chain conformational effects that localize compatibilizing comonomers at the block–block interface. These altered chain conformations are supported by simulations with self-consistent field theory (SCFT) and lead to the observed changes in domain spacing. However, the trends seen in the order–disorder transition are not captured by SCFT simulations or effective χ parameters, measured in the disordered phase by approximating the copolypeptoid as a uniform block. The disagreement between measured thermodynamic properties and coarse-grained approaches like SCFT and effective χ points to the

importance of molecular-scale effects in sequence-defined materials. Additionally, a reversal in relative disordering temperatures between forward and inverse taper sequences is observed compared to previous studies, likely due to a combination of sequence definition at the monomer lengthscale and the use of a "styrene-like" compatibilizing side chain, rather than a true polystyrene repeat unit. These results demonstrate that comonomer sequence tunes chain conformation and segregation strength, suggesting that sequence design could be used to target desired properties and morphologies in block copolymer materials while retaining important chemical functionalities.

This chapter was reproduced in part with permission from: A. L. Patterson, S. P. O. Danielsen, B. Yu, E. C. Davidson, G. H. Fredrickson, R. A. Segalman. Sequence Effects on Block Copolymer Self-Assembly through Tuning Chain Conformation and Segregation Strength Utilizing Sequence-Defined Polypeptoids. *Macromolecules*, 2019, 52, 3, 1277–1286.

3.1 Introduction

Block copolymers with tunable compatibility enable direct control over segregation strength, a key driving force for self-assembly and blend compatibilization. The segregation strength of a block copolymer (χN) can be tuned by changing the block–block interaction parameter (χ), typically achieved by changing the chemical identity of one or both blocks, or the overall polymer size (N).[1] However, the χ parameter between blocks is difficult to predict, testing different materials can be synthetically impractical, and the choice of a particular chemistry or chain length is often integral to the function of the resulting material. With these restrictions, targeting and tuning block copolymer properties can be challenging.

One strategy toward tuning segregation strength is to incorporate compatibilizing groups into one or both blocks.[2,3] Experimental approaches have leveraged advances in controlled polymerization chemistries to produce smoothly-varying composition profiles that span the length of the chain (gradients), modify just the block junction (tapers), or insert comonomer-rich domains along the length of the chain, resulting in desirable morphologies and greatly reduced T_{ODT}s.[4-11] Further, molecular simulations have predicted that changing the sequence on the monomer lengthscale can affect dynamics, chain conformations, and morphologies, suggesting that synthetic control of not only composition profiles but comonomer sequence could lead to designing materials with predictable properties.[12-14] However, traditional synthetic approaches produce a disperse population of chains and cannot control the placement of single monomers, preventing experimental access to these precise sequences. Some synthetic strategies have been developed that target fine sequence control (often through sequence-defined macromonomers or iterative orthogonal reactions), and biopolymers such as polypeptides and nucleic acids are inherently sequence-defined, but until very recently, most of these approaches have either been limited in production scale for use in bulk polymer physics studies or are not able to access arbitrary sequences.[15-23] There is considerable opportunity to experimentally investigate the range of promising behaviors expected for these precise materials.

Synthesized at large scale via highly efficient solid-phase synthesis,[24] polypeptoids (*N*-substituted polyglycines) are emerging materials for polymer applications where sequence plays a critical role in function. The exact sequence control afforded with this model system has led to discoveries in foldamers and self-assembling nanostructures in solution, and in bulk studies of crystallization and self-assembling systems for ion transport.[25-31] Pure polypeptoid and polystyrene–polypeptoid diblock copolymers have been shown to self-assemble into a variety of bulk microstructures.[32-36] In the study of polystyrene–polypeptoid

materials, phenyl side chains incorporated into the polar polypeptoid block acted as compatibilizing groups, lowering the order–disorder transition temperature in a similar manner to gradient and taper copolymers.[36] With behavior resembling that of traditional polymer systems and unique synthetic control, polypeptoids are poised for studying precise compositional and sequence effects.

The present study demonstrates the ability for sequence control of comonomers to directly tune both the chain conformations and segregation strength of self-assembling block copolymers, resulting in differences in domain spacing and phase stability. Sequences with compatibilizing groups distributed along the chain length are observed to have smaller domain spacings and lower order–disorder transition temperatures than tapered sequences, likely due to chain conformations made possible by localization of compatibilizing groups at the microdomain interface. These conclusions are supported by simulations performed with self-consistent field theory (SCFT). The order–disorder transition temperature (T_{ODT}) is also observed to be a function of sequence, but the trend in T_{ODT}s does not match that seen with SCFT or effective interaction parameters (extracted from scattering measurements in the disordered melt). We conclude that sequence-dependent chain conformations dominate the observed geometric and thermodynamic properties, and that coarse-grained approaches do not capture the molecular-scale physics at play in sequence-defined materials.

3.2 Experimental methods

3.2.1 Materials

Solvents and reagents were purchased from commercial suppliers and used without further purification unless otherwise noted. Rink amide MBHA resin was purchased from Novabiochem at 0.78 mmol/g loading. Anhydrous dimethylformamide (DMF) and diisopropylethylamine (DIPEA) were used in click reactions. HPLC-grade tetrahydrofuran

(THF), water, and acetonitrile were used for precipitations, lyophilization, and MALDI-MS sample preparation. Styrene, ethyl-α-bromoisobutyrate (EBiB), and N,N,N′,N″,N″-pentamethyldiethyltriamine (PMDETA) were filtered through alumina immediately before use.

3.2.2 Synthesis of alkyne-terminated polypeptoids

Polypeptoids were synthesized as previously described.[24] First, rink amide resin (0.78 mmol/g, 300 gmol scale) was deprotected twice with 4-methylpiperidine (30 eq, 20% v/v in DMF). Bromoacetic acid (12 eq, 0.6 M in DMF) and diisopropylcarbodiimide (DIC, 11.5 eq, 59% v/v in DMF) were added and mixed for 20 min. The bromide chain end was then displaced with an amine (methoxyethylamine (Nme), phenylethylamine (Npe), or phenylpropylamine (Npp), 16 eq, 1M in DMF) for 1 hr. The resin was washed with DMF five times between each synthetic step. After the desired sequence was synthesized, an additional unit was added in the same method, displacing with propargylamine (Nprg) to add an alkyne endgroup. Finally, the chain end was acetylated with a solution of equimolar acetic anhydride and pyridine (8 eq, 0.4 M in DMF), washed with DMF and dichloromethane (DCM), and dried with nitrogen flow. Polypeptoids were cleaved from the resin using 40 mL of a trifluoroacetic acid (TFA) cleavage cocktail with the composition DCM:TFA:H_2O (48.75 : 48.75 : 2.5) for 10 min. The resin was filtered and rinsed with more cleavage cocktail and DCM. The collected solution was dried *in vacuo* and lyophilized twice from acetonitrile:water (1:1) solutions to yield white powders. *Note: TFA is a volatile strong acid. Evaporation was performed with a cold trap at –90 °C. Precautions were taken to isolate TFA waste streams.* Polypeptoid molecular weight was confirmed by MALDI-MS and UPLC-MS.

3.2.3 Synthesis of azide-terminated polystyrene

First, bromine-terminated polystyrene (PS) was synthesized via atom transfer radical polymerization (ATRP). EBiB (146 gL, 1 eq), PMDETA (42 gL, 0.2 eq), and styrene (5 g, 48 eq) were combined in an oven-dried Schlenk flask. The solution was sparged with nitrogen for 30 min before adding copper (I) bromide (29 mg, 0.2 eq). The mixture was further degassed with three freeze–pump–thaw cycles (to pressures <100 mTorr), and then stirred under a nitrogen atmosphere at 100 °C until the mixture solidified, approximately 24 hours. The solid was dissolved in THF, filtered through alumina to remove copper compounds, and then precipitated into 1 L methanol. The filtered polymer was dried in vacuo overnight at 35 °C before being redissolved in DMF (at 200 mg/mL) and combined with sodium azide (90 mg, 1.5 eq). The reaction was stirred overnight at room temperature, then precipitated twice into 1 L methanol, stirring the second precipitation overnight to fully separate trace sodium azide. *Note: Sodium azide forms toxic and explosive hydrazoic acid when in contact with strong acids. Precautions were taken to isolate azide waste streams.* The final polymer was filtered and dried overnight *in vacuo* at 35 °C to yield a white solid. Molecular weight was determined by GPC against PS standards to be M_n = 5200 g/mol, Đ = 1.12.

3.2.4 Synthesis of polystyrene–polypeptoid diblock copolymers

In a typical reaction, alkyne-terminated polypeptoid (100 mg) was combined with azide-terminated polystyrene (220 mg, 2 eq) and anhydrous DMF (3 mL) in an oven-dried flask. DIPEA (37 µL, 10 eq) and PMDETA (22 µL, 5 eq) were added, and the solution was sparged with nitrogen for 30 min. In a separate, oven-dried Schlenk flask, ascorbic acid (19 mg, 6 eq) and copper (I) bromide (15 mg, 5 eq) were added, and the flask was evacuated and backfilled with nitrogen three times. The sparged solution was added to the Schlenk flask with a degassed syringe, and the mixture was further degassed with three freeze–pump–thaw cycles (to pressures <100 mTorr), before stirring under static vacuum at 50 °C for 40 hours. The

solution was then diluted with DMF and filtered through alumina to remove copper compounds. The filtrate was concentrated *in vacuo* and precipitated from THF into a mixture of 2:3 cyclohexane:hexanes to remove excess polystyrene. The precipitate was dried *in vacuo* before purifying by preparatory GPC with THF as the eluent. A final precipitation of the isolated product in 2:3 cyclohexane:hexanes and drying *in vacuo* yielded a clear, glassy solid. Purified block copolymer was characterized by MALDI-MS to ensure block coupling and the absence of unreacted homopolymer. The typical purity characterization via GPC was not possible for this system, as the polypeptoid interacts with the column, producing an artificially low molecular weight and thus an immeasurable shift in peak elution time for the block copolymer versus the polystyrene homopolymer.

3.2.5 Matrix-assisted laser desorption ionization mass spectrometry (MALDI-MS)

MALDI-MS was performed on a Bruker Microflex LRF MALDI TOF mass spectrometer. All solutions were prepared in HPLC-quality THF. Samples were dissolved at 200 gM and combined 1:1 vol/vol with 10 mg/mL dithranol (polypeptoids) or 20 mg/mL *trans*-2-[3-(4-*tert*-butylphenyl)-2-methyl-2-propenylidene]malonitrile (DCTB) with AgTFA added at 0.1 mg/mL to aid in ionization of polystyrene-containing materials. All matrix–sample mixtures were spotted (1 gL) onto a polished steel MALDI target plate (Bruker). Mass spectra were collected in positive reflectron (polypeptoids) or linear mode (diblocks copolymers), summing at least 600 shots. Mass peaks were calibrated against peptide and protein standards (Bruker, prepared as prescribed) in a mass range of 600–18,000 Da.

3.2.6 Ultra performance liquid chromatography mass spectrometry

UPLC-MS was performed on a Waters Xevo G2-XS, equipped with a time-of-flight mass spectrometer utilizing electrospray ionization. Samples were dissolved at 100 gM in appropriate acetonitrile/water mixtures for analysis (with 0.1% formic acid). Separation was

achieved on a Waters BEH C18 column with eluent gradients of 5–80% acetonitrile in water to 100% acetonitrile over 8 minutes. Polypeptoid materials were detected by UV absorption at 214 nm. Doubly, triply, and quadruply charged species were detected, with the addition of two, three, or four ions (H^+ or Na^+), respectively.

3.2.7 Gel permeation chromatography (GPC)

Analytical chromatography was performed on a Waters e2695 GPC at 35 °C with THF as the eluent (Figure 3.1). The instrument was equipped with an Agilent 6gm MiniMIX-D column, Waters 2414 differential refractive index detector, and Waters 2998 PDA detector (monitoring at 214 nm and 254 nm). Molecular weights were calibrated using polystyrene standards in the range 350–350,000 Da, and the polymer was determined to have Mn = 5200 g/mol with Đ = 1.12.

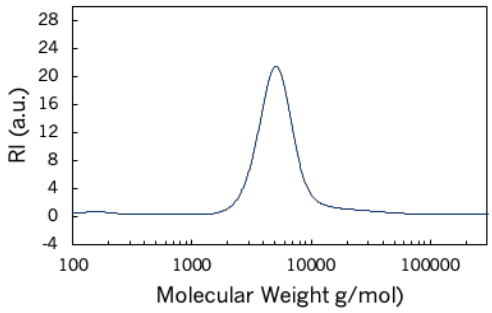

Figure 3.1 Characterization of azide-terminated polystyrene (GPC)

Preparatory GPC (prep-GPC) was performed on a similar Waters system equipped with an Agilent 10gm MIXED-D column, with THF as the eluent.

3.2.8 Small-angle X-ray scattering (SAXS)

Samples were prepared by sealing one side of aluminum washers with Kapton tape, with Kapton film blocking the adhesive in the center. Dry diblock copolymer samples were added to the center and annealed at reduced pressure (4×10^{-8} Torr) at 170 °C for at least 3 hours,

then cooled at 1 °C/min to 110 °C and annealed for at least 16 hours to form equilibrium bulk morphologies. After cooling to room temperature in vacuum, the second side of the washer was sealed.

SAXS was performed at the Advanced Light Source (ALS, beamline 7.3.3),[37] the Stanford Synchrotron Radiation Lightsource (SSRL, beamline 1-5), the National Synchrotron Light Source II (NSLS-II, beamline 11-BM), and the Advanced Photon Source (APS, beamline 12-ID-B). The beamlines were configured with X-ray energies of 10–14 keV with sample-to-detector distances of 2.8–3.6 m. Order–disorder transitions were determined at SSRL, with heating performed on a home-built stage, where temperature was measured directly at the sample position to ensure accuracy. After being loaded into the heating stage, samples were heated above 100 °C and allowed to equilibrate for 30 min before heating monotonically, equilibrating 5–15 min at each temperature before collecting exposures (Figure 3.2). Calibration using silver behenate standards, circular averaging, and correction for empty cell scattering were performed using the Nika package for Igor Pro.[38]

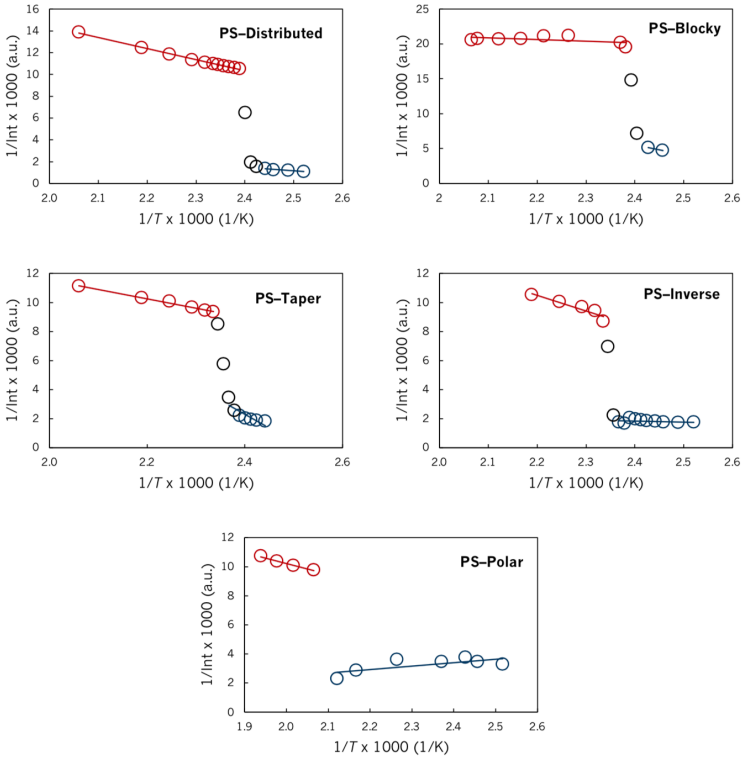

Figure 3.2 Measuring T_{ODT} from temperature-dependent SAXS

The location of the discontinuity marks the order–disorder transition temperature.

3.2.9 Self-consistent field theory

An SCFT framework was employed in which the sequence defined block copolymers are modeled as an incompressible melt of discrete Gaussian chains, with one bead of specified type for each polypeptoid residue.[39] The PS block was reduced to a discrete chain with one bead per reference volume of 0.1 nm^3 and elaborated to a chain of 50 beads consistent with the measured molecular weight and literature density. Periodic boundary conditions were applied, and a variable cell technique allows for cell relaxation.[40] To obtain a candidate morphology unit-cell structure, the symmetry of the corresponding space group was enforced on all fields and the simulation cell. The modified diffusion equations associated with forward and backward chain propagators were solved pseudospectrally.[41,42] Fields were

relaxed to saddle-point configurations using a semi-implicit scheme.[39,43] Phase boundaries were located by comparing the intensive mean-field free energies of the candidate phases.

The three binary χ values were set in the following ratio: χ_{PS-Nme}:χ_{PS-Npe}:$\chi_{Nme-Npe}$ 1.0:0.8:0.2. The two polystyrene–polypeptoid χs were each measured at 220 °C via application of the random phase approximation (RPA) to SAXS curves of the disordered phase. The Nme–Npe χ was estimated based on reference 32 and by comparing SCFT predictions to experiment. Density profiles reported here are shown at $\chi_{PS-Nme}N = 25$.

3.3 Synthesis of target polystyrene–polypeptoid diblock copolymers

Four polystyrene-*b*-copolypeptoid diblock copolymers were designed to share a common composition, and were expected to form ordered morphologies with accessible order–disorder transitions.[36] Two classes of sequences were synthesized, with compatibilizing groups distributed along the polypeptoid chain length (in blocks of 1 or 3) or tapered from the block junction (either forward or inverse) (Figure 3.3). The sequences were selected based on a fit statistic (sum of squared residuals) that was calculated against target composition profiles from all permutations of 27 and 9 beads, representing 27 polar side chains and 9 compatibilizing side chains. The composition at each unit was defined by a moving window average that sampled three repeat units to each side of the target bead, and the permutation with the lowest fit statistic was selected for each sequence (Figure 3.4).

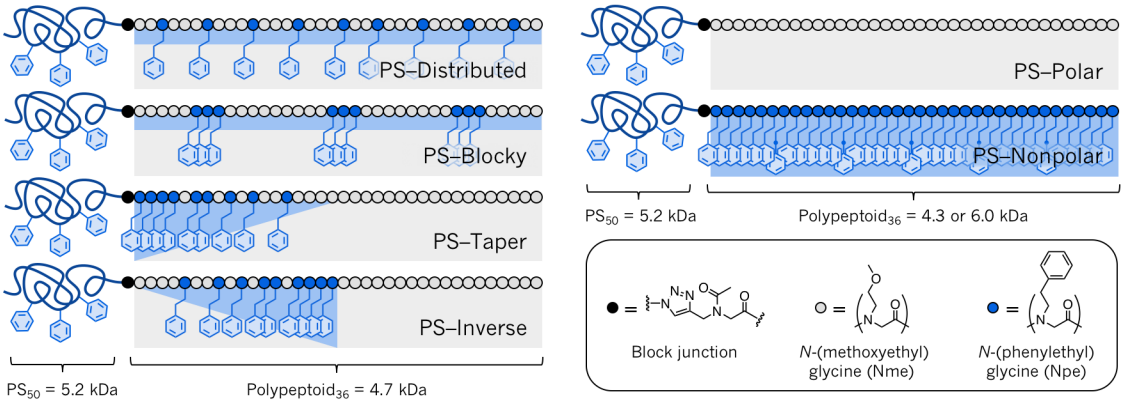

Figure 3.3 Summary of polystyrene-*b*-polypeptoid diblock copolymers

Four copolypeptoids with identical composition (left) were designed with compatibilizing groups distributed along the chain (as single units or blocks of three) or tapered from the block junction (forward or inverse). These sequences, a non-compatibilized sequence, and a fully-compatibilized sequence (right) were each clicked to polystyrene to form sequence-defined diblock copolymers.

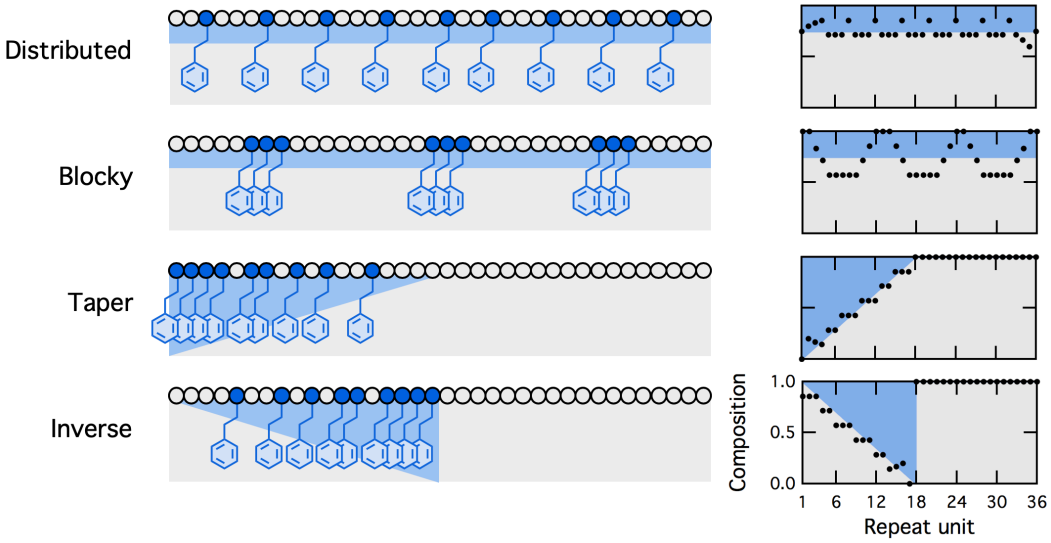

Figure 3.4 Polypeptoid sequence design

Schematics of sequences (left) and corresponding plots of local composition of Nme as a function of repeat unit (right). Local composition was defined by a rolling window average that sampled three units to each side of the center bead.

Alkyne-terminated polypeptoids were successfully synthesized via solid phase synthesis using the submonomer method[24] and are summarized in Table 3.1. Two polypeptoid repeat units were chosen: a polar side chain to encourage self-assembly (*N*-(2-methoxyethyl) glycine, Nme), and another to mimic the phenyl side chains of polystyrene to tune

compatibility (*N*-(2-phenylethyl)glycine, Npe). The all-polar sequence was synthesized as a homopolypeptoid of Nme. The all-nonpolar sequence was synthesized as a copolypeptoid of Npe and *N*-(2-phenylpropyl)glycine (Npp) to prevent crystallization.[29] Solid-phase polypeptoid synthesis produced the target sequences with high fidelity (Figure 3.5).

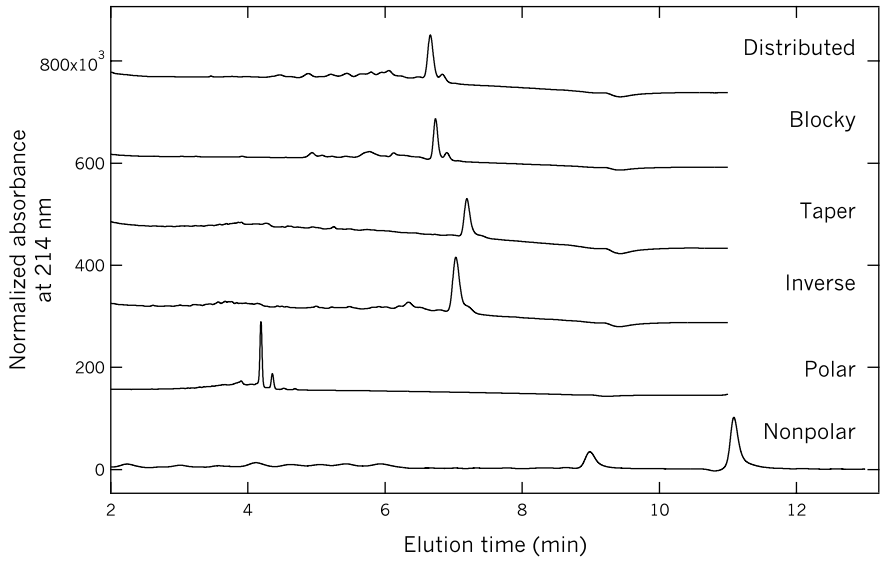

Figure 3.5 Characterization of target polypeptoid materials (UPLC-MS)

UPLC-MS chromatograms are shown with normalized absorption at 214 nm plotted against elution time and are vertically offset for clarity. The largest peak represents the target sequence for all materials, and impurities visible as small peaks at lower elution times are polypeptoid chains missing one, two, three, etc. repeat units.

Block copolymers were synthesized by conjugating alkyne-terminated polypeptoids with azide-terminated polystyrene via copper-mediated azide–alkyne click chemistry. All materials were synthesized from the same batch of azido-polystyrene, with low dispersity ($Đ = 1.12$). Extreme care was taken to purify diblock copolymers from unreacted homopolymer. Precipitation followed by prep-GPC yielded isolated diblocks with effectively no homopolymer impurities, as determined by MALDI-MS (Figure 3.6). A summary of molecular properties is shown in Table 3.1.

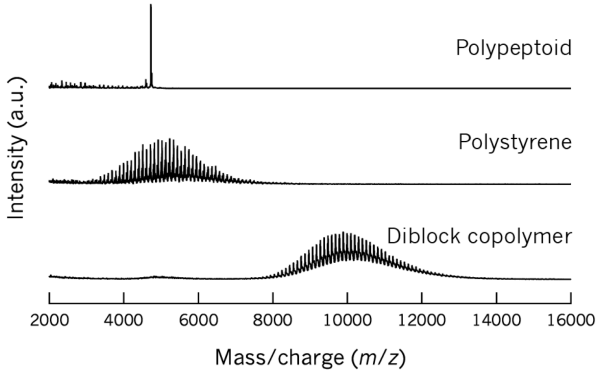

Figure 3.6 MALDI-MS of polypeptoid, polystyrene, and diblock copolymer

Representative MALDI mass spectrometry of the constituent blocks and diblock copolymer after purification. The material shown is PS–Distributed. Spectra are vertically offset for clarity.

Table 3.1 Summary of polypeptoids synthesized and their characteristics

Sequence name	Sequence	Mass (observed/ theoretical)
Distributed	Ac-Nprg-NmeNme$(NpeNme_3)_4$NpeNme$_2$$(NpeNme_3)_3$NpeNme$_2$	4712.0/4712.6
Blocky	Ac-Nprg-$Nme_5Npe_3Nme_9Npe_3Nme_8Npe_3Nme_5$	4712.9/4712.6
Taper	Ac-Nprg-Npe_4NmeNpe$_2$NmeNpeNmeNpeNme$_2$NpeNme$_{22}$	4712.1/4712.6
Inverse	Ac-Nprg-Nme_4NpeNme$_2$NpeNmeNpeNmeNpe$_2$NmeNpe$_4$Nme$_{18}$	4712.1/4712.6
Polar	Ac-Nprg-Nme_{36}	4298.1/4298.4
Nonpolar	Ac-Nprg-$Npe_6(NppNpe_5)_5$	6027.3/6027.2

3.4 Self-assembly and chain conformation effects

Both domain spacing and order–disorder transition temperature were found to depend on sequence, likely due to a combination of two factors: chain conformation effects arising from the localization of compatibilizing groups and tuning of the segregation strength between blocks. First, domain spacing is discussed in the context of possible preferred chain conformations. Next, order–disorder transitions are compared with effective χ parameters, calculated by applying the random phase approximation to X-ray scattering of the disordered phase, and simulations using self-consistent field theory. Overall, it is found that sequence-dependent chain conformations dominate the observed behaviors, as "smearing out" of the sequence to measure an effective χ and coarse-grained simulations both fail to capture thermodynamic transitions that arise from molecular-scale effects.

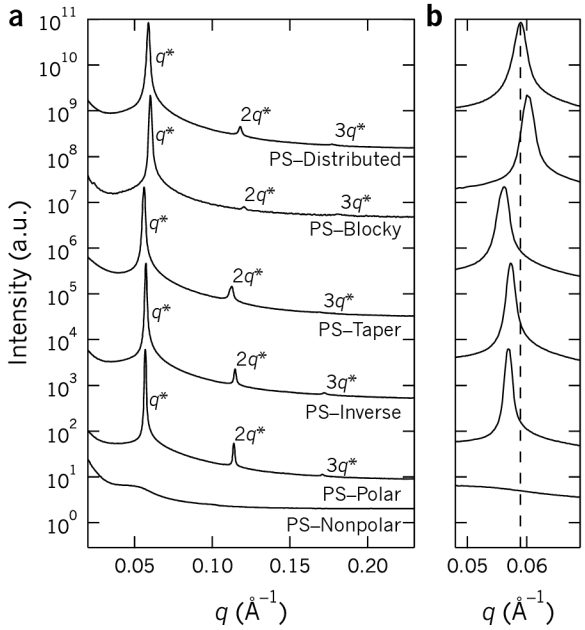

Figure 3.7 Small-angle X-ray scattering of polystyrene–polypeptoid diblock copolymers

a) Peaks at integer multiples of the primary peak (q^*) show that all materials form a lamellar morphology except the nonpolar block copolymer. b) Magnifying the low-q region reveals differences in primary peak position. The dashed line is a guide to the eye centered at q^* of PS–Distributed. Data shown were collected at room temperature and are vertically offset for clarity.

All PS–copolypeptoid diblock copolymers formed lamellar microstructures, assigned via small-angle X-ray scattering (SAXS) by the appearance of a sharp primary peak (q^*) and peaks at integer multiples of q^* (Figure 3a). Domain spacing was calculated from the position of the primary scattering peak as $d = 2\pi/q^*$ (Figure 3b), and was found to vary significantly with sequence, despite all sequence-defined materials sharing the exact same composition and length (Figure 3.8a, Table 3.2).

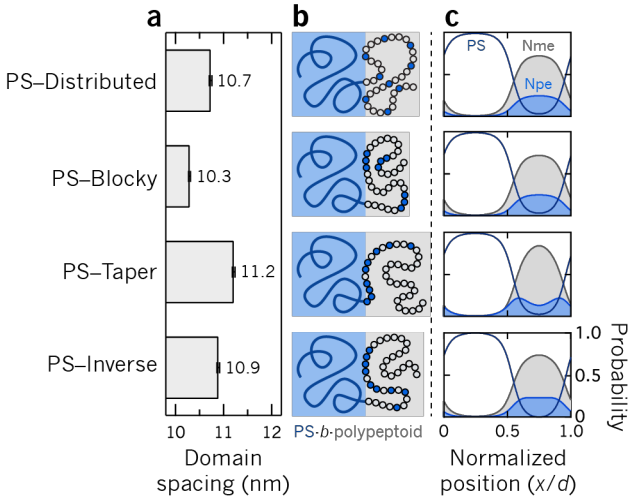

Figure 3.8 Domain spacing and chain conformation

a) Domain spacing of lamellar sequence-defined diblock copolymers as measured by SAXS. Error bars arise from limited instrument resolution in q and residuals to fits to the primary scattering peak by a Gaussian function. b) Schematics of representative chain conformations that result in the measured domain spacings. c) Density profiles for components within the lamellar domain as predicted by SCFT.

Simulations performed with self-consistent field theory reproduce the relative domain spacings measured by SAXS as $d_{PS–Taper} > d_{PS–Inverse} > d_{PS–Distributed} > d_{PS–Blocky}$, and the distribution of components within the lamellar domain varies as a function of sequence, as shown in simulated density profiles (Figure 4c). Notably, the compatibilizing Npe groups of PS–Taper are strongly localized at the domain interfaces, reflecting their placement in the sequence near the block junction and their affinity for the polystyrene-rich region. The distributed sequences (PS–Distributed and PS–Blocky) have more compatibilizing groups in the center of the domain, and PS–Inverse has an intermediate profile.

Table 3.2 Self-assembly of PS–polypeptoid diblock copolymers

Sample name	PS M_n (g/mol)[a]	PS Đ[a]	Polypeptoid mass (g/mol)	$f_{peptoid}$	Morphology	Domain spacing (± 0.03 nm)	T_{ODT} (± 1 °C)
PS–Distributed	5200	1.12	4712	0.44	LAM	10.73 nm	143 °C
PS–Blocky	5200	1.12	4712	0.44	LAM	10.29 nm	143 °C
PS–Taper	5200	1.12	4712	0.44	LAM	11.21 nm	151 °C
PS–Inverse	5200	1.12	4712	0.44	LAM	10.89 nm	153 °C
PS–Polar	5200	1.12	4298	0.42	LAM	11.06 nm	205 °C
PS–Nonpolar	5200	1.12	6027	0.51	DIS	N.A.	N.A.

"LAM" denotes lamellar, "DIS" denotes disordered. [a]PS number-average molecular weight (M_n) and dispersity (Đ) were determined by GPC against polystyrene standards. The volume fraction of peptoid ($f_{peptoid}$) was calculated using a polypeptoid density of 1.18 g/cm^3, as measured in reference 36, and polystyrene density of 1.04 g/cm^3. The order–disorder transition temperature (T_{ODT}) was determined by temperature-dependent SAXS.

The variation in domain spacing can be rationalized with an enthalpic argument, where the system's energy is lowered by adopting chain conformations that minimize the enthalpy of mixing (Figure 3.8b). The system suffers an energetic penalty when polar and nonpolar side chains are forced to mix, but this unfavorable interaction can be avoided by inserting the nonpolar components of the polypeptoid into the polystyrene microdomain. This enthalpic effect alters the chain conformation in both the ordered and disordered phases, as evidenced by domain spacing and disordered phase radius of gyration that both track with sequence (Figure 3.9). However, the relative variation in R_g is smaller than that measured in domain spacing (plotted on proportional axes, the dashed lines in Figure 3.9 demonstrate the total variation in domain spacing with sequence; the variation in R_g is much within these bounds).

Since it is expected that $d \sim R_g$, the conformational effects stemming from the sequence of compatibilizing groups must be exaggerated in the ordered phase—where all of the nonpolar polypeptoid units have mainly polar polypeptoid as nearest neighbors, as opposed to the prevalence of nearby nonpolar polystyrene in the disordered phase.

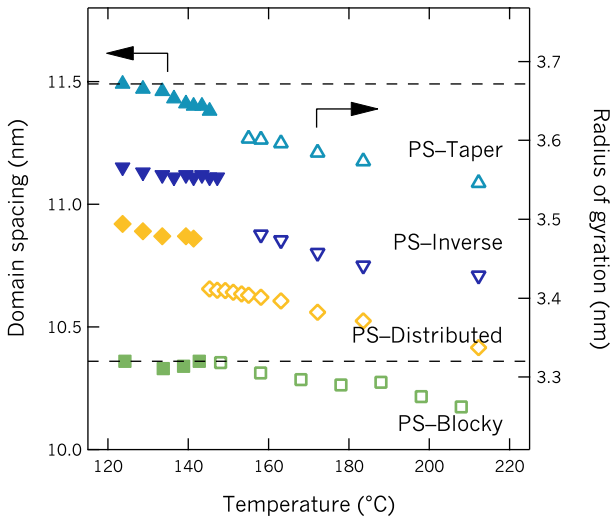

Figure 3.9 Characteristic lengthscales as a function of temperature and sequence

Domain spacing (left axis, closed symbols) was calculated using the primary scattering peak in the ordered state ($d = 2\pi/q^*$), and radius of gyration (right axis, open symbols) was taken from RPA fits in the disordered state. Values are plotted on proportional axes, and dashed lines indicate the total variation in domain spacing at 125 °C. All error bars are smaller than the markers.

The sequences with the smallest domain spacings are PS–Blocky and PS–Distributed (10.29 nm and 10.73 nm, respectively). All domain spacings have an error of ± 0.03 nm. These sequences have compatibilizing phenyl units distributed along the entire block length, which likely promotes flattened chain conformations that allow these nonpolar units to access the PS–polypeptoid interface more easily and lead to a smaller domain spacing. This hypothesis is supported by simulations performed with SCFT. Key regions of the polypeptoid block were selected as tracers (the chain middle and chain end, Figure 3.10a), and an example density profile for these tracers in the ordered lamellar phase is shown in Figure 3.10b, with probability (normalized by the maximum probability) plotted against position within the lamellar microdomain (normalized by domain spacing). For the sequences with distributed compatibilizing groups (PS–Distributed and PS–Blocky), the polypeptoid chain end is more likely to be at the PS–polypeptoid interface than for the tapered sequences or polar sequence

(Figure 3.10d), which causes these materials to have more compact chain conformations and smaller domain spacings.

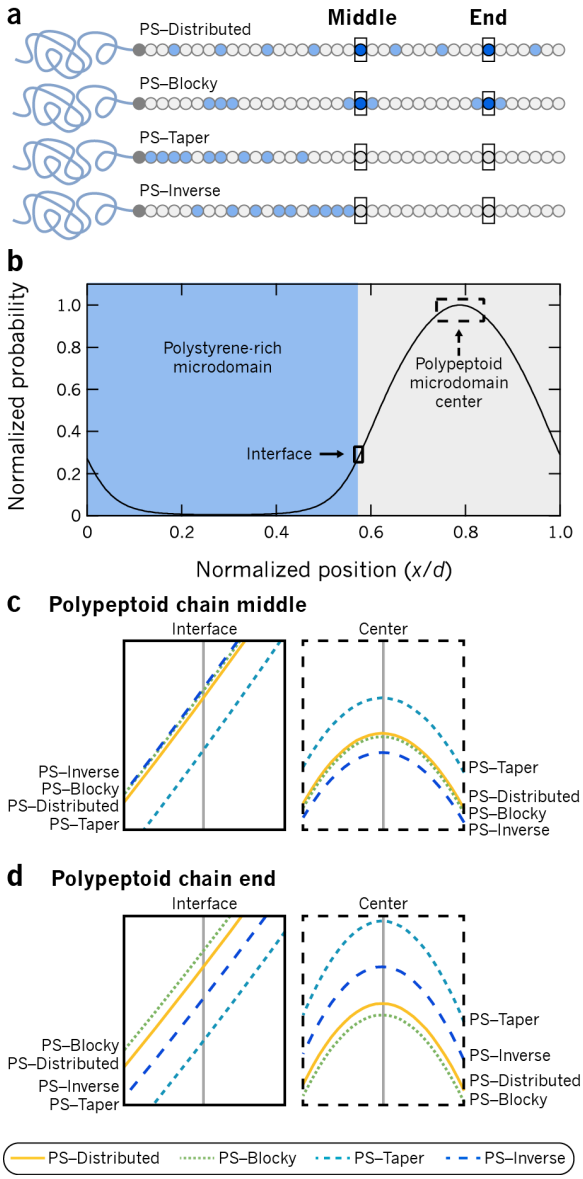

Figure 3.10 Composition profiles predicted by SCFT simulations

a) Two regions of the polypeptoid chain were chosen as tracers: the middle and near the chain end. b) A representative density profile is plotted against position within the lamellar microdomain, with the PS-rich region depicted on the left and polypeptoid-rich region on the right. Insets of the domain interface and polypeptoid domain center are shown for the c) middle region and d) chain end tracers. Comparing density profiles between sequences supports the existence of chain conformational effects in the ordered phase.

Conversely, the tapered sequence (PS–Taper) has the largest domain spacing (11.21 nm). With all of its compatibilizing groups placed near the block junction, a long polar tail is left to extend into and expand the domain. The inverse taper sequence (PS–Inverse) has elements of both these extremes and, as expected, an intermediate domain spacing (10.89 nm). Its compatibilizing units are concentrated toward the center of the block, allowing the middle of

the polypeptoid chain to localize at the PS interface and fold the chain into a more compact conformation. However, the lack of nonpolar units in the second half of the sequence may cause PS–Inverse to take on conformations that are more extended than the distributed sequences, whose chain ends have nonpolar units that can localize at the interface and thus shrink the domain. In Figure 3.10c, we see from simulations that, indeed, the middle of the Taper block is more likely to lie in the center of the polypeptoid domain than the middle of the Inverse block, whose nonpolar units are seen to migrate more strongly toward the interface. Further, the polar chain ends of both the Taper and Inverse blocks are much more likely to be in the polypeptoid microdomain center than either of the distributed sequences (Figure 3.10d).

3.5 Thermodynamic effects and segregation strength

Adding compatibilizing phenyl groups lowers the interaction parameter between the polar polypeptoid and nonpolar polystyrene blocks, with the precise sequence in which compatibilizing groups are incorporated resulting in variations in the order–disorder transition temperature and effective χ, despite the different copolypeptoid materials having the same composition. In addition to the geometric differences discussed above, these thermodynamic differences suggest that the details of monomer-level sequence are critical in dictating the segregation strength.

To quantify the segregation strength between blocks, we applied the random phase approximation (RPA) for a diblock copolymer melt to scattering profiles in the disordered phase,[1] extracting an effective χ parameter (χ_{eff}) as a function of sequence and temperature (see Appendix for fit details). We use the term "effective" interaction parameter to refer to a simple PS–polypeptoid χ, where the polypeptoid is considered to be a homogeneous or "smeared out" block for the purpose of fitting to the diblock copolymer RPA expression. This

approach was favored over other treatments, such as comparing the order–disorder transition to mean field theory predictions, due to suspected non-ideal chain conformations.

The disordered phase is accessible for all materials upon heating, as evidenced by the transition to a broad scattering peak corresponding to density fluctuations in the disordered melt that arise from the connectivity of the two dissimilar blocks. The q-position of the peak corresponds to the lengthscale of fluctuations (determined by the radius of gyration, R_g, of the block copolymer), and the breadth of the peak is determined by the strength of the interaction parameter. Due to a combination of unfavorable chain stretching at long lengthscales and dominant intrablock correlations at monomer lengthscales, the structure factor approaches zero intensity at both low- and high-q limits, respectively. Scattering curves were fit well with RPA (Figure 3.11) using χ_{eff}, R_g, and C as adjustable parameters, where C is a scaling constant that accounts for the arbitrary units of intensity and for constant prefactors related to scattering contrast and volume. It was assumed that the diblock copolymers were conformationally symmetric (statistical segment lengths for polystyrene and polypeptoids are similar, at 0.5 nm[44] and 0.4 nm[45], respectively). A reference volume of 0.1 nm^3 was used.

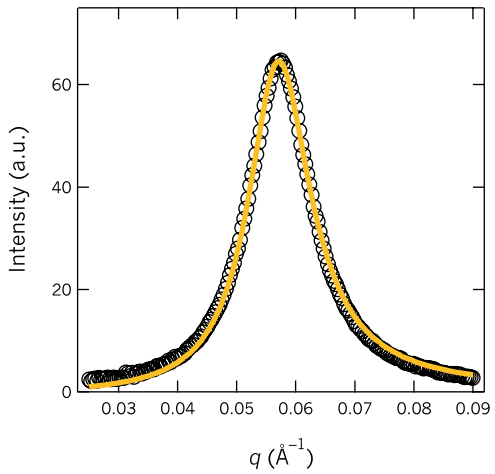

Figure 3.11 Fitting the random phase approximation to disordered scattering

Representative SAXS profile in the disordered phase, fit with the random phase approximation allowing effective interaction parameter (χ_{eff}), radius of gyration (R_g), and a scaling constant C to vary. Data are shown with black circles; the fit is shown with a yellow line. The example shown is PS–Distributed at 147 °C.

As expected, PS–Polar, with no compatibilizing groups, has the highest interaction parameter (Figure 3.12a). All sequence-defined diblock copolymers have lower χ_{eff} values, indicating that the incorporation of compatibilizing phenyl groups directly lowers the effective interaction parameter. Compatibilization is also evidenced by differences in order–disorder transition temperatures (Figure 3.12b). PS–Polar has the highest T_{ODT} at 205 °C, corroborating the high χ parameter measured between the polar polypeptoid and nonpolar polystyrene, especially given the small total molecular weight of ~10 kDa. By replacing 25% of the polar ether side chains with nonpolar phenyl groups, the T_{ODT} drops by as much as 62 °C, demonstrating a lowered interaction parameter with the polystyrene block.

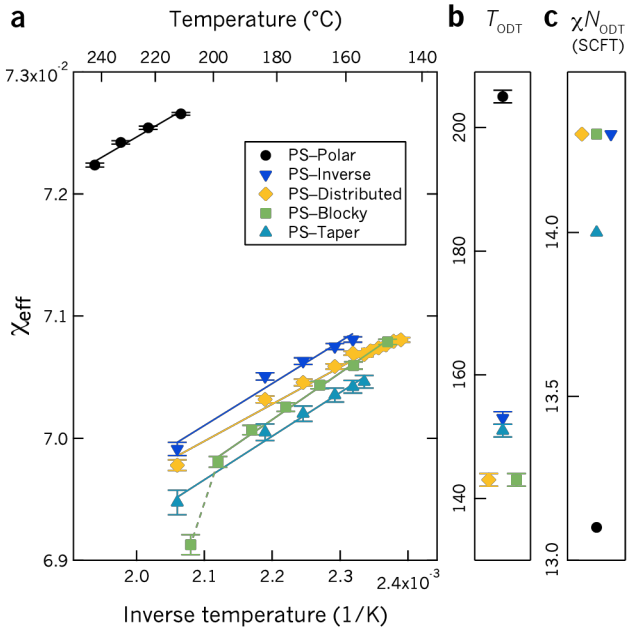

Figure 3.12 Comparison of thermodynamic factors (χ_{eff}, T_{ODT}, $\chi N_{ODT,SCFT}$)

a) The PS–polypeptoid effective interaction parameter (χ_{eff}) varies as a function of sequence and temperature. Solid lines are fits with the relationship $\chi_{eff} = A/T + B$, and error bars represent 95% confidence intervals from the fits. The dashed line is a guide to the eye and may signify a second order dependence on inverse temperature, possibly due to the breaking up of nonpolar aggregates of Npe side chains. b) Order–disorder transition temperature and c) χN at the ODT (as predicted by SCFT) both vary with sequence. Neither χ_{eff} nor χN_{ODT} reproduce the trends seen in the experimental T_{ODT}.

Among the sequence-defined copolypeptoid diblocks, the T_{ODT} varies markedly as a function of sequence (Figure 3.12b). The diblock copolymers with distributed sequences (PS–Distributed and PS–Blocky) disorder at the lowest temperature, both at 143 °C (± 1 °C for all T_{ODT}s). With compatibilizing groups distributed along the chain length, the nonpolar repeat units may be better solubilized in the polar polypeptoid, resulting in mixing (disordering) at lower temperatures upon heating. PS–Taper disorders at an intermediate temperature (151 °C), and PS–Inverse disorders at the highest temperature (153 °C). Comparing to references 8 and 9, the observed reversal of the relative transition temperatures between tapered and inverse tapered materials is likely due to a combination of two major differences between the systems: precise (versus average) sequence control and the use of a "styrene-like" compatibilizing group in this system. Dispersity in comonomer sequence is expected to affect relative phase stability, and the use of a "styrene-like" side chain leads to a weaker compatibilization between the two blocks compared to a

system that incorporates pure styrene repeat units into the polypeptoid block (which is impossible to do with the present chemistry).

Within the compatibilized materials, it is informative to compare the calculated χ_{eff} parameters with the measured order–disorder transition temperatures (Figure 3.12a and b), which might be expected to track together. First, the diblock copolymer with an inverse taper has the highest χ_{eff}, which is consistent with the result that it also disorders at the highest temperature. Apart from this material, the rest of the effective interaction parameters do not match their order–disorder transition temperatures: the tapered sequence has the lowest χ_{eff}, although it has the second highest disordering temperature, and the distributed sequences have intermediate χ_{eff}s but share the lowest disordering temperature. With this disagreement, it is important to consider that the order–disorder transition is inherently tied to both the ordered and disordered phases, because it corresponds to a point where their free energies coincide. Here, χ_{eff} is measured only in the disordered phase, and with sequence-dependent conformations in the ordered phase, this χ_{eff} does not necessarily describe the ordered phase or the transition to disorder. The lack of agreement between measured phase transitions and the relative order of effective χ parameters emphasizes the need for molecular-lengthscale information in applying RPA analyses to copolymer systems with varying distributions of comonomers. For example, this work implies that the application of a single χ parameter to a random copolymer may not fully capture the details of monomer-lengthscale distribution of functional groups, especially at short polymer lengths.

Further, if the effective χ concept were valid for these sequence-defined materials, then the domain spacing d in the lamellar phase could be related to χ_{eff} by a form imposed by SCFT: $d = R_g F(\chi_{eff}N)$, where R_g is the disordered phase radius of gyration and F is a dimensionless function of $\chi_{eff}N$. From the RPA fits above the order–disorder transition, we

find that the order of R_g parallels that of d (Figure 3.9), satisfying $d \sim R_g$ and indicating that some degree of the conformational effects detected in the ordered phase persist into the disordered phase. The function F is known numerically to be approximately 3.2 near the ODT at $\chi_{\text{eff}}N \sim 10$, and asymptotically scales as $(\chi_{\text{eff}}N)^{1/6}$ for strong segregation strength.[46] Furthermore, F is a monotonically increasing function of $\chi_{\text{eff}}N$, so a sequence-specific trend in χ_{eff} must translate into the same trend in d if the effective χ concept were to hold. Since this is not observed, we conclude that the notion of replacing a heterogeneous block by a "smeared out" homogenous block with an effective interaction parameter is too simplistic and has little predictive value for order–disorder transitions or ordered phase properties. Indeed, even for block polymers with purely homogeneous blocks, T_{ODT} and d are sensitive to block architecture and molecular weight, reflecting a complex balance of enthalpic interactions and conformational entropy in the ordered state.[47] It is therefore unreasonable to expect that sequence-dependent effects in polymers with heterogeneous blocks could be predicted by an effective χ deduced from the disordered state, and more complex descriptors that account for chain conformational effects should be pursued.

Finally, order–disorder transitions were calculated by SCFT simulations (Figure 3.12c) by comparing the intensive mean-field free energies of the candidate phases, employing the same three-χ framework and full sequence definition utilized in calculating the relative domain spacings above. A large difference is correctly predicted between PS–Polar and the rest of the materials, but the trends within the sequence-defined materials do not agree with those measured in experiment. While SCFT (mean-field theory) captures structural effects in the ordered phase well, such as the geometric effects seen in domain spacing and chain conformations, the location of the phase transition is sensitive to fluctuation effects in both disordered and ordered phases, so it is not surprising that the sequence-dependent trends in the order–disorder transition are not reproduced. This is further evidence that more

complex approaches that explicitly account for chain conformation should be pursued to describe systems with heterogeneous blocks.

3.6 Conclusions

A series of sequence-defined diblock copolymers was synthesized, and both morphological and thermodynamic effects were measured. It was found that domain spacing and order–disorder transition temperature are functions of sequence. The differences in these parameters are attributed to the dominating effect of an altered chain conformation in the ordered state that localizes compatibilizing groups at the polystyrene–polypeptoid interface.

Sequences with distributed compatibilizing groups have smaller domain spacings and lower order–disorder transition temperatures than those with compatibilizing groups tapered from the block junction (either forward or inverse). Simulations using self-consistent field theory reproduce the relative domain spacings and predict different distributions of compatibilizing groups within the polypeptoid domain based on sequence, supporting the suggested conformational effects in the ordered state. In the disordered state, altered chain conformations persist, as evidenced by relative radii of gyration that parallel the relative domain spacings. However, the mismatch between sequence-specific trends in order–disorder transition temperatures and effective interaction parameters (extracted from disordered phase scattering measurements) suggests that the effective χ concept has limited predictive value in anticipating T_{ODT} or ordered phase properties of sequence-specific block copolymers. Similarly, simulations performed with SCFT also do not match the trends seen in T_{ODT}, further demonstrating that these coarse-grained approaches do not capture thermodynamic trends seen in sequence-defined materials.

These results suggest that monomer-level sequence control influences both morphological and thermal properties via chain conformational effects. Exercising such

sequence control could lead to new materials with tunable self-assembly properties based on sequence alone.

3.7 Acknowledgements

The authors gratefully acknowledge funding from the National Science Foundation (NSF) Division of Materials Research (DMR) Polymers program (DMR-1608297) for synthesis and characterization of block copolymers and the NSF Condensed Matter and Materials Theory Program (DMR-1822215) for the SCFT simulations. A.L.P. gratefully acknowledges the NSF for a graduate research fellowship. Polypeptoid characterization and block copolymer purification were performed with guidance from Dr. Rachel Behrens and with support from the MRL Shared Experimental Facilities (supported by the MRSEC Program of the NSF, DMR-1720256; a member of the NSF-funded Materials Research Facilities Network). SCFT simulations utilized resources of the Center for Scientific Computing from the UCSB CNSI, MRL, and NSF MRSEC (DMR-1720256) and NSF CNS-1725797. X-ray scattering experiments utilized resources of the Advanced Light Source (a U.S. Department of Energy (DOE) Office of Science User Facility, DE-AC02-05CH11231; beamline 7.3.3), the Stanford Synchrotron Radiation Lightsource (supported by the U.S. DOE Office of Science, Office of Basic Energy Sciences, DE-AC02-76SF00515; beamline 1-5), the National Synchrotron Light Source II (a U.S. DOE Office of Science User Facility operated for the DOE Office of Science by Brookhaven National Laboratory, DE-SC0012704; beamline 11-BM), and the Advanced Photon Source (a U.S. DOE Office of Science User Facility operated for the DOE Office of Science by Argonne National Laboratory, DE-AC02-06CH11357; beamline 12-ID-B). A.L.P. thanks Dr. Morgan Schulze (UCSB) for X-ray scattering resources and Andrew Turner (MIT) for input in programming the sequence selection. The authors also thank Dr. Ron Zuckermann at the Molecular Foundry of the Lawrence Berkeley National Lab for helpful discussions regarding polypeptoid synthesis.

3.8 Appendix

*3.8.1 Peak fitting for determination of q**

Domain spacing (d) was determined by analysis of the primary scattering peak (q^*) from small-angle X-ray scattering as $d = 2\pi/q^*$. The error in q^* is a combination of error resulting from the goodness of fit to a Gaussian peak and instrumental error in the form of finite resolution in q. Peaks were fit using the `CurveFit` function in IgorPro:

```
CurveFit/ODR=2 gauss,
      waveInt[start,stop]
      /X=waveQ[start,stop]/D/R/I=1
      /XW=waveQerr[start,stop]
```

Where `waveInt` is the measured intensity, `waveQ` is the q vector, `waveQerr` is the error in q due to finite detector pixel size, and `start` and `stop` are integer data points that bound the peak (selected using the cursors). As there is no meaningful measurement of the error in intensity, approximated only as $\sqrt{I(q)}$, this source of error was not included in the fit for position q^*. Error in d was calculated through standard error propagation.

3.8.2 Random phase approximation

The random phase approximation for a diblock copolymer was employed to measure the effective χ of polystyrene–polypeptoid materials, treating the copolypeptoid chain as a single effective homogeneous block. The following expression for intensity as a function of q was used:

$$I(q) = \left(\frac{b_1}{v_1} - \frac{b_2}{v_2}\right)^2 S(q) = C\,S(q) = C\left(\frac{F(f,q,R_g)}{N} - 2\chi\right)^{-1}$$

Where:

$$F(f,q,R_g) = \frac{g(1,q,R_g)}{g(f,q,R_g)g(1-f,q,R_g) - \frac{1}{4}\left[g(1,q,R_g) - g(f,q,R_g) - g(1-f,q,R_g)\right]^2},$$

$g(f,q,R_g)$ is the Debye function:

$$g(f,q,R_g) = \frac{2\left[f(q^2{R_g}^2)+e^{-f(q^2{R_g}^2)}-1\right]}{(q^2{R_g}^2)^2},$$

and the scattering lengths (b_i) and volumes (v_i) are represented by a constant scalar C in order to account for the arbitrary units of scattering. Note that absolute scattering would utilize these parameters explicitly but was not necessary for measuring the trends presented here.

A summary of the dependence of χ_{eff} on inverse temperature is given below as the coefficients to linear fits of $\chi_{\text{eff}} = \text{A}/T + \text{B}$.

Material	A (K)	B
PS–Distributed	2.77 ± 0.10	0.06423 ± 0.00023
PS–Blocky	3.75 ± 0.15	0.06191 ± 0.00035
PS–Taper	3.37 ± 0.34	0.06261 ± 0.00078
PS–Inverse	3.03 ± 0.19	0.06380 ± 0.00043
PS–Polar	3.10 ± 0.14	0.06628 ± 0.00028

3.8.3 Applying the random phase approximation in Mathematica

The above structure factor $S(q)$ was defined in Mathematica as a model (`modelMaterial`) for each material as a function of volume fraction, q, R_g, N, and C. This model was called in a nonlinear fit with 95% confidence intervals to fit disordered scattering peaks:

```
fitMaterialTemp=
      NonlinearModelFit[
            dataMaterialTemp[[start;;stop]],{1,2}]],
            {modelMaterial,500>Rg>1,1>χ>0,C>0},
            {Rg,χ,C},q,ConfidenceLevel→0.95];
```

where `dataMaterialTemp` is a 4-column text file with q, Intensity, q error, and Intensity error, and `start` and `stop` are integers referring to data points bounding the disordered peak (selected using the cursors in IgorPro).

3.9 References

(1) Leibler, L. Theory of Microphase Separation in Block Copolymers. *Macromolecules* **1980,** *13* (6), 1602-1617.

(2) Beckingham, B. S.; Register, R. A. Synthesis and Phase Behavior of Block-Random Copolymers of Styrene and Hydrogenated Isoprene. *Macromolecules* **2011,** *44* (11), 4313-4319.

(3) Quinn, J. D.; Register, R. A. Microphase Separation in Block-Random Copolymers of Styrene, 4-Acetoxystyrene, and 4-Hydroxystyrene. *J. Polym. Sci. Pol. Phys.* **2009,** *47* (21), 2106-2113.

(4) Kim, J.; Gray, M. K.; Zhou, H. Y.; Nguyen, S. T.; Torkelson, J. M. Polymer blend compatibilization by gradient copolymer addition during melt processing: Stabilization of dispersed phase to static coarsening. *Macromolecules* **2005,** *38* (4), 1037-1040.

(5) Wong, C. L. H.; Kim, J.; Torkelson, J. M. Breadth of glass transition temperature in styrene/acrylic acid block, random, and gradient copolymers: Unusual sequence distribution effects. *J. Polym. Sci. Pol. Phys.* **2007,** *45* (20), 2842-2849.

(6) Jouenne, S.; Gonzalez-Leon, J. A.; Ruzette, A.-V.; Lodefier, P.; Tence-Girault, S.; Leibler, L. Styrene/butadiene gradient block copolymers: Molecular and mesoscopic structures. *Macromolecules* **2007,** *40* (7), 2432-2442.

(7) Mastroianni, S. E.; Epps, T. H., III Interfacial Manipulations: Controlling Nanoscale Assembly in Bulk, Thin Film, and Solution Block Copolymer Systems. *Langmuir* **2013,** *29* (12), 3864-3878.

(8) Singh, N.; Tureau, M. S.; Epps, T. H., III Manipulating ordering transitions in interfacially modified block copolymers. *Soft Matter* **2009,** *5* (23), 4757-4762.

(9) Roy, R.; Park, J. K.; Young, W. S.; Mastroianni, S. E.; Tureau, M. S.; Epps, T. H., III Double-Gyroid Network Morphology in Tapered Diblock Copolymers. *Macromolecules* **2011,** *44* (10), 3910-3915.

(10) Tsukahara, Y.; Nakamura, N.; Hashimoto, T.; Kawai, H.; Nagaya, T.; Sugimura, Y.; Tsuge, S. Structure and Properties of Tapered Block Polymers of Styrene and Isoprene. *Polym. J.* **1980,** *12* (7), 455-466.

(11) Lutz, J. F.; Schmidt, B. V. K. J.; Pfeifer, S. Tailored Polymer Microstructures Prepared by Atom Transfer Radical Copolymerization of Styrene and N-substituted Maleimides. *Macromol. Rapid Commun.* **2011,** *32* (2), 127-135.

(12) Seo, Y.; Brown, J. R.; Hall, L. M. Effect of Tapering on Morphology and Interfacial Behavior of Diblock Copolymers from Molecular Dynamics Simulations. *Macromolecules* **2015,** *48* (14), 4974-4982.

(13) Ganesan, V.; Kumar, N. A.; Pryamitsyn, V. Blockiness and Sequence Polydispersity Effects on the Phase Behavior and Interfacial Properties of Gradient Copolymers. *Macromolecules* **2012,** *45* (15), 6281-6297.

(14) Chang, L. W.; Lytle, T. K.; Radhakrishna, M.; Madinya, J. J.; Velez, J.; Sing, C. E.; Perry, S. L. Sequence and entropy-based control of complex coacervates. *Nat. Commun.* **2017,** *8*.

(15) Barnes, J. C.; Ehrlich, D. J. C.; Gao, A. X.; Leibfarth, F. A.; Jiang, Y. V.; Zhou, E.; Jamison, T. F.; Johnson, J. A. Iterative exponential growth of stereo- and sequence-controlled polymers. *Nat. Chem.* **2015,** *7* (10), 810-815.

(16) Jiang, Y.; Golder, M. R.; Nguyen, H. V. T.; Wang, Y. F.; Zhong, M. J.; Barnes, J. C.; Ehrlich, D. J. C.; Johnson, J. A. Iterative Exponential Growth Synthesis and Assembly of Uniform Diblock Copolymers. *J. Am. Chem. Soc.* **2016,** *138* (30), 9369-9372.

(17) Gutekunst, W. R.; Hawker, C. J. A General Approach to Sequence-Controlled Polymers Using Macrocyclic Ring Opening Metathesis Polymerization. *J. Am. Chem. Soc.* **2015,** *137* (25), 8038-8041.

(18) Fu, C. K.; Huang, Z. X.; Hawker, C. J.; Moad, G.; Xu, J. T.; Boyer, C. RAFT-mediated, visible light-initiated single unit monomer insertion and its application in the synthesis of sequence-defined polymers. *Polym. Chem.* **2017,** *8* (32), 4637-4643.

(19) Solleder, S. C.; Meier, M. A. R. Sequence Control in Polymer Chemistry through the Passerini Three-Component Reaction. *Angew. Chem., Int. Ed.* **2014,** *53* (3), 711-714.

(20) Berthet, M. A.; Zarafshani, Z.; Pfeifer, S.; Lutz, J. F. Facile Synthesis of Functional Periodic Copolymers: A Step toward Polymer-Based Molecular Arrays. *Macromolecules* **2010,** *43* (1), 44-50.

(21) Al Ouahabi, A.; Kotera, M.; Charles, L.; Lutz, J. F. Synthesis of Monodisperse Sequence-Coded Polymers with Chain Lengths above DP100. *ACS Macro Lett.* **2015,** *4* (10), 1077-1080.

(22) Boz, E.; Wagener, K. B.; Ghosal, A.; Fu, R. Q.; Alamo, R. G. Synthesis and crystallization of precision ADMET polyolefins containing halogens. *Macromolecules* **2006,** *39* (13), 4437-4447.

(23) Baughman, T. W.; Chan, C. D.; Winey, K. I.; Wagener, K. B. Synthesis and morphology of well-defined poly(ethylene-co-acrylic acid) copolymers. *Macromolecules* **2007,** *40* (18), 6564-6571.

(24) Zuckermann, R. N.; Kerr, J. M.; Kent, S. B. H.; Moos, W. H. Efficient Method for the Preparation of Peptoids [Oligo(N-substituted glycines)] by Submonomer Solid-Phase Synthesis. *J. Am. Chem. Soc.* **1992,** *114* (26), 10646-10647.

(25) Nam, K. T.; Shelby, S. A.; Choi, P. H.; Marciel, A. B.; Chen, R.; Tan, L.; Chu, T. K.; Mesch, R. A.; Lee, B. C.; Connolly, M. D.; Kisielowski, C.; Zuckermann, R. N. Free-floating ultrathin two-dimensional crystals from sequence-specific peptoid polymers. *Nat. Mater.* **2010,** *9* (5), 454-460.

(26) Murnen, H. K.; Rosales, A. M.; Jaworsk, J. N.; Segalman, R. A.; Zuckermann, R. N. Hierarchical Self-Assembly of a Biomimetic Diblock Copolypeptoid into Homochiral Superhelices. *J. Am. Chem. Soc.* **2010,** *132* (45), 16112-16119.

(27) Armand, P.; Kirshenbaum, K.; Falicov, A.; Dunbrack, R. L.; Dill, K. A.; Zuckermann, R. N.; Cohen, F. E. Chiral N-substituted glycines can form stable helical conformations. *Folding Des.* **1997,** *2* (6), 369-375.

(28) Gorske, B. C.; Mumford, E. M.; Gerrity, C. G.; Ko, I. A Peptoid Square Helix via Synergistic Control of Backbone Dihedral Angles. *J. Am. Chem. Soc.* **2017,** *139* (24), 8070-8073.

(29) Rosales, A. M.; Murnen, H. K.; Zuckermann, R. N.; Segalman, R. A. Control of Crystallization and Melting Behavior in Sequence Specific Polypeptoids. *Macromolecules* **2010,** *43* (13), 5627-5636.

(30) Greer, D. R.; Stolberg, M. A.; Kundu, J.; Spencer, R. K.; Pascal, T.; Prendergast, D.; Balsara, N. P.; Zuckermann, R. N. Universal Relationship between Molecular Structure and Crystal Structure in Peptoid Polymers and Prevalence of the cis Backbone Conformation. *J. Am. Chem. Soc.* **2018,** *140* (2), 827-833.

(31) Rosales, A. M.; Segalman, R. A.; Zuckermann, R. N. Polypeptoids: a model system to study the effect of monomer sequence on polymer properties and self-assembly. *Soft Matter* **2013,** *9* (35), 8400-8414.

(32) Sun, J.; Teran, A. A.; Liao, X. X.; Balsara, N. P.; Zuckermann, R. N. Nanoscale Phase Separation in Sequence-Defined Peptoid Diblock Copolymers. *J. Am. Chem. Soc.* **2013,** *135* (38), 14119-14124.

(33) Sun, J.; Teran, A. A.; Liao, X. X.; Balsara, N. P.; Zuckermann, R. N. Crystallization in Sequence-Defined Peptoid Diblock Copolymers Induced by Microphase Separation. *J. Am. Chem. Soc.* **2014,** *136* (5), 2070-2077.

(34) Sun, J.; Liao, X. X.; Minor, A. M.; Balsara, N. P.; Zuckermann, R. N. Morphology–Conductivity Relationship in Crystalline and Amorphous Sequence-Defined Peptoid Block Copolymer Electrolytes. *J. Am. Chem. Soc.* **2014,** *136* (42), 14990-14997.

(35) Sun, J.; Jiang, X.; Siegmund, A.; Connolly, M. D.; Downing, K. H.; Balsara, N. P.; Zuckermann, R. N. Morphology and Proton Transport in Humidified Phosphonated Peptoid Block Copolymers. *Macromolecules* **2016,** *49* (8), 3083-3090.

(36) Rosales, A. M.; McCulloch, B. L.; Zuckermann, R. N.; Segalman, R. A. Tunable Phase Behavior of Polystyrene–Polypeptoid Block Copolymers. *Macromolecules* **2012,** *45* (15), 6027-6035.

(37) Hexemer, A.; Bras, W.; Glossinger, J.; Schaible, E.; Gann, E.; Kirian, R.; MacDowell, A.; Church, M.; Rude, B.; Padmore, H. A SAXS/WAXS/GISAXS Beamline with Multilayer Monochromator. *J. Phys.: Conf. Ser.* **2010,** *247*.

(38) Ilavsky, J. Nika: software for two-dimensional data reduction. *J. Appl. Crystallogr.* **2012,** *45*, 324-328.

(39) Fredrickson, G. H., *The Equilibrium Theory of Inhomogeneous Polymers*. Oxford Science Publications: Oxford, UK, 2006.

(40) Barrat, J. L.; Fredrickson, G. H.; Sides, S. W. Introducing variable cell shape methods in field theory simulations of polymers. *J. Phys. Chem. B* **2005,** *109* (14), 6694-6700.

(41) Rasmussen, K. O.; Kalosakas, G. Improved numerical algorithm for exploring block copolymer mesophases. *J. Polym. Sci. Pol. Phys.* **2002,** *40* (16), 1777-1783.

(42) Tzeremes, G.; Rasmussen, K. O.; Lookman, T.; Saxena, A. Efficient computation of the structural phase behavior of block copolymers. *Phys. Rev. E* **2002,** *65* (4), 041806-(1-5).

(43) Ceniceros, H. D.; Fredrickson, G. H. Numerical solution of polymer self-consistent field theory. *Multiscale Model Simul.* **2004,** *2* (3), 452-474.

(44) Chain Dimensions and Entanglement Spacings. In *Physical Properties of Polymers Handbook*, Mark, J. E., Ed. AIP Press: Woodbury, NY, 1996.

(45) Rosales, A. M.; Murnen, H. K.; Kline, S. R.; Zuckermann, R. N.; Segalman, R. A. Determination of the persistence length of helical and non-helical polypeptoids in solution. *Soft Matter* **2012,** *8* (13), 3673-3680.

(46) Matsen, M. W.; Bates, F. S. Unifying weak- and strong-segregation block copolymer theories. *Macromolecules* **1996,** *29* (4), 1091-1098.

(47) Matsen, M. W. Effect of Architecture on the Phase Behavior of AB-Type Block Copolymer Melts. *Macromolecules* **2012,** *45* (4), 2161-2165.

Chapter 4

Interfacial mixing in self-assembled sequence-defined materials

The degree of mixing of dissimilar components in self-assembled block copolymers determines important properties such as phase stability, interfacial tension, and domain size. Here, the effect of precise comonomer sequence on interfacial and mixing properties is measured via small angle X-ray scattering utilizing a polystyrene-*b*-polypeptoid diblock copolymer system, where the polypeptoid block is composed of highly-segregating (polar) and compatibilizing (nonpolar) repeat units. When compatibilizing groups are distributed along the polypeptoid chain, the presence of neighboring polar groups suppresses interfacial mixing and causes the interfacial width to narrow, while materials with tapered sequences promote interfacial mixing and larger interfacial widths. The tapered sequences have stronger localization of compatibilizing groups at the polystyrene–polypeptoid interface, as

supported by simulations with self-consistent field theory, and thus more pure domain centers, while the distributed sequences allow for more in-domain mixing of polystyrene into the polypeptoid domain. Along with the sequence-driven nonideal chain conformations shown recently, the final state of mixing and resulting geometry of sequence-defined self-assembled lamellae is shown to be determined by the combined effects of interfacial mixing, in-domain mixing, and the accompanying segmental repulsion.

4.1 Introduction

Understanding the interface between dissimilar components of block copolymers is key to targeting applications such as blend compatibilization and self-assembly. Tunable interfacial modifiers hold promise for blend and surfactant systems, where tethering across a high-surface-tension interface is desirable for high-performance blends and emulsions [REF Coates Science 2017, Coates Macromolecules 2018]. In bulk self-assembled block copolymers, the composite-like mechanical properties rely on the segregation of distinct domains and are modulated by the character of the interface between them: whether sharp or mixed.[1-3] Furthermore, self-assembling block copolymers are useful for applications that require patterning on nanometer length scales, and the fidelity of the pattern is determined partly by the sharpness of the interface between distinct domains.

In all of these applications, the chemistry of the components can be modified to increase segregation across the interface, usually through choosing high-χ systems,[4,5] introducing specific interactions,[6] or blending in judicious additives.[7,8] Controlling comonomer sequence is a promising yet relatively unexplored design tool to tune the thermodynamics of mixing dissimilar components without changing the chemistries. Semibatch methods to produce tapered and gradient composition profiles have been shown to influence the properties of self-assembled melts (influencing thermal phase stability, phase windows, mixing-induced broad glass transition temperatures and interfacial widths), as well as

enhance blend compatibilization.[9-16] However, the semibatch synthetic strategy cannot produce monomer-lengthscale sequence definition, so the effects of finely-controlled comonomer sequence are relatively unexplored.[17-19] Recent work utilized sequence-defined polypeptoids (*N*-substituted glycines) in lamellae-forming diblock copolymers to study the influence of compatibilizing comonomer sequence on self-assembly.[20] It was found that sequence significantly impacts domain spacing, due to nonideal chain conformations driven by localizing compatibilizing groups at the block–block interface. Further, the segregation strength between blocks was clearly modulated, evidenced by order–disorder transitions varying up to 10 °C by changing sequence alone. Interfacial thickness is known to vary inversely with the Flory–Huggins interaction parameter (χ) as $t \sim \chi^{-\alpha}$, where in the limite of inifinite molecular weight homopolymers, the scaling parameter α is $\frac{1}{2}$, and for block copolymers subject to fluctuation effects $\alpha \approx \frac{5}{6}$ in the range of physically-relevant χ values ($\chi \ll 1$).[21-24] While it was found that sequence-specific analyses must be employed to quantify χ differences based on sequence, the differences in segregation strength implied by the different order–disorder transition temperatures are likely to manifest as a variation in interfacial thickness.

Here we show that controlling sequence on the comonomer length scale affects the interfacial width of lamellar polystyrene-*b*-polypeptoid diblock copolymers, where the polypeptoid block is either a homopolymer of a polar ether side chain or a sequence-defined copolymer of the polar side chain with compatibilizing phenyl side chains (Figure 4.1). The tapered sequences are found to have wider interfaces, and distributed sequences possess comparably narrow interfacial widths to the fully polar, non-compatibilized material. The interfacial widths are quantified using structure factor analysis of well-resolved small angle X-ray scattering peaks. Furhter, the distribution of individual components in the self-

assembled domains is simulated with self-consistent field theory, which together elucidate the roles of interphase mixing, in-domain mixing, and unfavorable segmental interactions in forming lamellae with varying interfacial thicknesses.

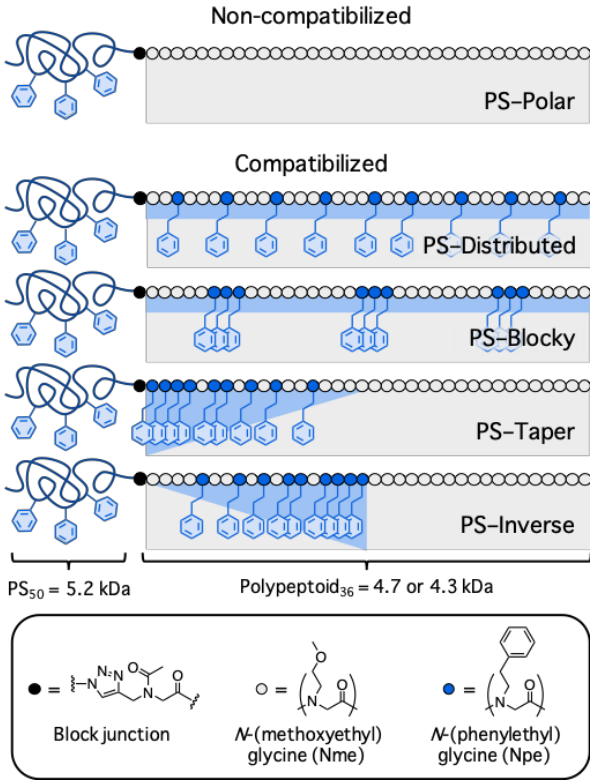

Figure 4.1. Summary of polystyrene-*b*-polypeptoid materials. A non-compatibilized diblock copolymer (top, PS–Polar) and four sequence-defined diblock copolymers with identical composition (bottom four) were synthesized.

4.2 Methods

4.2.1 Synthesis and characterization of PS–polypeptoid diblock copolymers

Synthesis and characterization procedures are detailed in a recent paper.[20] In short, styrene and (*n*-butyl)acrylate were polymerized via atom-transfer radical polymerization, and the chain end was substituted with sodium azide. The resulting azide-functionalized polymers were characterized with gel permeation chromatography (GPC), where polystyrene was measured against polystyrene standards, and Mark–Houwink parameters for specifically low

molecular weight poly(*n*-butyl)acrylate[25] were used to convert from poly(methyl methacrylate) standards to poly(*n*-butyl)acrylate. Polypeptoids were grown via the solid-phase submonomer method[26] with an additional terminal unit incorporating an alkyne side chain. Polypeptoids were analyzed with matrix-assisted laser desorption ionization mass spectrometry (MALDI-MS) and ultra-performance liquid chromatography mass spectrometry (UPLC-MS). Azide-terminated polystyrene (PS) or poly(n-butyl acrylate) (PnBA) were conjugated to alkyne-terminated polypeptoid using copper-mediated azide–alkyne click, and excess homopolymers were removed via precipitation and preparatory GPC (PS) or chromatography on alumina (PnBA). See reference 20 for further details and Table 4.1 for characteristics of the synthesized blocks.

Table 4.1. Characteristics of constituent blocks. [a]Calculated from UPLC-MS traces.

Block identity	Mn (g/mol)	Đ	d (± 0.02, g/cm^3)
PS–N_3	5200	1.12	1.03
PnBA–N_3	4900	1.15	1.03
$Nme_{27}Npe_9$–≡	4712	<1.04a	1.26
Nme_{36}–≡	4296	<1.04[a]	1.26

4.2.2 SAXS

Diblock copolymers were loaded into aluminum washers, with one side sealed with Kapton tape with Kapton film blocking the adhesive in the center. Samples were thermally annealed at high temperature in high vacuum (170 °C for ≥3 h, 3×10^{-8} Torr), cooled slowly (≤ 1 °C/min) to 110 °C, and annealed overnight before cooling slowly to room temperature in vacuum and sealing the other side of the washer. Small-angle X-ray scattering (SAXS) was performed at the National Synchrotron Light Source II (NSLS-II, Brookhaven National Lab), configured with an X-ray energy of 13.5 keV and sample–detector distance of 3 m. All measurements are reported at room temperature.

Data were calibrated with silver behenate standards, reduced using circular averaging, and corrected for empty cell scattering and q-independent background scattering (approximated as a constant fit to high q). Individual reflections were fit with Voigt peaks[27] with linear baselines to obtain peak intensities (areas).

4.2.3 Pycnometry

Polystyrene, poly(*n*-butyl)acrylate, and polypeptoid samples were thermally annealed above their glass transition temperatures in high vacuum (3×10^{-8} Torr) before cooling slowly to room temperature to produce glassy solids devoid of air bubbles. Sample volumes were measured with a Micromeritics AccuPyc II 1340 gas pycnometer using the gas displacement technique with helium. Five purge cycles were followed by five measurements. Dividing the mass (measured separately) by the average volume yielded sample densities.

4.2.4 Self-consistent field theory

An SCFT framework was employed in which the sequence defined block copolymers are modeled as an incompressible melt of discrete Gaussian chains, with one bead of specified type for each polypeptoid residue.[28] The PS block was reduced to a discrete chain with one bead per reference volume of 0.1 nm^3 and elaborated to a chain of 50 beads consistent with the measured molecular weight and literature density. Periodic boundary conditions were applied, and a variable cell technique allows for cell relaxation.[29] The integro-difference equations associated with forward and backward chain propagators were solved pseudospectrally.[30,31] Fields were relaxed to saddle-point configurations using a semi-implicit scheme.[28,32]

The three binary χ values were set in the following ratio: $\chi_{PS–Nme}$:$\chi_{PS–Npe}$:$\chi_{Nme–Npe}$ 1.0:0.8:0.2. The two polystyrene–polypeptoid χs were each measured at 220 °C via

application of the random phase approximation (RPA) to SAXS curves of the disordered phase. The Nme–Npe χ was estimated based on reference 33 and by comparing SCFT predictions to experiment. Density profiles reported here are shown at $\chi_{PS-Nme}N = 25$ unless otherwise noted.

4.2.5 Lamellar model with diffuse interfaces

The scattering from a lamellar multicomponent material with diffuse interfaces is derived below, following Roe and Beckingham, *et al.*[34,35] This approach to measure interfacial width utilizes peak intensities from well-defined scattering peaks, rather than the high-q scattering tail used historically to measure interfacial widths,[36,37] as it is less prone to error from subtracting the unknown background.

The structure factor of a perfectly-oriented, one-dimensional lamellar stack contributes to the scattering intensity as:

$$I_{\text{ideal,1D}}(q) \sim \Delta\rho^2 \sin^2\left(\frac{q d_A}{2}\right) q^{-2} \qquad (4.1)$$

where $\Delta\rho$ is the difference in scattering length density (electron density) between the two domains and d_A is the thickness of a layer of block A (in a few paragraphs, it will be shown that this d_A can be chosen arbitrarily without loss of generality). In this system, the electron density difference between polystyrene and polypeptoid (~75 e^-/nm^3) vastly outweighs the small electron density difference between Nme and Npe polypeptoid repeat units (~1 e^-/nm^3), so nearly all of the scattering arises from PS–polypeptoid contrast.

In a real system, there are many grains of lamellar structures randomly oriented in three-dimensional space, and the scattering we measure is the ideal 1D scattering multiplied by the Lorentz correction q^{-2},[38,39] yielding the familiar Porod decay of q^{-4}:

$$I_{\text{ideal,isotropic}}(q) \sim \Delta\rho^2 \sin^2\left(\frac{q d_A}{2}\right) q^{-4} \qquad (4.2)$$

Equation (4.2) represents the azimuthally-averaged isotropic scattering of randomly oriented lamellar sheets, and is still "ideal" in that it has perfectly sharp interfaces (modeled as step functions in scattering length density, Figure 4.2a). A correction must be made to account for diffuse interfaces at the lamellar domain boundaries, as there is always some degree of mixing between dissimilar blocks in real systems. This interfacial mixing is modeled by convoluting a smoothing function (often chosen to be Gaussian) with the ideal, sharp interface to create a smoothly-varying scattering length density profile (Figure 4.2b and c). The Fourier transform of this real-space Gaussian smoothing leads to a Gaussian decay in q-space of the structure factor peaks, modifying the ideal q^{-4} behavior as:

$$I_{\text{diffuse,isotropic}}(q) \sim \Delta\rho^2 \sin^2\left(\frac{q d_A}{2}\right) q^{-4} e^{-\sigma^2 q^2} \qquad (4.3)$$

where σ^2 is the variance of the real-space Gaussian. Equation (4.3) describes the envelope in which scattering peak intensities will be found for a real lamellar material.

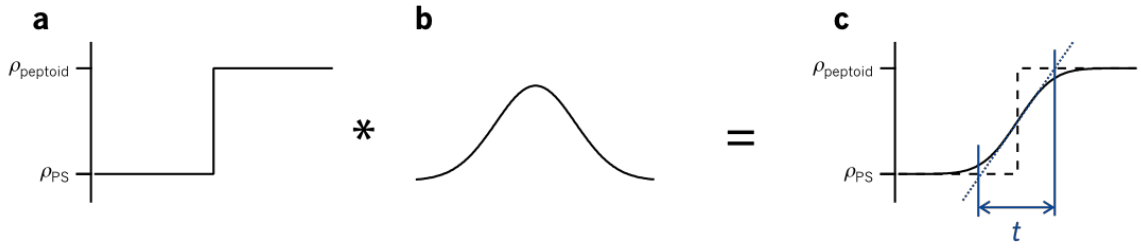

Figure 4.2. Construction of diffuse interface.

Real systems have diffuse interfaces, modeled by the convolution of (a) the ideal (step-function) change in scattering length density with (b) a Gaussian smoothing function, yielding (c) a smooth variation in electron density in the interfacially-mixed region, with interfacial thickness $t = \sqrt{2\pi}\sigma$.

Peaks only occur when the Bragg condition $q = \frac{2\pi n}{d}$ is met, where d is the full lamellar domain spacing, so the intensity of peaks of order n go as:

$$I(n) \sim \Delta\rho^2 \sin^2(\pi n \varphi_A) n^{-4} e^{-2\pi n^2 (t/d)^2} \qquad (4.4)$$

where $\varphi_A=d_A/d$ is the volume fraction of domain A and t is the interfacial width, related to σ as $t = \sqrt{2\pi}\sigma$ and illustrated in Figure 4.2c. Because $\sin^2(x)$ is even around $x= \ /2$, the argument $n\varphi_A$ is the same whether we choose A such that $\varphi_A>1/2$ or $\varphi_A<1/2$; this is Babinet's reciprocity theorem. For consistency, we set $\varphi_A = \varphi_{peptoid} < 1/2$ throughout this paper. By comparing the sharp interface model (equation (4.3)) and diffuse interface model (equation (4.4)) against measured peak intensities, it is clear that the materials studied here are much better modeled by a diffuse interface (Figure 4.4).

4.3 SAXS analysis of self-assembled diblock copolymers

All samples formed well-ordered, isotropically oriented lamellae with periods of ~10 nm. Azimuthal averaging of the 2D scattering patterns reflects the structure of many grains (the beam size is 200 × 200 gm, and sample thickness is 800 gm), producing 1D scattering data with good statistics and at least two higher order reflections for all samples ($2q^*$ and $3q^*$, Figure 4.3).

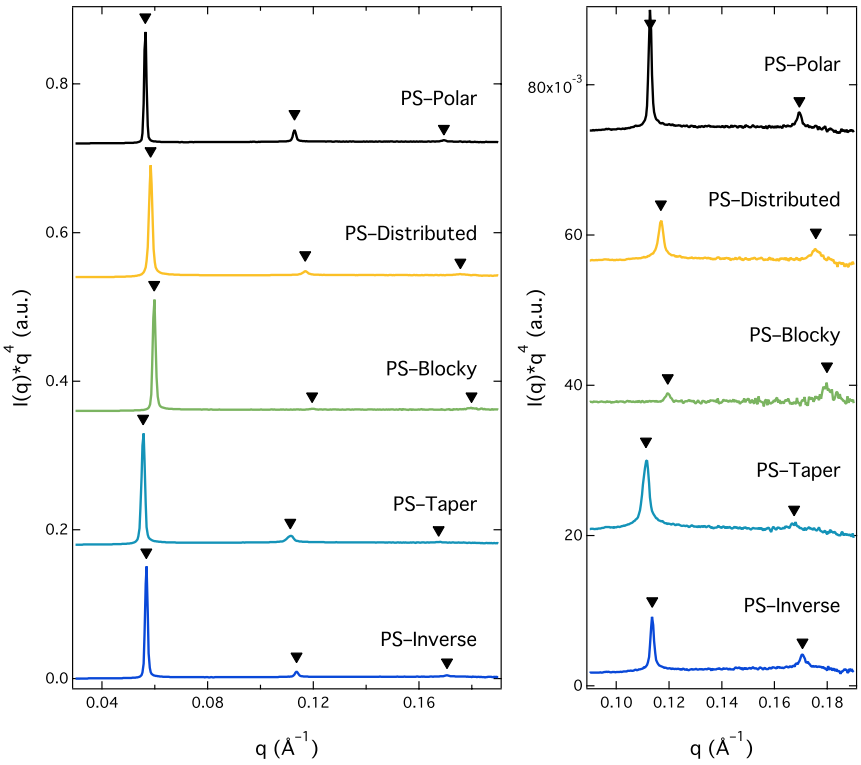

Figure 4.3. Porod-corrected small-angle X-ray scattering (SAXS) of PS–polypeptoid diblock copolymers (right is zoomed in on the 2q* and 3q* region).

All diblock copolymers studied form well-ordered lamellae with 2q* and 3q* higher order reflections, indicated by black triangles. Spectra have been scaled to have identical q* amplitudes.

Interfacial thicknesses were robustly calculated by fitting the diffuse interface model to scattering peak intensities of each material. The area of each scattering peak was found by fitting individual Voigt peaks with a local linear baseline that accounts for unknown background; sensitivity analyses show that the choice of baseline leads to a <5% variation in peak area, which contributes a 1% variation in interfacial width (smaller than the error arising from goodness of fit of the peak). In applying the diffuse interface model (equation (4.4)), interfacial thickness (t) and volume fraction (φ_{peptoid}) were allowed to vary, as well as a scaling factor that accounts for the use of arbitrary units of intensity. Figure 4.4 demonstrates the goodness of fit for Porod-corrected scattering of an example material (PnBA–Polar). Variation in φ_{peptoid} affects the positions of the extrema (from the

$\sin^2(\pi n \varphi_A)$ term), and the overall downward trend in intensity with increasing reflection number n is due to the diffuse interface (described by the $e^{-2\pi n^2 (t/d)^2}$ decay factor). Scattering and peak areas from Porod-corrected scattering ($I(q)*q^4$) are shown to emphasize the differences in the behavior with and without a diffuse interface.

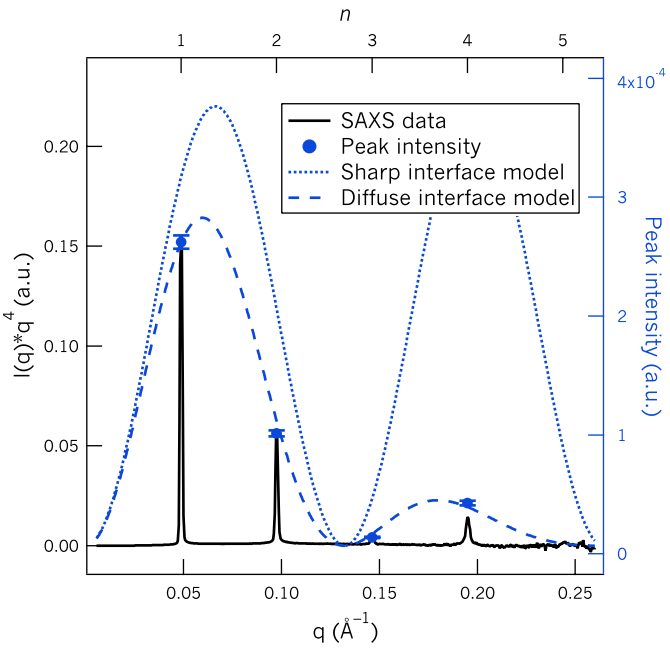

Figure 4.4. Example fit of diffuse models to the SAXS data.

Porod-corrected scattering intensity ($I(q)*q^4$) is plotted versus scattering vector q in black (left axis). The integrated peak intensities are superimposed as blue markers, along with envelopes fit using the sharp interface model (dotted blue line) and diffuse interface model (dashed blue line) (right axis). The diffuse interface is clearly a better model for capturing the measured behavior. The example shown is PnBA–Polar.

It is important to note that the X-ray scattering contrast in this system is dominated by the electron density difference between polystyrene and polypeptoid (~75 e^-/nm^3), vastly outweighing the small electron density difference between Nme and Npe polypeptoid repeat units (1 e^-/nm^3). We can be confident that nearly all of the scattering arises from PS–polypeptoid contrast, justifying the use of a simple two-layer model, even with variation expected in the distribution of Nme and Npe polypeptoid units.

4.4 Effect of sequence on interfacial thickness

Fits of SAXS peak intensities to equation (4.4) demonstrate that interfacial thickness varies as a function of sequence, with materials comprising tapered sequences having larger interfacial thicknesses than those with distributed sequences or the non-compatibilized polypeptoid block. This variation in interfacial thickness is rationalized by calculating the compatibilizing group content in the interphase with self-consistent field theory simulations.

With the highest segregation strength,[20] the non-compatibilized PS–Polar block copolymer was found to have the smallest interfacial width at 2.57 ± 0.03 nm (Figure 4.5). Previous work with the polystyrene–polypeptoid system has shown that replacing 25% of the polar polypeptoid units with nonpolar compatibilizing groups lowers the order–disorder transition by over 50 °C, likely indicating a lower χ, although it was found that sequence-specific models must be implemented to quantify this difference. Following $t \sim \chi^{-\alpha}$, the interfacial thicknesses of the compatibilized materials are expected to be larger than the non-compatibilized PS–Polar and be influenced by chain conformations that localize compatibilizing nonpolar polypeptoid units at the block–block interface. When compatibilizing groups are added, the interfacial thickness increases for the tapered sequences, but remains narrow for the distributed sequences, despite 25% of the polypeptoid units being replaced with phenyl side chains that promote mixing.

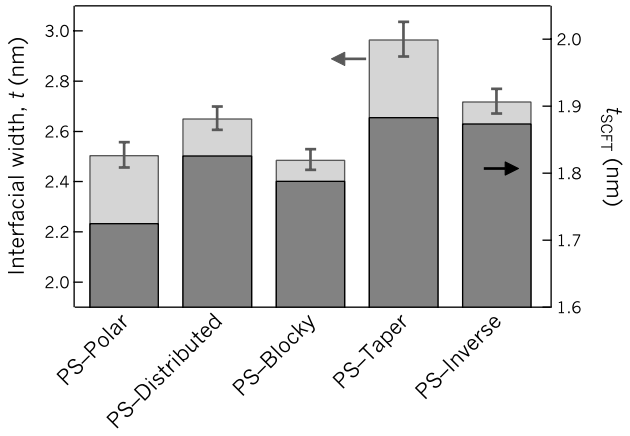

Figure 4.5. Interfacial widths of lamellar PS–polypeptoid diblock copolymers, calculated from fits of the diffuse interface model (equation (4)) to SAXS peak intensities.

PS–Taper has the largest interfacial thickness at 2.97 ± 0.06 nm, followed by PS–Inverse with t = 2.72 ± 0.05 nm. PS–Taper has all of its compatibilizing groups placed near the block junction in its primary sequence, so it has the fewest polar polypeptoid units close to PS and the greatest potential for block–block mixing, resulting in the wider interface measured. Literature studies of forward versus inverse tapers in polystyrene–polyisoprene (PS–PI) block copolymers found the reverse result: using X-ray reflectivity, Luo, et al. found the inverse taper has a larger interfacial thickness than the forward taper (10.5 nm versus 5.2 nm, respectively).[12] In this PS–polypeptoid system, the smaller taper size (~2500 g/mol versus ~7500 g/mol) and the use of a "styrene-like" compatibilizing group increases the overall propensity for mixing compared to the PS-PI system, likely causing the increased interfacial width observed for the forward taper relative to the inverse taper.

The distributed sequences have smaller interfacial thicknesses than the tapered ones: PS–Distributed (2.65 ± 0.05 nm) and PS–Blocky (2.49 ± 0.04 nm). Unexpectedly, the interfacial thickness of PS–Blocky matches that of the totally non-compatibilized PS–Polar (2.51 ± 0.05 nm), despite having 25% of its polar repeat units replaced with compatibilizing groups and an order–disorder transition depressed by 62 °C. The distribution of the

nonpolar groups throughout an overall polar matrix likely narrows the interfacial width while still promoting disordering on a whole-chain length scale upon heating.

Simulations with self-consistent field theory (SCFT), explicitly incorporating comonomer sequence and the three binary χ values, give insight into the distribution of components in the self-assembled domains. While PS–polypeptoid is a fairly high-χ system ($\chi \approx 0.08$ with little temperature dependence, using reference volume $v_0 = 0.1$ nm^3),[20] the block copolymers studied here are relatively small (~10 kDa total), so the segregation strength χN is much less than 100 and therefore far from the strong segregation limit. With a relatively low χN, we expect a fair amount of mixing between polypeptoid and polystyrene, and for even the center of the lamellar microdomains to contain a small amount of the other block. In fact, simulations show that at $\chi N = 25$, the domain centers are approximately 5% the opposite block identity (Figure 4.6).

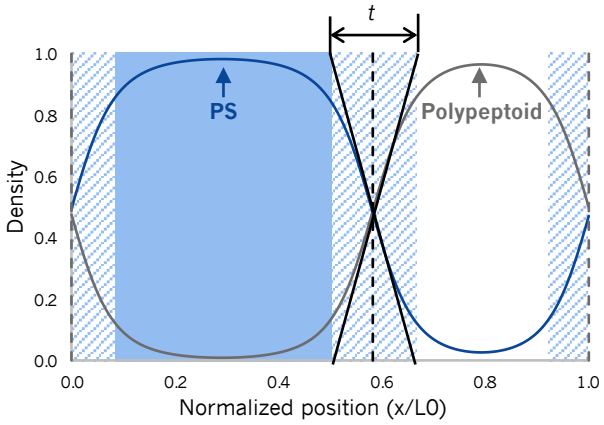

Figure 4.6. Representative simulated density profiles of polystyrene and polypeptoid in the lamellar structure. The interfacial thickness *t* is indicated as constructed from tangents to the interface.

By tracking the locations of polar Nme polypeptoid units and nonpolar compatibilizing Npe units in the simulations, we can visualize how the sequence-driven chain conformations are affecting the interfacial width. The distribution of Npe groups is illustrated in Figure 4.7a. The interphase is 50% polystyrene and 50% polypeptoid, but the proportion of Nme and Npe

groups comprising the interfacial polypeptoid depends on the sequence. The Npe content of the interfacial polypeptoid in the distributed sequences (PS–Distributed and PS–Blocky) is identical to the whole-chain Npe content (25% Npe). While we expect that folded chain conformations allow compatibilizing Npe units to migrate toward the interface, shrinking the domain spacing in these distributed sequences, the interface-directed compatibilizing groups are covalently tethered to neighboring polar groups, which must accompany them to the interfacial region. This covalent restriction causes the interphase polypeptoid composition to reflect the overall composition of 1:3 (or 9:27 Npe:Nme), as it is not possible to increase Npe content without also increasing Nme content in these sequences. With polar Nme groups forced to be at the interface, there is stronger local repulsion between polypeptoid and polystyrene, likely causing the narrow interfacial widths of PS–Distributed and PS–Blocky. This result suggests that blocky-distributed sequence design could be implemented to improve processability while maintaining high-fidelity interfaces, matching the narrow interfacial width of the non-compatibilized material while decreasing the order–disorder temperature by 62 °C.

The interfacial regions of the tapered sequences have slightly higher Npe content than the distributed sequences, with the interphase of PS–Inverse having 26% Npe units, and that of PS–Taper having the highest fraction of Npe units at 33%. Putting this comparison in terms of individual compatibilizing Npe units: for a single chain, the distributed sequences have 5 Npe units in the polypeptoid region, <4 in the interphase, and <1 in the polystyrene region, on average. For PS–Taper, these numbers shift to 3 Npe units in the polypeptoid, 5 in the interphase, and 1 in the polystyrene region (Figure 4.7b); PS–Inverse lies between the two extremes. In other words, the compatibilizing groups of the tapered materials are more likely to reside in the interphase than those of the distributed sequences, whose interfacial region has the same composition of peptoid as the polypeptoid domain.

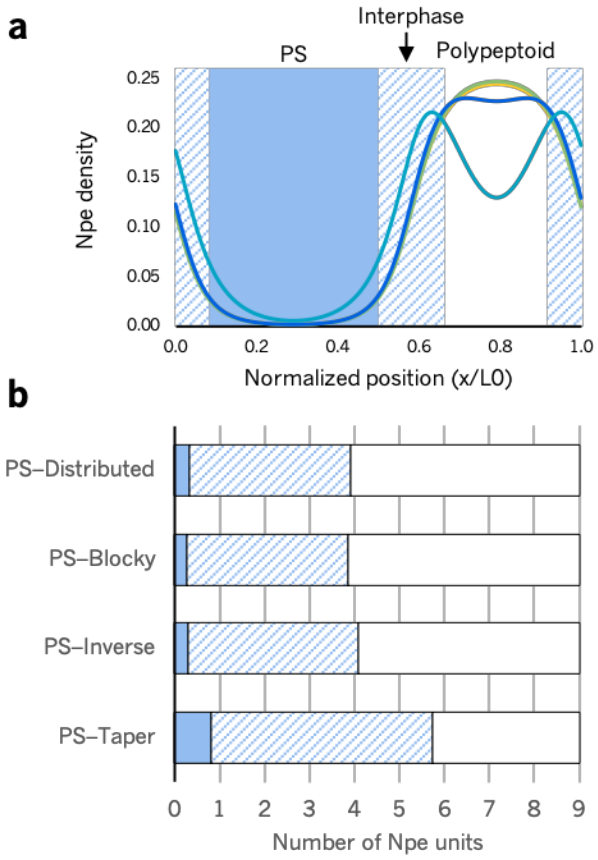

Figure 4.7. A) SCFT predictions of distribution of Npe compatibilizing unit in lamellar domains. B) Distribution of compatibilizing Npe polypeptoid units between microphases. The tapered sequence has more Npe units in the interfacial region.

4.5 Relationship between interfacial thickness and volume fraction

The $\sin^2(n\pi\varphi_A)$ term in the lamellar structure factor is very sensitive to volume fraction φ_A, so by fitting both interfacial thickness and φ_A, accurate volume fractions can be measured (Figure 4.8).

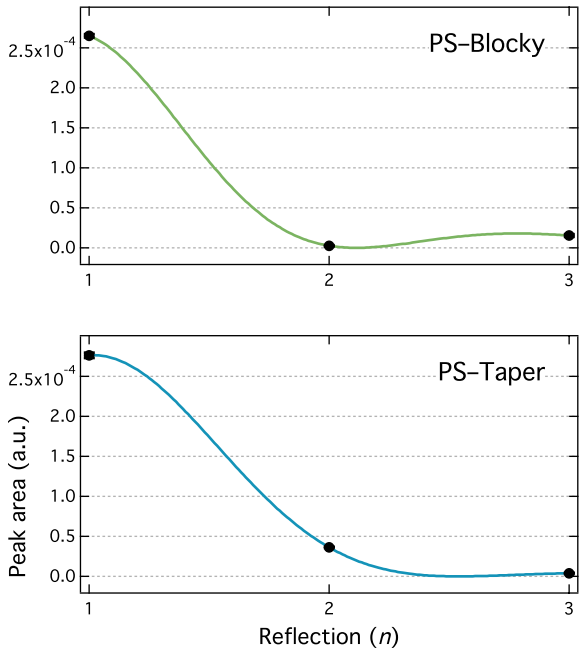

Figure 4.8. Example fits to scattering peaks to Porod-corrected peaks areas of PS–Blocky and PS–Taper. The decay with increasing *n* indicates the contribution from the diffuse interface, while the sinusoidal behavior stems from the lamellar structure factor, whose period is set by $\varphi_{peptoid}$.

The polypeptoid and polystyrene densities and molecular weights are very well known in this study, and the theoretical volume fraction for all sequence-defined materials is $\varphi_{peptoid,calc} = 0.43$, and for PS–Polar, $\varphi_{peptoid,calc} = 0.40$. Fitting to SAXS peaks, three of the five samples match the expected volume fractions (PS–Distributed, PS–Inverse, and PS–Polar), while PS–Taper has a lower $\varphi_{peptoid,SAXS}$ and PS–Blocky has a higher $\varphi_{peptoid,SAXS}$ (Table 4.2). These two materials also represent the extremes in domain spacings and interfacial widths, so further analysis of this discrepancy is merited.

Table 4.2. Self-assembly parameters for PS–polypeptoid diblock copolymers.

Sample	d (nm)	φ_{calcd}	t (nm)	φ_{fit}
PS–Polar	11.1	0.40	2.51 ± 0.03	0.40
PS–Distributed	10.8	0.43	2.65 ± 0.06	0.43
PS–Blocky	10.5	0.43	2.49 ± 0.06	0.47
PS–Taper	11.3	0.43	2.97 ± 0.06	0.39
PS–Inverse	11.1	0.43	2.78 ± 0.03	0.42

Since the domain spacing is also changing between the sequences, a clearer comparison is made between the absolute distribution of microdomain sizes. Figure 4.9 shows schematically the absolute sizes of polypeptoid and polystyrene domains (calculated as $d_{\text{peptoid}} = \varphi_{\text{peptoid}} d$ and $d_{\text{PS}} = \left(1 - \varphi_{\text{peptoid}}\right) d$). A surprising result becomes apparent: the most "folded" chain conformation (PS–Blocky) seems to have the largest polypeptoid domain, while the most "extended" chain conformations (PS–Taper) seems to have the smallest, with the polystyrene domain varying in size in an opposite trend.

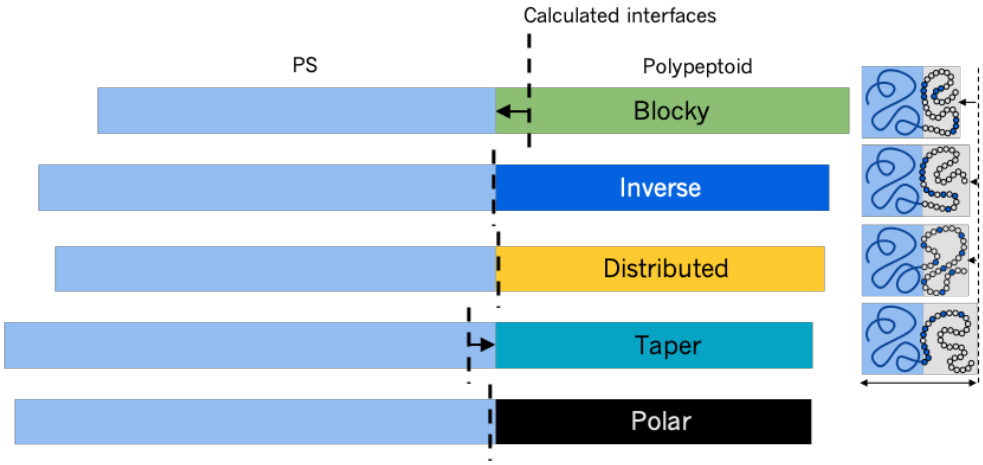

Figure 4.9. Visualization of polypeptoid (left) and polystyrene (right) portions of the total domain spacing. Bar lengths are drawn to scale and have been visually aligned at the interface determined by SAXS. Chain conformations are reproduced at the right.

The main cause of this seeming disagreement is the degree of in-domain mixing, i.e., the amount of polystyrene mixed into the center of the polypeptoid domain and vice versa. For all samples, SCFT reveals more segmental mixing in the polypeptoid-rich domain, indicated by the increased density of polystyrene in the polypeptoid region versus the lower density of polypeptoid in the polystyrene region (emphasized at $\chi_{\text{PS–Nme}}N$=15 in Figure 4.10a). Asymmetric in-domain mixing will shift mass into the polypeptoid domain from the PS domain, increasing φ_{peptoid}. In the extreme cases within the sequence-defined materials, PS–Blocky has the most in-domain mixing and also the largest positive deviation from the calculated volume fraction (polystyrene is swelling the polypeptoid domain), while PS–

Taper has the least in-domain mixing and the largest negative deviation from the calculated volume fraction (polystyrene is more strongly localized in the polystyrene domain) (Figure 4.10b and c). The comparison of PS–Taper and PS–Polar agrees with results found previously for PS–PI taper and diblock copolymer systems.[3]

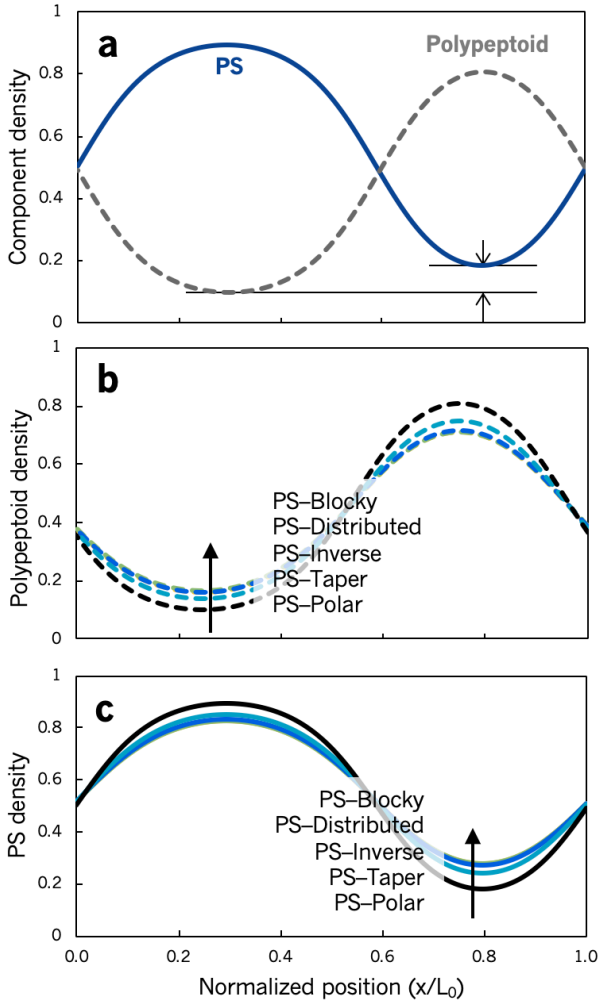

Figure 4.10. SCFT simulations of PS and polypeptoid densities at $\chi_{PS\text{–}Nme}N$=15

A) Overall composition profiles for PS and polypeptoid (example shown in PS–Polar). There is more intermixing of PS into the polypeptoid domain than vice versa. B) Total polypeptoid density and C) PS density for different sequences. There is more in-domain mixing for the distributed sequences and less for the tapered sequences, with PS–Polar having the least.

Further, the polypeptoid domain of the distributed sequences are composed of 24% Npe versus Nme, while the polypeptoid domain of PS–Taper is only 16% Npe. With more of the

unfavorable Nme–Npe contacts in the distributed sequences, it is possible that their polypeptoid domains are expanded versus that of PS–Taper, further exaggerating the asymmetry in volume fraction. The sum of the effects of chain conformation, interfacial mixing, in-domain mixing, and number of repulsive contacts results in asymmetric distributions of materials in the domains (Figure 4.11).

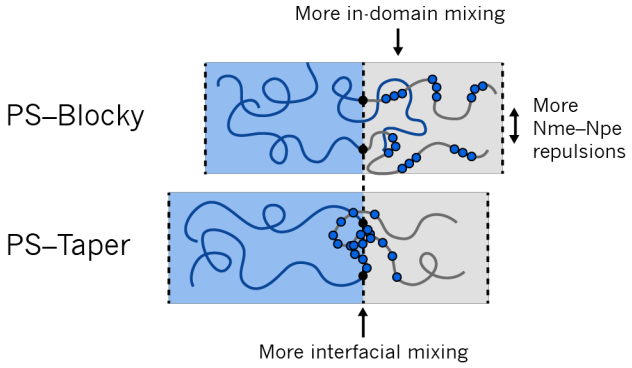

Figure 4.11. The combination of interfacial and in-domain mixing, chain conformation, and number of repulsive contacts leads to variation in domain spacing, interfacial thickness, and volume fraction.

4.6 Comparison to higher-χ system

To study the effects of interaction parameter χ on interfacial width, an analogous series was synthesized with poly(*n*-butyl)acrylate (PnBA) conjugated to the same five polypeptoid blocks shown above. Application of the random phase approximation to PnBA–Polar and PS–Polar indicated that the PnBA series has a higher χ than the PS series (Figure 4.12). As expected, this higher χ leads to smaller interfacial thicknesses (0.5 nm smaller in all cases except PnBA–Taper, which has measurable excess homopolymer and therefore a narrowed interfacial width). The same trends with sequence are seen in the fully purified samples in this analogous series, but with smaller absolute differences between sequences due to the overall smaller interfacial widths. This comparison shows that sequence design has a greater potential for tuning interfacial width in lower-χ systems, while higher-χ systems approach the same narrow interfacial width regardless of sequence.

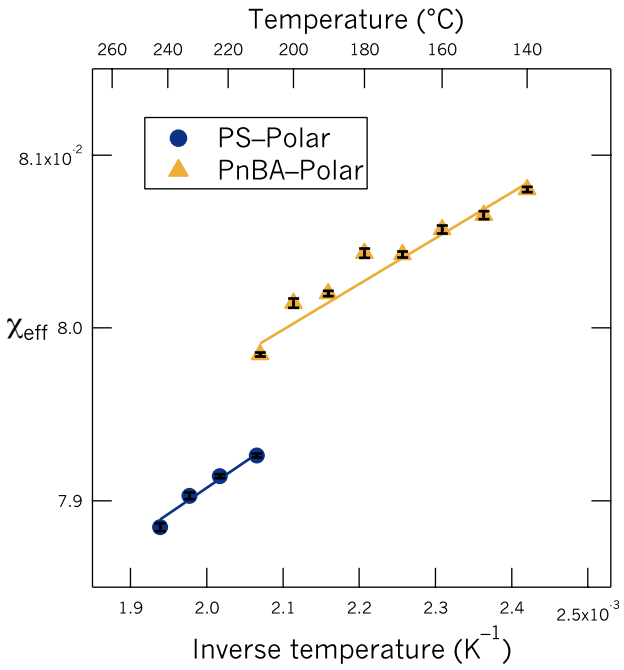

Figure 4.12. Interaction parameters (χs) for PS–Polar and PnBA–Polar diblock copolymers, as measured through application of the random phase approximation to disordered scattering curves.

Table 4.3. Self-assembly parameters for PnBA–polypeptoid diblock copolymers

Sample	d (nm)	φ_{calcd}	t (nm)	φ_{fit}
PnBA–Polar	12.9	0.40	1.98 ± 0.02	0.37
PnBA–Distributed	12.0	0.42	2.26 ± 0.03	0.40
PnBA–Blocky	12.0	0.42	2.15 ± 0.03	0.40
PnBA–Taper	12.2	0.42	2.21 ± 0.01	0.37
PnBA–Inverse	12.1	0.42	2.22 ± 0.02	0.40

4.7 Conclusions

This work demonstrates that, in addition to altering chain conformation, comonomer sequence significantly impacts the thermodynamics of mixing at both the microdomain interface and centers. At the interface, tapered sequences of compatibilizing groups are enriched in these nonpolar groups, broadening the interface, while the domain centers are more pure in polystyrene or polypeptoid. Distributed sequences have sharp interfaces due to the necessity of neighboring polar groups to accompany compatibilizing groups to the

interface, but the forced mixing of polar and nonpolar peptoid units expands the polypeptoid domain and invites more polystyrene into the domain center. The combination of these effects—chain conformation, interfacial mixing, in-domain mixing, and penalized comonomer contacts—demonstrates the rich behavior of sequence-defined polymers and the ability to tune morphological properties with comonomer sequence alone.

4.8 Acknowledgements

The authors gratefully acknowledge funding from the National Science Foundation (NSF) Division of Materials Research program (DMR-1608297) for synthesis and characterization of block copolymers and the NSF Condensed Matter and Materials Theory Program (DMR-1822215) for self-consistent field theory simulations. A.L.P. gratefully acknowledges the NSF for a graduate research fellowship. Polypeptoid characterization and block copolymer purification were performed with Dr. Rachel Behrens at the MRL Shared Experimental Facilities, supported by the MRSEC Program of the NSF, a member of the NSF-funded Materials Research Facilities Network (DMR-1720256). SCFT simulations utilized resources of the Center for Scientific Computing (DMR-1720256) and NSF (CNS-1725797). X-ray scattering was performed at the National Synchrotron Light Source II, a U.S. Department of Energy Office of Science User Facility (DE-SC0012704; beamline 11-BM). The authors thank Bryan Beckingham (University of Auburn) for helpful discussions regarding fitting interfacial widths from X-ray scattering, and Ron Zuckermann (Molecular Foundry, Lawrence Berkeley National Lab) for helpful discussions regarding polypeptoid synthesis.

4.9 References

(1) Shen, M.; Kaelble, D. H. On Viscoelastic Behavior of a Styrene-Butadiene-Styrene (S-B-S) Block Copolymer. *J Polym Sci Pol Lett* **1970,** *8* (3), 149-&.

(2) Hashimoto, T.; Tsukahara, Y.; Tachi, K.; Kawai, H. Structure and Properties of Tapered Block Polymers .4. Domain-Boundary Mixing and Mixing-In-Domain Effects

on Microdomain Morphology and Linear Dynamic Mechanical Response. *Macromolecules* **1983,** *16* (4), 648-657.

(3) Hashimoto, T.; Tsukahara, Y.; Kawai, H. Structure And Properties Of Tapered Block Polymers Of Styrene And Isoprene .2. Dynamic Mechanical Responses And Their Structural Interpretations. *Polym. J.* **1983,** *15* (10), 699-711.

(4) Kennemur, J. G.; Yao, L.; Bates, F. S.; Hillmyer, M. A. Sub-5 nm Domains in Ordered Poly(cyclohexylethylene)-block-poly(methyl methacrylate) Block Polymers for Lithography. *Macromolecules* **2014,** *47* (4), 1411-1418.

(5) Azuma, K.; Sung, J.; Choo, Y.; Rokhlenko, Y.; Dwyer, J. H.; Schweitzer, B.; Hayakawa, T.; Osuji, C. O.; Gopalan, P. Self-Assembly of an Ultrahigh-chi Block Copolymer with Versatile Etch Selectivity. *Macromolecules* **2018,** *51* (16), 6460-6467.

(6) Luo, Y. D.; Montarnal, D.; Treat, N. J.; Hustad, P. D.; Christianson, M. D.; Kramer, E. J.; Fredrickson, G. H.; Hawker, C. J. Enhanced Block Copolymer Phase Separation Using Click Chemistry and Ionic Junctions. *ACS Macro Lett.* **2015,** *4* (12), 1332-1336.

(7) Tirumala, V. R.; Daga, V.; Bosse, A. W.; Romang, A.; Ilavsky, J.; Lin, E. K.; Watkins, J. J. Well-Ordered Polymer Melts with 5 nm Lamellar Domains from Blends of a Disordered Block Copolymer and a Selectively Associating Homopolymer of Low or High Molar Mass. *Macromolecules* **2008,** *41* (21), 7978-7985.

(8) Luo, Y. D.; Kim, B.; Montarnal, D.; Mester, Z.; Pester, C. W.; McGrath, A. J.; Hill, G.; Kramer, E. J.; Fredrickson, G. H.; Hawker, C. J. Improved Self-Assembly of Poly(dimethylsiloxane-b-ethylene oxide) Using a Hydrogen-Bonding Additive. *Journal of Polymer Science Part a-Polymer Chemistry* **2016,** *54* (14), 2200-2208.

(9) Singh, N.; Tureau, M. S.; Epps, T. H., III Manipulating ordering transitions in interfacially modified block copolymers. *Soft Matter* **2009,** *5* (23), 4757-4762.

(10) Roy, R.; Park, J. K.; Young, W. S.; Mastroianni, S. E.; Tureau, M. S.; Epps, T. H., III Double-Gyroid Network Morphology in Tapered Diblock Copolymers. *Macromolecules* **2011,** *44* (10), 3910-3915.

(11) Mastroianni, S. E.; Epps, T. H., III Interfacial Manipulations: Controlling Nanoscale Assembly in Bulk, Thin Film, and Solution Block Copolymer Systems. *Langmuir* **2013,** *29* (12), 3864-3878.

(12) Luo, M.; Browns, J. R.; Remy, R. A.; Scott, D. M.; Mackay, M. E.; Halv, L. M.; Epps, T. H. Determination of Interfacial Mixing in Tapered Block Polymer Thin Films: Experimental and Theoretical Investigations. *Macromolecules* **2016,** *49* (14), 5213-5222.

(13) Kim, J.; Gray, M. K.; Zhou, H. Y.; Nguyen, S. T.; Torkelson, J. M. Polymer blend compatibilization by gradient copolymer addition during melt processing: Stabilization of dispersed phase to static coarsening. *Macromolecules* **2005,** *38* (4), 1037-1040.

(14) Kim, J.; Mok, M. M.; Sandoval, R. W.; Woo, D. J.; Torkelson, J. M. Uniquely broad glass transition temperatures of gradient copolymers relative to random and block copolymers containing repulsive comonomers. *Macromolecules* **2006,** *39* (18), 6152-6160.

(15) Wong, C. L. H.; Kim, J.; Torkelson, J. M. Breadth of glass transition temperature in styrene/acrylic acid block, random, and gradient copolymers: Unusual sequence distribution effects. *J. Polym. Sci. Pol. Phys.* **2007,** *45* (20), 2842-2849.

(16) Mok, M. M.; Pujari, S.; Burghardt, W. R.; Dettmer, C. M.; Nguyen, S. T.; Ellison, C. J.; Torkelson, J. M. Microphase separation and shear alignment of gradient copolymers: Melt rheology and small-angle X-ray scattering analysis. *Macromolecules* **2008,** *41* (15), 5818-5829.

(17) Seo, Y.; Brown, J. R.; Hall, L. M. Effect of Tapering on Morphology and Interfacial Behavior of Diblock Copolymers from Molecular Dynamics Simulations. *Macromolecules* **2015,** *48* (14), 4974-4982.

(18) Brown, J. R.; Seo, Y. M.; Sides, S. W.; Hall, L. M. Unique Phase Behavior of Inverse Tapered Block Copolymers: Self Consistent Field Theory and Molecular Dynamics Simulations. *Macromolecules* **2017,** *50* (14), 5619-5626.

(19) Ganesan, V.; Kumar, N. A.; Pryamitsyn, V. Blockiness and Sequence Polydispersity Effects on the Phase Behavior and Interfacial Properties of Gradient Copolymers. *Macromolecules* **2012,** *45* (15), 6281-6297.

(20) Patterson, A. L.; Danielsen, S. P. O.; Yu, B.; Davidson, E. C.; Fredrickson, G. H.; Segalman, R. A. Sequence Effects on Block Copolymer Self-Assembly through Tuning Chain Conformation and Segregation Strength Utilizing Sequence-Defined Polypeptoids. *Macromolecules* **2019,** *52* (3), 1277-1286.

(21) Semenov, A. N. Theory of Block-Copolymer Interfaces in the Strong Segregation Limit. *Macromolecules* **1993,** *26* (24), 6617-6621.

(22) Shull, K. R. Mean-Field Theory of Block Copolymers: Bulk Melts, Surfaces, and Thin Films. *Macromolecules* **1992,** *25* (8), 2122-2133.

(23) Ohta, T.; Kawasaki, K. Equilibrium Morphology of Block Copolymer Melts. *Macromolecules* **1986,** *19* (10), 2621-2632.

(24) Helfand, E.; Tagami, Y. Theory of Interface Between Immiscible Polymers. *J. Chem. Phys.* **1972,** *57* (4), 1812.

(25) Gruendling, T.; Junkers, T.; Guilhaus, M.; Barner-Kowollik, C. Mark-Houwink Parameters for the Universal Calibration of Acrylate, Methacrylate and Vinyl Acetate Polymers Determined by Online Size-Exclusion Chromatography-Mass Spectrometry. *Macromol. Chem. Phys.* **2010,** *211* (5), 520-528.

(26) Zuckermann, R. N.; Kerr, J. M.; Kent, S. B. H.; Moos, W. H. Efficient Method for the Preparation of Peptoids [Oligo(N-substituted glycines)] by Submonomer Solid-Phase Synthesis. *J. Am. Chem. Soc.* **1992,** *114* (26), 10646-10647.

(27) Ruland, W. Integral Width of Convolution of a Gaussian and a Cauchy Distribution. *Acta Crystallogr* **1965,** *18*, 581-&.

(28) Fredrickson, G. H., *The Equilibrium Theory of Inhomogeneous Polymers*. Oxford Science Publications: Oxford, UK, 2006.

(29) Barrat, J. L.; Fredrickson, G. H.; Sides, S. W. Introducing variable cell shape methods in field theory simulations of polymers. *J. Phys. Chem. B* **2005,** *109* (14), 6694-6700.

(30) Rasmussen, K. O.; Kalosakas, G. Improved numerical algorithm for exploring block copolymer mesophases. *J. Polym. Sci. Pol. Phys.* **2002,** *40* (16), 1777-1783.

(31) Tzeremes, G.; Rasmussen, K. O.; Lookman, T.; Saxena, A. Efficient computation of the structural phase behavior of block copolymers. *Phys. Rev. E* **2002,** *65* (4), 041806-(1-5).

(32) Ceniceros, H. D.; Fredrickson, G. H. Numerical solution of polymer self-consistent field theory. *Multiscale Model Simul.* **2004,** *2* (3), 452-474.

(33) Sun, J.; Teran, A. A.; Liao, X. X.; Balsara, N. P.; Zuckermann, R. N. Nanoscale Phase Separation in Sequence-Defined Peptoid Diblock Copolymers. *J. Am. Chem. Soc.* **2013,** *135* (38), 14119-14124.

(34) Roe, R.-J., *Methods of X-Ray and Neutron Scattering in Polymer Science*. Oxford University Press: 198 Madison Ave, New York, New York 10016, 2000.

(35) Beckingham, B. S.; Register, R. A. Architecture-Induced Microphase Separation in Nonfrustrated A-B-C Triblock Copolymers. *Macromolecules* **2013,** *46* (9), 3486-3496.

(36) Ruland, W. Small-Angle Scattering of 2-Phase Systems - Determination and Significance of Systematic Deviations from Porods Law. *J. Appl. Crystallogr.* **1971,** *4* (Feb1), 70-&.

(37) Hashimoto, T.; Shibayama, M.; Kawai, H. Domain-Boundary Structure of Styrene-Isoprene Block Co-Polymer Films Cast from Solution .4. Molecular-Weight Dependence of Lamellar Microdomains. *Macromolecules* **1980,** *13* (5), 1237-1247.

(38) Shibayama, M.; Hashimoto, T. Small-Angle X-Ray-Scattering Analyses of Lamellar Microdomains Based on a Model of One-Dimensional Paracrystal with Uniaxial Orientation. *Macromolecules* **1986,** *19* (3), 740-749.

(39) Cser, F. About the Lorentz correction used in interpretation of small-angle X-ray scattering data of semicrystalline polymers. *J. Appl. Polym. Sci.* **2001,** *80* (3), 358-366.

Conclusions

Chapter 5

Conclusions and outlook

In summary, this dissertation demonstrates the role of comonomer sequence in two applications: surface design for antifouling coatings and block copolymer design for bulk self-assembly. In both cases, polypeptoids have been leveraged as precise materials with tunable functionality, length, and comonomer sequence.

In Chapter 2, a modular coating platform was utilized to make comparisons between polymer backbone chemistry, side chain backbone chemistry, and side chain sequence in antifouling/fouling release performance and chemical presentation. All coatings became more hydrophilic by soaking in water, suggesting rearrangement of the components in response to environment. X-ray photoelectron spectroscopy (performed in vacuum on soaked samples) revealed that peptide-functionalized coatings and PDMS-based coatings rearranged quickly to the vacuum-state presentation, while peptoid-functionalized PEO retained side chains at the surface even in vacuum. The initial settlement of model *Ulva linza* and *Navicula incerta* algae was strongly influenced by the side chain backbone chemistry, with lower initial settlement for peptide-functionalized coatings, while fouling release properties were dominated by the polymer backbone chemistry and generally improved with the addition of peptoid side chains. Correlating physicochemical properties and fouling

performance is critical for designing next-generation coatings, and this work elucidates the roles of each component's chemistry and length scale in amphiphilic (multi-component) coating designs.

In addition to tailoring surface design, precise copolymer materials also tune the structure and properties of bulk self-assembled systems. In Chapter 3, the role of comonomer sequence is investigated in the self-assembly of a lamellae-forming diblock copolymer. The adoption of nonideal chain conformations (supported by SCFT simulations) results in modulation of the periodic domain spacing, driven by the localization of compatibilizing comonomers at the block–block interface. Further, the thermal stability of the self-assembled phase is significantly altered by both the addition of compatibilizing groups and their placement in the sequence, with distributed sequences having lower order–disorder transition temperatures, and it is shown that sequence-specific models must be used to quantify these thermodynamic differences. The geometric effects of compatibilizing group placement are further explored in Chapter 4, focusing on the role of sequence in promoting interfacial and in-domain mixing. X-ray scattering analysis enables the quantification of the interfacial thickness for each sample, which also varies as a function of sequence, where tapered sequences have more interfacial mixing and distributed sequences do not broaden the interface versus a totally uncompatibilized block copolymer. This study builds on the initial results described in Chapter 3 to reach a clearer picture of how comonomer sequence affects chain conformation, in-domain mixing and phase stability, and interfacial mixing.

While this work represents significant progress in determining the roles of precise comonomer placement, it is just the beginning of utilizing polymer sequence as a design tool to target both surface and bulk properties of multicomponent polymer materials. An important extension of this work would be incorporating sequence-defined copolymers as

compatibilizers in homopolymer–homopolymer blends. The lessons learned in this work about chain conformation and interfacial behavior, along with continued collaboration with simulation, will inform the synthesis of designer surfactants for industrially-relevant mixed systems. The Segalman group is well-poised to explore these studies, as the versatility of polypeptoid chemistry lends itself to a variety of blend systems by exchanging side chain functionality to match the homopolymers of interest. Blend studies would give insight into the role of sequence in interfacial tension and coarsening, and dynamic secondary ion mass spectrometry (dSIMS) experiments with model homopolymer bilayers would provide insight into copolymer accumulation at these interfaces.

Understanding the effect of comonomer sequence on chain conformation raises the possibility of further enhancing nonideal chain conformations with specific interactions, such as hydrogen bonding. Pursuing such nonideal polymer shapes could lead to interesting chain packing and phase behavior relevant to both neat self-assembly and blends.

Further, while this work is placed squarely in the lamellar phase window, the effects of comonomer sequence at phase boundaries would be interesting to pursue, especially in collaboration with theory to predict key sequences to synthesize. The ability to control morphology with sequence instead of composition would open doors to functional self-assembled materials whose "loading" of particular functionalities or components could be tuned independently of their morphology.

While polypeptoid synthesis has advanced to produce sufficient quantities of precise materials, a challenge yet to be addressed is the low production of *block copolymers* containing these materials. In Chapters 3 and 4 of this work, the conjugation of polypeptoid and polystyrene blocks had low conversion, and the need for absolute purity further diminished the yield. This challenge precludes the study of bulk mechanical or rheological properties, which are expected to be interesting and illuminating in these unique materials. While it

would avoid the challenges from conjugating two distinct polymers together, the direct synthesis of polypeptoid-only block copolymers is limited by the reaction efficiency of each step, and even with very high efficiencies, is not yet routine.

Multi-component polymeric materials will continue to be at the forefront of new technologies, and the results described here emphasize the utility of precise comonomer sequence as a design tool to target a wide range of applications. With ever-improving synthetic techniques and characterization tools, the place of comonomer sequence design will continue to be strengthened in future materials research.